University of Southampton

Faculty of Engineering, Science and Mathematics

School of Ocean and Earth Science

Physical and biological forcings on the carbonate chemistry in the North Atlantic Ocean

by

Cynthia Dumousseaud

Thesis for the degree of Doctor of Philosophy

May 2010

UNIVERSITY OF SOUTHAMPTON

ABSTRACT

FACULTY OF ENGINEERING, SCIENCE AND MATHEMATICS

SCHOOL OF OCEAN AND EARTH SCIENCE

Doctor of Philosophy

PHYSICAL AND BIOLOGICAL FORCINGS ON THE CARBONATE CHEMISTRY IN THE NORTH ATLANTIC OCEAN

by Cynthia Dumousseaud

The atmospheric concentration of CO_2 has risen considerably since the industrial revolution, and the subsequent uptake of atmospheric CO_2 by the oceans has affected the carbonate system and caused a reduction in the pH of the oceans. Model estimates involving future CO_2 emission scenarios have predicted a significant increase of oceanic Dissolved Inorganic Carbon concentrations by the end of the century, corresponding to a decrease in oceanic pH by up to 0.4. In order to observe and predict changes in primary productivity and community structure in the oceans associated with future climate change, precise measurements of all the carbonate system parameters are important. The natural processes affecting the seasonal and regional variations of the carbonate chemistry are still poorly understood and sustained monitoring programs are required in order to determine the importance of hydrographical and biogeochemical forcings. The relationships between physical and biological parameters and carbonate system parameters were investigated in several regions of the North Atlantic Ocean, allowing a better understanding of the natural processes affecting the carbonate system in this ocean basin. For this purpose, the seasonal and inter-annual variability of the carbonate system in the Northeast Atlantic Ocean was studied through a ship of opportunity program, allowing observations of the short-term processes affecting the carbonate system and air-sea CO_2 fluxes. The results showed contrasting effects of winter mixing and sea surface temperature on the carbonate system and the air-sea CO_2 fluxes. In addition, the distributions of the carbonate system parameters were determined in the Iceland Basin and in the sub-tropical Northeast Atlantic Ocean. The carbonate system in the Iceland Basin was characterized by mesoscale variability associated to the presence and development of an eddy dipole in the study region; while the sub-tropical Northeast Atlantic Ocean showed spatial variability in all the chemical parameters, associated with coastal upwelling and remineralization in an oxygen minimum zone. Although the physics appeared to be the main forcing on the carbonate system in this study, the role of biology in the seasonality of the carbonate system is highly important. However, physical forcings tend to set the level for biological drawdown and therefore highly contribute to the variability of the carbonate system and CO_2 fluxes.

Contents

List of Figures vi
List of Tables viii
Declaration of authorship ix
Declaration of supervision x
Acknowledgements xi

Chapter 1. Introduction 1
1.1. The global carbon cycle and the oceanic CO_2 pump 2
1.1.1. The solubility pump 3
1.1.2. The biological pump 4
1.2. The carbonate system 5
1.2.1. Dissolved Inorganic Carbon 6
1.2.2. Total alkalinity 7
1.2.3. Fugacity and partial pressure of CO_2 8
1.2.4. pH 8
1.2.5. Processes affecting the carbonate system 9
1.3. Ocean acidification 11
1.3.1. Calcifying organisms 11
1.3.2. Ocean monitoring 12
1.4. Objectives 14
1.5. Thesis outline 14

Chapter 2. Carbonate system measurements 16
2.1. Introduction 17
2.2. Oceanic pH measurements 18
2.2.1. Definition of pH scales 18
2.2.2. TRIS buffer 19
2.2.2.1. Buffer preparation 19
2.2.2.2. Buffer calibration 22
2.2.3. Potentiometric system 27
2.2.3.1. System description 27
2.2.3.2. System preparation and operation 29
2.2.3.3. Accuracy and precision 30
2.2.3.4. System performance 31
2.2.4. Spectrophotometric measurement 32

2.2.4.1. Overview 32
2.2.4.2. Indicator solution 33
2.2.4.3. Calculation 34
2.2.4.4. Discussion 35
2.3. DIC and TA measurements 35
2.3.1. The VINDTA 3C 35
2.3.2. Dissolved Inorganic Carbon 36
2.3.3. Total Alkalinity 37
2.4. Calculation of the carbonate system 37
2.5. Conclusion 39

Chapter 3. Contrasting effects of temperature and winter mixing on the seasonal and inter-annual variability of the carbonate system in the Northeast Atlantic Ocean 41
3.1. Introduction 44
3.2. Methods 45
3.2.1. Area of study 45
3.2.2. Sampling 46
3.2.3. DIC and TA measurements 47
3.2.4. Coccolithophore abundance 49
3.2.5. Air-Sea CO_2 flux calculation 49
3.2.6. External sources of data 50
3.3. Results and discussion 51
3.3.1. Salinity, temperature and nitrate 51
3.3.2. Dissolved oxygen anomaly and chlorophyll *a*-fluorescence 51
3.3.3. Total Alkalinity 54
3.3.4. Dissolved Inorganic Carbon 56
3.3.5. Seasonal variability of DIC and nitrate 56
3.3.6. Influence of winter mixing on the carbonate system variability 58
3.3.7. Air-Sea CO_2 fluxes 60
3.4. Conclusions 64

Chapter 4. Control of the carbonate system by upwelling and respiration in the sub-tropical Northeast Atlantic Ocean 65
4.1. Introduction 67
4.2. Methods 69
4.3. Results and discussion 72
4.3.1. Surface distributions of hydrographic, biological and chemical properties 72

4.3.2. Meridional distributions of hydrographic, biological and chemical properties... 76
4.3.3. Influence of coastal upwelling on air-sea CO_2 fluxes 78
4.3.4. Oxygen minimum zone 79
4.4. Conclusions 83

Chapter 5. Mesoscale variability of the carbonate chemistry in the Iceland Basin 84
5.1. Introduction 85
5.2. Methods 86
5.2.1. Area of study 86
5.2.2. Sampling 86
5.2.3. DIC and TA measurements 87
5.2.4. Underway pH measurements 88
5.3. Inter-consistency of the carbonate system measurements 88
5.4. Results and discussion 89
5.4.1. Surface distribution of the parameters 89
5.4.2. Depth distributions of the parameters 92
5.4.3. Mesoscale variability associated with an eddy dipole 93
5.4.4. Differences between the two eddies 94
5.5. Conclusions 97

Chapter 6. Summary and perspectives 98
6.1. Introduction 99
6.2. Summary 99
6.3. Recommendations and perspectives 102
6.3.1. Quality controlled carbonate system databases 102
6.3.2. Importance of climate models 102
6.3.2.1. Ocean circulation 103
6.3.2.2. High latitudes 104
6.3.3. Carbon sequestration and geo-engineering 104
6.3.4. Atlantic Ocean vs. Pacific Ocean 105

Appendices 106
References 115

List of Figures

Figure 1.1. Effects of various processes on the carbonate system parameters 9
Figure 1.2. Long-term trends of surface oceanic pH 13

Figure 2.1. Platinization of the hydrogen electrodes..... 23
Figure 2.2. Preparation of the silver/silver chloride electrodes. 24
Figure 2.3. Bath instrumentation and cell bath 24
Figure 2.4. Drawing and picture of the potentiometric pH system 30
Figure 2.5. Continuous pH measurements. 31
Figure 2.6. Comparison of pCO_2 and pH data 32

Figure 3.1. Location of the FerryBox route 46
Figure 3.2. Monthly mean of SSS, SST, nitrate, O_2 anomaly and chl *a*-fluo..... 52
Figure 3.3. SeaWIFS chlorophyll-*a* distribution..... 54
Figure 3.4. Monthly mean concentrations of TA, nTA, DIC and nDIC 55
Figure 3.5. Argo float temperature data and mixed layer depths..... 59
Figure 3.6. Calculated air-sea CO_2 fluxes..... 61
Figure 3.7. Monthly mean oceanic and atmospheric pCO_2 and wind speed data..... 62

Figure 4.1. D326 cruise track and stations location 69
Figure 4.2. Surface distributions of S, T, nitrate, phosphate, density, and chl-*a* 74
Figure 4.3. Surface distributions of DIC, TA, nDIC, and nTA..... 75
Figure 4.4. Surface distributions of pH, pCO_2, air-sea CO_2 flux and wind speed 75
Figure 4.5. Depth distributions of temperature, salinity, TA, DIC, O_2 and density... 77
Figure 4.6. Depth profiles of dissolved oxygen, DIC, nDIC, and TA 80
Figure 4.7. Depth distribution of dissolved oxygen..... 81
Figure 4.8. DIC and AOU relationship between 100 m and 4000 m..... 82
Figure 4.9. Depth profiles of Ω_{Ca} and Ω_{Ar} 82

Figure 5.1. Surface and deep circulation in the North Atlantic Sub-polar Gyre..... 85
Figure 5.2. D321 cruise track and associated survey area. 87
Figure 5.3. Underway surface water distributions 90
Figure 5.4. Depth profile measurements (0 to 150 m) 91
Figure 5.5. ADCP vector plot and approximate location of the two eddies 92

Figure 5.6. SST and chl-*a* satellite images..... 93
Figure 5.7. Depth profiles of the casts sampled within the eddy cores..... 95
Figure 5.8. Profile distributions of nitrate and DIC in the cyclonic and anti-cyclonic eddy cores and outside the eddy dipole..... 96
Figure 5.9. Surface pH distributions at the beginning and the end of the cruise. 97

Figure 6.1. Surface water distributions of temperature, DIC, salinity, and TA..... 100

Figure A.1. Comparison of DIC measured and calculated (chapter 3)..... 107
Figure A.2. Comparison of TA measured and calculated (chapter 4). 108
Figure A.3. Comparison of pH measured and calculated (chapter 4)..... 109
Figure A.4. Correlation observed between underway DIC, TA and SST data; and between underway DIC, TA and SSS data (chapter 4)..... 110
Figure A.5. Correlation observed between depth distributions of S and T, DIC and T, and TA and S (chapter 4). 111
Figure A.6. Correlation observed between depth distributions of DIC and T, NO_3 and DIC, PO_4 and DIC, and TA and S (chapter 5). 112
Figure A.7. Correlation observed between sea surface DIC and temperature..... 113
Figure A.8. Correlation observed between sea surface TA and salinity..... 114

List of Tables

Table 2.1. Chemical composition of the TRIS buffer solution. 21
Table 2.2. Calculated carbonate parameters using the different sets of constants. ... 39
Table 2.3. Errors associated with the recalculation of the carbonate system. 39

Table 3.1. Crossing dates (Portsmouth to Bilbao) between 2005 and 2007. 46
Table 3.2. Observed and estimated seasonal amplitude of DIC 57
Table 3.3. Effect of varying parameters on the air-sea CO_2 flux calculation 63

Table 4.1. Hydrographic and chemical characteristics of the water masses 78

Table 5.1. List of the CTD casts and their positions related to the eddies location .. 94

Table 6.1. Pearson product-moment correlation coefficient (r) 101

Declaration of authorship

I, Cynthia Dumousseaud, declare that this thesis entitled “Physical and biological forcings on the carbonate chemistry in the North Atlantic Ocean” and the work presented in it are my own, and have been generated by me as the result of my own original research.

I confirm that:

1. This work was done wholly or mainly while in candidature for a research degree at this University.
2. Where any part of this thesis has previously been submitted for a degree or any other qualification at this University or any other institution, this has been clearly stated.
3. Where I have consulted the published work of others, this is always clearly attributed.
4. Where I have quoted from the work of others, the source is always given. With the exception of such quotations, this thesis is entirely my own work.
5. I have acknowledged all main sources of help.
6. Where the thesis is based on work done by myself jointly with others, I have made clear exactly what was done by others and what I have contributed myself.

Signed: .....

Date: .....

Graduate School of the

National Oceanography Centre, Southampton

This PhD dissertation by *Cynthia Dumousseaud* has been produced under the supervision of the following persons:

Supervisors

Prof. Eric Achterberg
Dr. Toby Tyrrell
Dr. David Hydes
Dr. Matt Mowlem

Chair of Advisory Panel

Prof. Peter Statham

Acknowledgements

Firstly, I would like to thank my supervisors Eric Achterberg, Toby Tyrrell, David Hydes, and Matt Mowlem for making this work possible and for providing me guidance and helpful advices throughout this study. Further acknowledgements go to Duncan Purdie and Nick Bates (BIOS) for the review of this thesis and for their helpful comments.

I would also like to thank all the persons involved in the FerryBox crossings and the D321 and D326 cruises. More particularly I would like to thank the captain, officers and crew of the RRS *Discovery*, the P&O MV *Pride of Bilbao* and the MV *Santa Maria*; John Allen, PSO of the D321 cruise; Adrian Martin; Rosalind Pidcock; Mark Stinchcombe and Matthew Patey for the oxygen and nutrient analysis; Mark Moore, Anastasia Charalampopoulou, Mike Lucas and Duncan Purdie for the chlorophyll-*a* measurements; Alex Forryan for the satellite images; Claire Powell for the help with sample collection; Lesley Salt; Jenny Andrew and Julie Collins from British Oceanographic Data Centre (BODC) and Ben Moat for assistance with the wind speed data; P&O Ferries Ltd., UK, and Seatrade Reefer Chartering, Belgium, for providing access to their ships; the FerryBox team for the help provided in the maintenance of the FerryBox system and on the calibration crossings, and more particularly Sue Hartman, Jon Campbell, Charlene Bargeron, Navjit Sagoo, Holly Niner, and Angus Roberts for their help with data collection and analysis; Elizabeth Kent and Werenfrid Wimmer for their helpful comments; Andrew Dickson (Scripps) for sharing is expertise on TRIS buffer preparation; David Pearce (Cefas) and John Wood (Ruthern Instrument) for their technical support and advices in the operation of the potentiometric pH system used in this study; as well as Cedric Floquet, Mark Moore, Nigel Eastwood, Neil Jenkinson, Mark Hartman, Alberto Borges and Jon Campbell who also provided valuable help. Additional thanks go to Ute Schuster and Nick Hardman-Mountford for providing me access to their fCO_2 and pCO_2 data; and the WUN Research Mobility Program.

Finally, I would like to thank family and friends who supported me throughout my studies; and more importantly my parents, Gaëlle, Benjamin, Amandine, Ben, Anthony, Estelle, Flo, Roz, Anastasia, Thanos, Sergio, Alex, Sofia, Hao, Aurélie and Nicolas, Bethan, Lorna, Daria, Kat, Clara and Lev, Christina, Polly, Rich, Craig, Matt, Stinch, Pete, Xi, Aaron, Bronwyn, Paul, Maria, Ian, and many others.

This thesis was funded by a NOCS PhD studentship.

Chapter 1

Introduction

1.1. The global carbon cycle and the oceanic CO_2 pump

Since the industrial revolution, the atmospheric concentration of CO_2 has increased from 280 ppm in the late 1700s to almost 390 ppm in 2009 (Hofmann et al. 2009), reaching levels significantly higher than determined for the past 650,000 years (IPCC 2007). This increase was associated with anthropogenic activities including fossil fuel combustion and deforestation (Royal Society 2009 and 2005; Falkowski et al. 2000).

Different emission scenarios have predicted a further increase leading to concentrations of over 800 ppm by the end of this century, corresponding to a global temperature increase of between 2 to 4 °C (Royal Society 2009; IPCC 2007; IPCC 2001). Although the uncertainties associated with these estimates are significant (Watson 2008), the consequent risks of high atmospheric CO_2 concentrations are known and the expected changes will have considerable impact on the oceans, with sea level rise and ocean acidification (IPCC 2007; Royal Society 2005; Caldeira and Wicket 2003; Wolf-Gladrow et al. 1999). The process of ocean acidification is associated with the chemical changes occurring due to the enhanced CO_2 content in the oceans. While some of the effects of high atmospheric CO_2 concentrations are already noticeable, others are more uncertain and will require detailed research efforts.

The global carbon cycle is regulated by carbon exchange between the atmosphere, the land, and the oceans (Sarmiento and Gruber 2002). More particularly, the land and the oceans, two major reservoirs of carbon (Sarmiento and Gruber 2002), play a significant role in regulation of the atmospheric CO_2 concentrations through net uptake of anthropogenic CO_2. The oceanic carbon pool is by far the largest, and is estimated to be about 38000 PgC (~93%). It is followed by the terrestrial carbon pool (2300 PgC, ~5.6%), and the atmospheric carbon pool (590 PgC, ~1.4%) (Sarmiento and Gruber 2006; Sarmiento and Gruber 2002).

The amount of anthropogenic CO_2 accumulated in the oceans can be estimated (Gruber et al. 1996; Sabine et al. 2004; Touratier and Goyet 2004a and b; Touratier et al. 2007; Goyet et al. 2009). This allows a better estimate of past and future changes in the global carbon cycle and anthropogenic CO_2 uptake. The principal

methods currently used to calculate anthropogenic CO_2 are the TrOCA method (tracer combining oxygen, dissolved inorganic carbon and total alkalinity; Touratier and Goyet 2004a and b); and the ΔC^* method, which uses a carbon tracer to separate anthropogenic CO_2 from the measured DIC concentrations (Gruber et al. 1996).

In the period since the industrial revolution until 1994, the oceans have absorbed almost half of the anthropogenic CO_2 emitted to the atmosphere, corresponding to a global oceanic sink of 118 ± 19 Pg C (Sabine et al. 2004). An annual mean oceanic CO_2 uptake of 1.6 ± 0.9 Pg C yr^{-1}, estimated from surface oceanic pCO_2 measurements obtained between 1970 and 2007 (Takahashi et al. 2009), represents a large portion of the CO_2 emitted to the atmosphere as a result of fossil fuel burning. This value is in agreement with other recent estimates of 1.4 ± 0.7 Pg C yr^{-1} and 1.7 ± 0.4 Pg C yr^{-1} for the period 1995 to 2000, obtained both from observations and general circulation models (Gruber et al. 2009). The fossil fuel CO_2 emissions were estimated as 7.2 Pg C yr^{-1} for the period 2000-2005 (IPCC 2007); as opposed to 5.4 ± 0.3 Pg C yr^{-1} in the 1980s (Sarmiento and Gruber 2002).

This rapid increase in the annual anthropogenic CO_2 emissions hence shows the need to reduce our current emissions. Without the oceanic CO_2 uptake, the actual atmospheric concentration would be close to 450 ppm (Doney et al. 2009a). The oceanic carbon cycle is governed by biological and physical processes, described respectively as the biological pump and the solubility pump, which together control the oceanic CO_2 uptake (Falkowski et al. 2000).

1.1.1. The solubility pump

The oceanic solubility pump is governed by the physical and chemical processes acting to transport CO_2 from the surface ocean to the deep ocean. The solubility of CO_2 in sea water is inversely correlated with the sea water temperature, and the efficiency of the solubility pump therefore increases with increasing latitude (Zeebe and Wolf-Gladrow 2001). The oceanic thermohaline circulation plays an important role in the solubility pump, with the formation and sinking of cold and dense water masses at higher latitudes contributing to the sequestration of anthropogenic CO_2 (Falkowski et al. 2000). On the other hand, upwelling regions can act as a source of

CO_2 to the atmosphere due to CO_2 supersaturated deep waters being brought to the surface (Falkowski et al. 2000).

Climate models have predicted a decrease in the solubility pump efficiency associated with future climate change due to changes in ocean circulation (i.e. enhanced stratification) and increase in sea surface temperature. This could have a considerable impact on the global carbon cycle as the ability of the oceans to absorb anthropogenic CO_2 will be reduced (Bopp et al. 2001).

1.1.2. The biological pump

The biological pump is composed of the soft tissue pump, which transfers POC to depth, and of the carbonate pump, which transfers mineral $CaCO_3$ to the deep waters. The biological carbon pump is therefore responsible for the removal of carbon from the euphotic zone, exporting it to the deeper layer of the oceans (De La Rocha and Passow 2007). The pump functions through CO_2 uptake and formation of particulate organic carbon by photoautotrophs, and subsequent sinking of this organic carbon. Vertical transport by zooplankton and advection of dissolved organic matter also play an important role in the carbon export process (Urrère and Knauer 1981; Copin-Montégut and Avril 1993; Steinberg et al. 2000). The fraction of organic carbon exported to the deep ocean is characteristic of the efficiency of the biological pump (De La Rocha and Passow 2007). The biological pump plays an important role in the global carbon cycle: by transporting carbon to the deep ocean, transfer of CO_2 from the atmosphere to the ocean is possible, hence accentuating the solubility pump and reducing the rapid increase in atmospheric CO_2 (Anderson and Totterdell 2004).

The efficiency of the biological pump is dependent on a range of processes, and is low in High Nutrient Low Chlorophyll (HNLC) regions where primary productivity is limited by factors other than the availability of major nutrients such as nitrate and phosphate. These factors include light (de Baar et al. 2005), zooplankton grazing (Landry et al. 1997; Cullen 1991), and dissolved iron (Martin et al. 1991; Martin and Fitzwater 1988).

The efficiency of the biological pump is described by the *f*-ratio. Introduced by Eppley and Peterson (1979), it represents the fraction of new production over total

primary production, and is used to estimate the export flux from the surface layer to the deep ocean. The difference between new production (obtained from nitrate inputs to the euphotic zone) and regenerated production (obtained from nutrient recycling in the surface waters) was first noted by Dugdale and Goering (1967). However, while surface nitrification was then assumed negligible, later studies showed that this process was occurring at shallower depth (i.e. Dore and Karl 1996), and in relatively large proportions (Yool et al. 2007), leading to an overestimation of new production and of the *f*-ratio. A recent estimate showed that up to 50% of the surface nitrate used by phytoplankton comes from surface nitrification (oxidation of ammonia to nitrate) rather than from the deep ocean (Yool et al. 2007), and careful use of the *f*-ratio in quantifying carbon export is therefore recommended.

The carbonate pump is an important component of the biological pump and is responsible for the precipitation and dissolution of calcium carbonate, hence controlling the carbonate system in the oceans. Coccolithophores (major producers of calcium carbonate; Broerse et al. 2000), along with foraminifera and pteropods, are the main contributors to the carbonate pump.

1.2. The carbonate system

The carbonate system is governed by equations 1.1 to 1.6 and the associated thermodynamics equilibrium constants (see chapter 2). The four chemical species of the carbonate system in sea water are the bicarbonate ion (HCO_3^-), the carbonate ion (CO_3^{2-}), the free (aqueous) carbon dioxide $CO_{2(aq)}$, and carbonic acid (H_2CO_3). The transfer of CO_2 from the atmosphere to the oceans strongly affects the carbonate system (equations 1.1 to 1.6) through an increase in the bicarbonate ion concentration and a decrease in the carbonate ion concentration (Zeebe and Wolf-Gladrow 2001; Falkowski et al. 2000).

The carbonate system controls the formation of calcium carbonate ($CaCO_3$) by calcifying organisms, a process which also leads to the formation of CO_2 (equation 1.4). The carbonate pump has the potential to increase the CO_2 concentration in sea water (Ridgwell and Zeebe 2005; Zeebe and Wolf-Gladrow 2001). This has been observed in regions of the open ocean following intense calcification events, leading

to an increase in CO_2 of as much as 50 µatm (Robertson et al. 1994; Holligan et al. 1993). However, most of the CO_2 formed during calcium carbonate formation is converted to bicarbonate ions (equation 1.5), associated to the buffering process of the oceans (Zeebe and Wolf-Gladrow 2001). The ratio of CO_2 released during calcification over the precipitated carbonate was estimated as 0.6 at an atmospheric CO_2 concentration of 350 µatm, but is expected to increase to up to 0.78 with future increase in atmospheric CO_2 concentration (Frankignoulle et al. 1994).

$$CO_2\ (g) = CO_2\ (aq) \qquad (1.1)$$

$$CO_2\ (aq) + H_2O = H_2CO_3 \qquad (1.2)$$

$$H_2CO_3 = H^+ + HCO_3^- \qquad (1.3)$$

$$Ca^{2+} + 2HCO_3^- = CaCO_3 + CO_2 + H_2O \qquad (1.4)$$

$$CO_2 + CO_3^{2-} + H_2O = 2HCO_3^- \qquad (1.5)$$

The carbonic acid (H_2CO_3) and aqueous carbon dioxide (CO_2 (aq)) are chemically not separable (Zeebe and Wolf-Gladrow 2001, Dickson et al. 2007), and equations 1.2 and 1.3 are therefore combined to form equation 1.6.

$$CO_2^*\ (aq) + H_2O = H^+ + HCO_3^- \qquad (1.6)$$

Where $CO_2^*\ (aq) = CO_2\ (aq) + H_2CO_3$

(g) and (aq) refer to the gaseous and aqueous states, respectively

Dissolved Inorganic Carbon (DIC), Total Alkalinity (TA), pH, and partial pressure (or fugacity) of CO_2 are the four parameters of the carbonate system directly measureable in seawater. The measurement of any two of these four variables allows the calculation of the other carbonate system parameters, such as the concentrations of bicarbonate and carbonate ions, via the use of the carbonate system equilibrium constants (cf. chapter 2).

1.2.1. Dissolved Inorganic Carbon

The DIC concentration of a sample of seawater is defined as the sum of the concentrations of all the inorganic forms of carbon dioxide present in the sample:

$$DIC = [CO_2^*] + [HCO_3^-] + [CO_3^{2-}] \quad (1.7)$$

Where $[CO_2^*] = [CO_2] + [H_2CO_3]$

It represents the biggest carbon pool in the ocean and is chemically constituted of bicarbonate ion (88.6%), carbonate ion (10.9%), and of carbon dioxide and carbonic acid (0.5%) (Sarmiento and Gruber 2006). Standard procedure for the determination of the DIC content of a seawater sample is available (Dickson et al. 2007; Dickson and Goyet 1994), and will be described in detail in chapter 2.

1.2.2. Total alkalinity

The notion of total alkalinity is difficult, and different definitions can be found in the literature (Zeebe and Wolf-Gladrow 2001). The most accurate definition is given by Dickson (1981):

> *"The total alkalinity of a sample of sea water is defined as the number of moles of hydrogen ion equivalent to the excess of proton acceptors (bases formed from weak acids with a dissociation constant $K \leq 10^{-4.5}$ at 25 °C and zero ionic strength) over proton donors (acids with $K > 10^{-4.5}$) in 1 kilogram of sample".*

$$TA = [HCO_3^-] + 2[CO_3^{2-}] + [B(OH)_4^-] + [OH^-] + [HPO_4^{2-}] + 2[PO_4^{3-}] + [SiO(OH)_3^-] + [NH_3] + [HS^-] - [H^+]_F - [HSO_4^-] - [HF] - [H_3PO_4] \quad (1.8)$$

Where $[H^+]_F$ is the free hydrogen ion concentration (cf. section 2.2).

In addition to the carbon dioxide species, other acid-base systems significantly contribute to TA (equation 1.8). These include boric acid, water, and minor nutrient species with acid-base properties such as silicate, phosphate and ammonia (Wolf-Gladrow et al. 2007; Dickson 2010). In most waters however, the terms NH_3 and HS^- can be neglected as these ions are usually present in very small amounts (Dickson et al. 2007). The method for the determination of TA in sea water will be described in detail in chapter 2.

1.2.3. Fugacity and partial pressure of CO_2

The fugacity and partial pressure of CO_2 in seawater (fCO_2 and pCO_2 respectively, in µatm) are defined as the fugacity and partial pressure of CO_2 in air which is in equilibrium with the sea water sample. They are obtained from the measurement of the mole fraction of CO_2 in seawater, xCO_2 (µmol mol^{-1}), by equilibrating a large volume of seawater with a small, fixed volume of air. The partial pressure of CO_2 is proportional to the mole fraction of CO_2 according to equation 1.9 (Dickson et al. 2007).

$$pCO_2 = xCO_2 \times p \qquad (1.9)$$

Where p is the total pressure of the mixture in atm

The fugacity is about 0.3 to 0.4% lower than the partial pressure due to the non-ideal nature of the gas phase (which does not strictly follow Henry's law) taken into account in the fugacity measurement (Zeebe and Wolf-Gladrow 2001). The fugacity of CO_2 can be obtained from the partial pressure using equation 1.10 (Dickson et al. 2007):

$$fCO_2 = pCO_2 \times \exp\left(p\frac{B + 2\delta}{RT}\right) \qquad (1.10)$$

Where B is the virial coefficient of pure CO_2 in cm^3 mol^{-1}, δ is the virial coefficient of CO_2 in air (cross virial coefficient) in cm^3 mol^{-1}, R is the gas constant (= 8.314472) in J K^{-1} mol^{-1}, and T is the temperature in Kelvin.

1.2.4. pH

The notion of pH has been introduced by Sørensen (1909) with the definition of the logarithmic pH scale. It is defined as the negative logarithm of the concentration of hydrogen ions (equation 1.11).

$$pH = -\log [H^+] \qquad (1.11)$$

The description of the two recommended methods currently in use for the determination of pH in seawater and the preparation of the buffer used to calibrate pH measurements will be discussed in detail in the next chapter.

1.2.5. Processes affecting the carbonate system

A number of biological (e.g. calcium carbonate precipitation and dissolution, photosynthesis, respiration), chemical (e.g. CO_2 uptake and release) and physical (e.g. mixing) processes affect the carbonate system. The effects of these processes on the carbonate system parameters are shown in Figure 1.1 (Zeebe and Wolf-Gladrow 2001). While CO_2 uptake and release processes only affect the DIC concentrations, biological processes affect both DIC and TA. In case of calcium carbonate ($CaCO_3$) production or dissolution, there is a larger effect on TA than on DIC: each mole of $CaCO_3$ precipitated or dissolved leads to a decrease or increase of 1 mole of DIC and 2 moles of TA. On the other hand, photosynthesis or respiration tend to decrease or increase DIC and have minor effects on TA mainly due to nitrate uptake or release (Zeebe and Wolf-Gladrow 2001; Brewer and Goldman 1976; Bates et al. 2009).

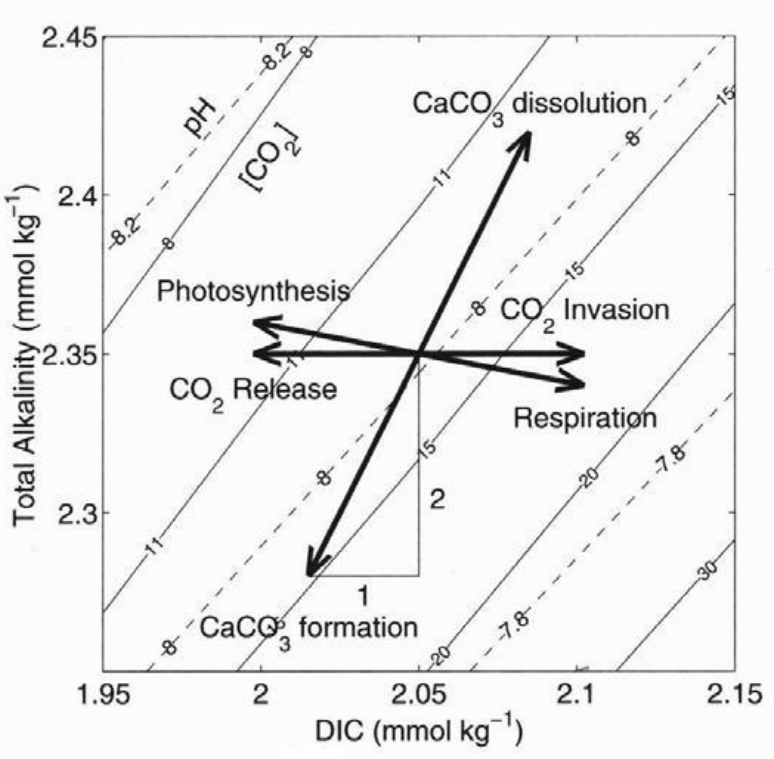

Figure 1.1. Effects of various processes on the carbonate system parameters (from Zeebe and Wolf-Gladrow 2001). Solid and dashed lines represent the levels of dissolved CO_2 concentration (in µmol kg^{-1}) and pH, respectively.

The effect of nitrogen uptake/release on TA also depends on the type of nitrogen assimilated/remineralized: while nitrate and nitrite uptake tend to increase TA, a

decrease in TA is observed when ammonium is the source of nitrogen (Wolf-Gladrow et al. 2007). However, the changes in pH due to biogeochemical and physical processes are more difficult to quantify due to the natural buffering capacities of the ocean (Soetaert et al. 2007).

Other biological processes affecting the carbonate system variables include nitrification (oxidation of ammonia into nitrate), nitrogen fixation, denitrification (reduction of nitrate via nitrite to N_2), remineralization of POC (production of ammonia or nitrate), and iron and manganese reduction (Soetaert et al. 2007; Wolf-Gladrow et al. 2007).

The carbonate system in seawater presents some natural buffer capacities which can be described by the Revelle factor (Revelle and Suess 1957). The buffer factor (RF_0) represents the percent change in *p*CO2 (or *f*CO_2) causes by a 1% change in DIC at constant TA (Zeebe and Wolf-Gladrow 2001; equation 1.12). Due to these buffering capacities, the increase in DIC (and related decrease in pH) associated with the oceanic uptake of CO_2 from the atmosphere is lower than expected. However, the capacity of the oceans to absorb CO_2 is inversely proportional to the Revelle factor. With increasing oceanic pCO_2 due to increasing atmospheric CO_2 concentration, the Revelle factor increases, slowly reducing the buffering capacity of the oceans.

$$\mathrm{RF}_0 = \frac{d[\mathrm{CO}_2]/\mathrm{CO}_2}{d\mathrm{DIC}/\mathrm{DIC}} \qquad (1.12)$$

Approximately 80% of the variation in TA in the surface ocean is related to changes in salinity (Wolf-Gladrow et al. 2007; Friis et al. 2003; Millero et al. 1998a), including freshwater addition (e.g. precipitation, river inputs, sea-ice melting) and removal processes (e.g. evaporation or sea-ice formation) (Bates et al. 2009). The salinity normalization of TA is therefore useful to characterize the changes in TA due to biogeochemical processes such as calcium carbonate precipitation and production of particulate organic matter (Wolf-Gladrow et al. 2007; Millero et al. 1998a). Although this normalization presents some limitations (Friis et al. 2003), it can be used to compare the TA distribution between regions where the salinity deviates from 35, such as at high and low-latitudes (Millero et al. 1998a).

1.3. Ocean acidification

As a consequence of the absorption of about half of the anthropogenic CO_2 emissions since the industrial revolution (Sabine et al. 2004), the surface ocean pH has decreased by 0.1 and is expected to further decrease by as much as 0.4 by the end of the century, depending on future CO_2 emissions scenarios (Orr et al. 2005, Caldeira and Wickett 2003; Wolf-Gladrow et al. 1999). Model estimates have predicted a global increase in DIC of 12% by the end of the century, as a result of a doubling of atmospheric CO_2 concentrations, with a corresponding decrease of the carbonate ion concentration ($[CO_3^{2-}]$) of 60% (Feely et al. 2004). This decrease in carbonate ion concentration would lead to a decrease in the saturation state of calcium carbonate (Ω), which will affect the precipitation and dissolution process of calcium carbonate, such that calcifying organisms would dissolve at shallower depths (Feely et al. 2004).

$$\Omega = \frac{[Ca^{2+}][CO_3^{2-}]}{K^*_{sp}} \qquad (1.13)$$

With K^*_{sp} the solubility product of calcium carbonate, expressed as (equation 1.14):

$$K^*_{sp} = [Ca^{2+}]_{sat}[CO_3^{2-}]_{sat} \qquad (1.14)$$

1.3.1. Calcifying organisms

Important phytoplankton organisms threatened by future changes in the carbonate chemistry are the coccolithophores, major producers of calcium carbonate (Broerse et al. 2000) and other calcifiers such as corals, foraminifera, and pteropods (Fabry 2008, Royal Society 2005). However, it is still not clear how coccolithophores and other calcifiers will be affected by changes in the carbonate system (Fabry 2008). Different experiments have shown varying results, in some cases with a decrease in calcification and the presence of malformed coccolithophores at enhanced pCO_2 levels (Zondervan et al. 2001; Riebesell et al. 2000), while in other cases, increased pCO_2 levels led to an increase in calcification rates (Iglesias-Rodriguez et al. 2008).

These different results could possibly be attributed to differences in the coccolithophore species under study (Fabry 2008).

Three different types of calcium carbonate are produced by marine organisms: calcite, magnesium calcite and aragonite. Calcite products are known to be less soluble than aragonite, but the incorporation of magnesium in the calcification process increases the solubility (Royal Society 2005; Dickson 2010). The differences in solubility properties observed between the different types of calcium carbonate produced by marine organisms suggest that they will not react equally to future changes in the carbonate chemistry.

1.3.2. Ocean monitoring

To observe and subsequently predict changes in the productivity and community structure in the ocean associated with the expected changes in the carbonate chemistry, precise measurements of the carbonate chemistry parameters are important. For this reason, accurate pH measurements, along with DIC, TA and pCO_2 measurements need to be conducted.

The monitoring of atmospheric carbon dioxide concentration was pioneered by David Keeling, who was the first to show the annual increase in atmospheric CO_2 (Keeling 1960). The Hawaii Ocean Time-Series (HOTS) and the Bermuda Atlantic Time-Series (BATS) programs were then established in 1988 to monitor the hydrographic, biological and chemical properties in sea water at station Aloha, Hawaii, and in the Sargasso Sea (Karl et al. 2003). These programs have provided since then monthly observations of the chemical properties of the water column in the North Pacific Sub-tropical Gyre and in the North Atlantic Sub-tropical Gyre, introducing the longest records in the world of carbon dioxide levels. Following this, numerous monitoring programs have been developed, including the ESTOC (European Station for Time-series in the Ocean, Canary Islands) station in the Northeast Atlantic Ocean, and the SEATS (South East Asia Time-Series) station in the South China Sea (Karl et al. 2003; Doney et al. 2009a).

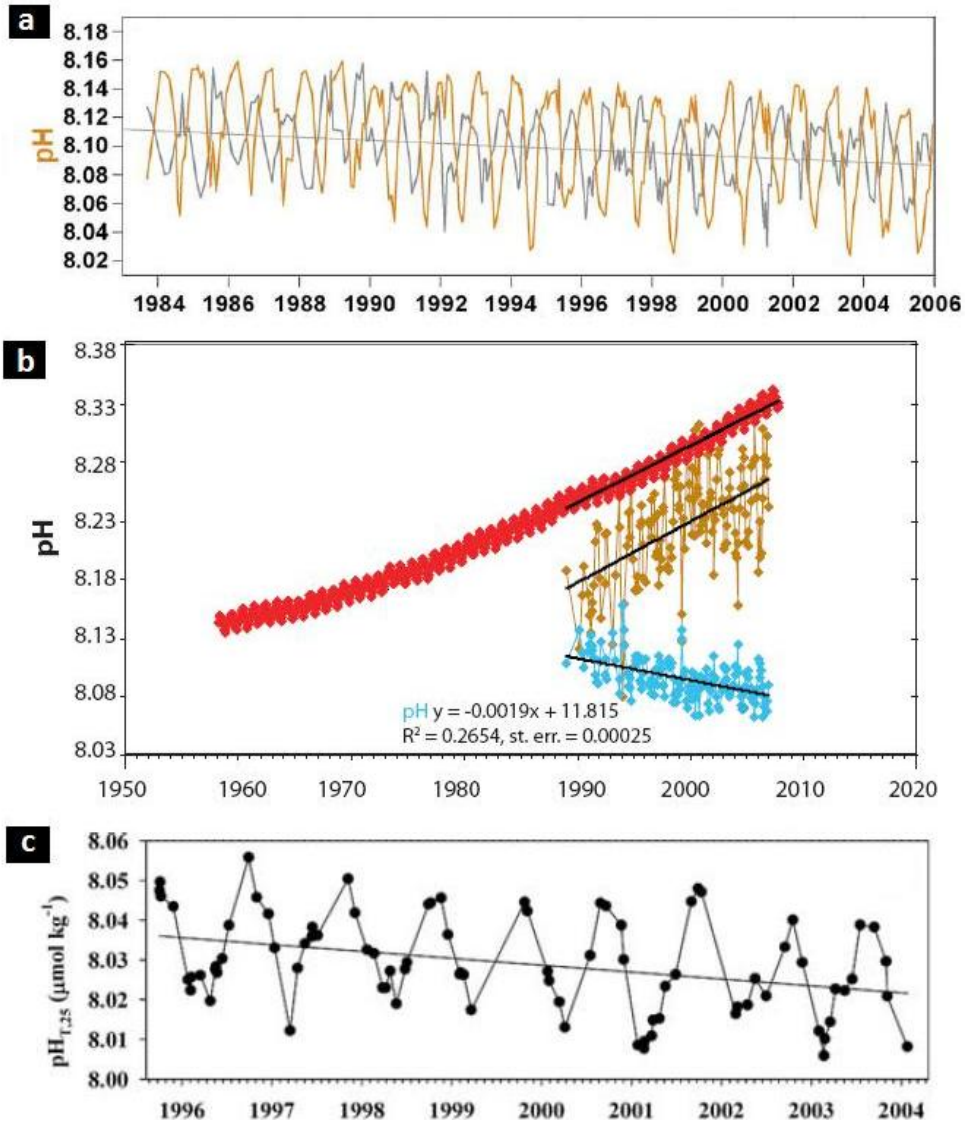

Figure 1.2. Long-term trends of surface oceanic pH observed at: (a) BATS and Hydrostation S in the North Atlantic Ocean (Figure adapted from Bates 2007); (b) Ocean Station ALOHA in the sub-tropical North Pacific Ocean (Figure adapted from Doney et al. 2009a); and (c) ESTOC station between 1995 and 2004 (Figure adapted from Santana-Casiano et al. 2007)

These time-series programs have helped us to understand biogeochemical processes in the oceans and allowed us to observe the changes that are taking place in the oceans. For example, the annual decrease in surface oceanic pH was estimated from three major ocean time-series program (Figure 1.2) to -0.0017 y^{-1} for BATS (Bates 2007), -0.0017 y^{-1} for the ESTOC station (Santana-Casiano et al. 2007), and -0.0019 y^{-1} for HOTS (Dore et al. 2009; Doney et al. 2009a).

1.4. Objectives

The current trend in oceanic pH involves an annual decrease of -0.0017 to -0.0019 (Bates 2007; Santana-Casiano et al. 2007; Dore et al. 2009). However, spatial and temporal pH variations of 0.3 have been estimated (Royal Society 2005). Therefore, it is of particular importance to understand all the processes, both natural and anthropogenic, driving changes in the oceanic carbonate system in order to allow an improved prediction of the effects of ocean acidification on ecosystem structure and functioning. More particularly, we need to understand the biological and physical controls on the carbonate system. The aim of this study is to observe the natural variations of the carbonate chemistry in the North Atlantic Ocean and to determine the strength of the key forcing processes through measurements of Dissolved Inorganic Carbon, Total Alkalinity and oceanic pH.

1.5. Thesis outline

A description of the methods available to determine pH in sea water is given in chapter 2. The challenges encountered with analytical measurement and calibration are also examined. This chapter provides a detailed description for the preparation of pH buffers in artificial sea water, required to obtain high quality pH measurements. The methods used in this study for the determination of DIC and TA are described, as well as the constants used for the calculation of the carbonate system parameters.

As explained above, ocean monitoring is required to track changes in the carbonate chemistry due to increasing atmospheric CO_2 concentrations, and to observe the natural spatial, seasonal and inter-annual variability. The use of ships of opportunity is an important tool for ocean monitoring. A two-year study of the carbonate system conducted as part of the FerryBox program is presented in chapter 3. The observations reveal inter-annual variability in the carbonate system and air-sea CO_2 fluxes associated with differences in temperature and winter mixing.

Coastal upwelling regions can bring low-pH and CO_2 enriched waters to the surface ocean (Feely et al. 2008) and are important environments to study the potential impact of ocean acidification. The spatial variability of the carbonate system in the

sub-tropical North Atlantic associated with coastal upwelling and an oxygen minimum zone is described and discussed in chapter 4.

The North Atlantic Ocean, and more particularly the Iceland Basin, is characterized by strong mesoscale activity. The distribution of the carbonate system parameters and their variability associated with the presence of an eddy dipole in this oceanic area is presented in chapter 5, along with a detailed interpretation of the measured carbonate system parameters.

Finally, chapter 6 gives a summary of the work undertaken as part of this PhD project, including a comparison and discussion of the different results presented in the previous chapters, such as spatial and temporal variability in the North Atlantic Ocean and differences in the forcing factors involved in the natural variability of the carbonate system. Some recommendations and perspectives for future work regarding climate change and the global carbon cycle are also discussed.

Chapter 2

Carbonate system measurements

2.1. Introduction

The importance of achieving high accuracy and high precision pH measurements on a continuous and long term basis (i.e. as part of a time-series program) has been discussed in chapter 1. Total Alkalinity (TA) and Dissolved Inorganic Carbon (DIC) analyses constitute so far the most accurate and reliable measurements of the carbonate system. However, no autonomous systems are currently available for the measurement of these variables. Continuous pH measurements, along with partial pressure of CO_2 (pCO_2), DIC and TA measurements, are necessary to obtain a good understanding of the seasonal and inter-annual variability, and long-term changes of the carbonate system.

The achievement of high quality oceanic pH measurements is however still a challenge but have considerably improved in recent years. Two methods are currently in use for the determination of pH in seawater and will be described in detail in this chapter: the potentiometric method and the spectrophotometric method. The potentiometric method is based on the measurement of the electromotive force of a cell composed of a glass pH electrode and a reference electrode, while the spectrophotometric method is based on the addition of an indicator dye to the seawater sample. Until the late 1980s the main difficulty encountered with the potentiometric pH measurement was due to the difference in ionic strength between the buffer and the sea water sample. These challenges have been overcome due to the development of artificial sea water buffers of similar ionic strength to that of the sample (Covington and Whitfield 1988).

Buffer solutions are extremely important in order to calibrate potentiometric pH measurements and their pH values must be well defined. However, for measurement in high ionic strength solutions, NBS (National Bureau of Standards) pH buffers have been shown to produce large differences between calibration and sample measurements (Whitfield et al. 1985). Instead, the use of the TRIS (2-amino-2-hydroxymethyl-1,3-propanediol) buffer, introduced by Smith and Hood (1964), has been recommended. To achieve a chemical composition close to sea water, the buffer is made up in artificial sea water prepared according to the protocol by Dickson et al. (2007). Such buffers have been shown to be relatively stable if stored in borosilicate bottles with a greased ground-glass stopper to prevent carbon dioxide or water vapor

exchange with the atmosphere (Nemzer and Dickson 2005; Dickson et al. 2007), with a small shift in pH over time (0.0005 pH unit per year). The recent introduction of spectrophotometric pH measurements has further increased the quality and frequency of oceanic pH measurements as they reduce errors encountered due to electrode failure or buffer preparation (Clayton and Byrne 1993; Bellerby et al. 1995; Dickson 2010). However, potentiometric pH measurements involve relatively simple and low-cost instrumentation.

2.2. Oceanic pH measurements

2.2.1. Definition of pH scales

Three different seawater pH scales have been defined, based on different definitions of the hydrogen ion concentration:

- The free hydrogen ion concentration scale (pH_F) uses the concentration of free hydrogen ions to define the hydrogen ion activity (Bates 1964). This pH scale does not take into account the influence of sulfate or fluoride ions (equations 2.1 and 2.2).

$$pH_F = -\log (a_{H+ (F)}) \quad (2.1)$$

$$a_{H+ (F)} \approx [H^+]_F \quad (2.2)$$

- The total hydrogen ion concentration scale (pH_T) was introduced by Hansson (1973). This scale takes into account the influence of sulfate ions but not of fluoride ions (equations 2.3 to 2.6).

$$pH_T = -\log (a_{H+ (T)}) \quad (2.3)$$

$$a_{H+(T)} \approx [H^+]_F + [HSO_4^-] \quad (2.4)$$

$$\approx [H^+]_F (1+ K_{HSO4}[SO_4^{2-}]) \quad (2.5)$$

$$K_{HSO4} = [HSO_4^-]/([H^+][SO_4^{2-}]) \quad (2.6)$$

  Where K_{HSO4} is the association constant for HSO_4^-.

- The seawater hydrogen ion concentration scale (pH_{SWS}) includes the influence of fluoride ions (Dickson and Riley 1979) in addition to the sulfate ions (equations 2.7 to 2.10).

$$pH_{SWS} = -\log(a_{H^+(SWS)}) \quad (2.7)$$

$$a_{H+(SWS)} \approx [H^+]_F + [HSO_4^-] + [HF] \quad (2.8)$$

$$\approx [H^+]_F (1 + K_{HSO4}[SO_4^{2-}] + K_{HF}[F^-]) \quad (2.9)$$

$$K_{HF} = [HF]/([H^+][F^-]) \quad (2.10)$$

Where K_{HF} is the association constant for HF.

The measurement of a single ion activity is impossible to achieve in practice and the use of the free scale is therefore not recommended (Covington and Whitfield 1988, Dickson 1993). The sea water scale can cause problems due to the uncertainties with the stability constants of HF (Dickson 1993). The total scale (pH_T) is the recommended scale (Dickson 1990; Dickson 2010) as it does not take into account the fluoride ions. The presence of sulfate ions in seawater needs to be taken into account when measuring the hydrogen ion concentration (i.e. pH) as it interacts with the hydrogen ion and thus perturbs the acid-base equilibrium in seawater (Dickson 1990).

The pH measurement is hence dependent on the scale used and a difference of up to 0.12 can be observed between the different scales (Zeebe and Wolf-Gladrow 2001). The potentiometric system described later in this chapter was calibrated with artificial seawater buffer (TRIS) containing sulfate, and the total hydrogen ion concentration scale should therefore be used in the pH calculation (Wedborg et al. 1999). A conversion between the different pH scales is possible, as shown in equation 2.11:

$$\begin{aligned} pH_F &= pH_T + \log(1 + K_{HSO4}[SO_4^{2-}]) \\ &= pH_{SWS} + \log(1 + K_{HSO4}[SO_4^{2-}] + K_{HF}[F^-]) \end{aligned} \quad (2.11)$$

2.2.2. TRIS buffer

2.2.2.1. Buffer preparation

The TRIS (2-amino-2-hydroxymethyl-1, 3-propanediol) buffer solution was made up in artificial sea water according to Dickson et al. (2007) and presented in Table 2.1. The calcium chloride ($CaCl_2$) and magnesium chloride ($MgCl_2$) solutions were

calibrated using the Mohr titration (Vogel 1978) and the hydrochloric acid (HCl) solution was calibrated using the Borax titration (Mellon and Morris 1925). The salts (NaCl, KCl, Na_2SO_4 and TRIS; Fisher Scientific analytical reagent grade) were dried at 110 °C for an hour in an oven prior to weighing. All solutions were prepared by weight, and the composition of the solution was scaled to the weight of the HCl added, the chloride concentration being the greatest source of error in the solution composition (Andrew Dickson, pers. comm.). Two batches of TRIS buffer were prepared and certified at the Scripps Institution of Oceanography (San Diego, USA) in Professor Andrew Dickson's laboratory, between June and July 2008 (WUN Research Mobility Programme). The process of the analysis and certification of these batches will be described in detail in section 2.3.2.

Silver nitrate titration (Mohr titration)

In order to determine the exact weight of the $CaCl_2$ and $MgCl_2$ solutions to add to the buffer solution (Table 2.1), their exact concentration needs to be determined. For this purpose, the $CaCl_2$ and $MgCl_2$ solutions (of approximately 1 mol kg^{-1}) were titrated with a gravimetric Mohr (silver nitrate) titration (Vogel 1978) with a precision better than 0.05%. The potassium chromate indicator solution was prepared by dissolving 5 g of K_2CrO_4 (Acros Organics) in 5 ml of de-ionized (Milli-Q) water to which a few drops of the silver nitrate ($AgNO_3$) solution were added. A red silver chromate precipitate should form and the solution was left to stand for 12 hours (overnight), then filtered and diluted to 100 ml with Milli-Q water. A few drops of the indicator (light yellow solution) were added before each titration in order to determine the end-point of the titration.

The standard silver nitrate (approximately 0.3 M) titrant solution ($AgNO_3$) was titrated with sodium chloride (NaCl, approximately 0.1g in 50 ml Milli-Q water) in order to determine its exact concentration. The titrated silver nitrate solution was then used for the titration of the $CaCl_2$ and $MgCl_2$ solutions. For this purpose, 0.5 g of the solution to titrate ($CaCl_2$ or $MgCl_2$) was introduced in a beaker (the exact weight added was carefully recorded) in approximately 80 ml Milli-Q water, and a few drops of the indicator were added. The weight of the beaker was recorded at that stage and the solution titrated with the silver nitrate solution until endpoint (characterized by an orange-red color). The weight of the beaker was recorded at the

end of the titration in order to determine the exact weight of silver nitrate solution added. The blank of the titration was determined with $CaCO_3$ following the same procedure by dissolving 0.1 g of $CaCO_3$ in 80 ml Milli-Q water.

	mol kg^{-1} H_2O	***Mw (g mol^{-1})***	***w(i)***	***density***	***buoyancy factor***	***mol kg^{-1} sol***	***g kg^{-1} sol***
NaCl	0.38762	58.443	22.6537	2.165	1.0004	0.37087	21.688
Na_2SO_4	0.02927	142.04	4.1575	2.68	1.0003	0.02801	3.981
KCl	0.01058	74.551	0.7888	1.984	1.00045	0.01012	0.755
$CaCl_2$	0.01075	110.99	1.1931	1.042	1.001	0.01029	10.286
$MgCl_2$	0.05474	95.211	5.2119	1.071	1.00097	0.05474	52.378
TRIS	0.08	121.136	9.6909	1.35	1.00074	0.07654	9.275
HCl	0.04	36.461	1.4584	1.018	1.00103	0.03827	38.272
$\Sigma w(i)$ in 1 kg H_2O = 45.154 g							
$m(Cl^-)$ = 0.56918 mol kg^{-1} H_2O							

Table 2.1. Chemical composition of the TRIS buffer solution (Dickson et al. 2007); recipe computed for 1000 g of solution, salinity = 35, and assuming a molality of 1 mol kg^{-1} for each of the solutions ($CaCl_2$, $MgCl_2$ and HCl).

Borax titration

In order to determine the exact weight of the HCl solution to introduce in the buffer solution, the exact concentration of the HCl solution also needs to be determined (Table 2.1). A gravimetric Borax (di-sodium tetraborate $Na_2B_4O_7.10H_2O$, Fisher Scientific analytical reagent grade) titration (Mellon and Morris 1925) was used to standardize the HCl solution (1 mol kg^{-1}) with a precision of 0.1%. The methyl red indicator used for the titration was water soluble and prepared at a 0.02% ratio (0.02 g in 100 ml Milli-Q water). For each titration, approximately 1 g of Borax was dissolved in 60 ml of Milli-Q water and titrated with the HCl solution. The weight of added HCl was carefully recorded, as well as the initial weight of Borax.

2.2.2.2. Buffer calibration

Two batches of high quality buffer (5 and 20 liters) were prepared at the Scripps Institution of Oceanography (UCSD, La Jolla, USA) and certified in Professor Andrew Dickson's laboratory during June and July 2008. The certified buffers allowed us to determine the accuracy of the potentiometric pH system as well as the quality of the buffer prepared at NOCS.

All the salts used for the preparation of the buffer were recrystallized in order to minimize possible contamination from bromide ions (Dickson 1990). The HCl solution (1 mol kg^{-1}) was made up from double-distilled concentrated HCl and was coulometrically titrated (precision better than 0.01%) in order to establish the exact acid concentration. The two batches of buffer prepared were bottled in 250 ml Pyrex glass bottles with greased ground stoppers according to the CRM bottling procedure (Dickson et al. 2007). The pH of the buffer was calculated according to Nemzer and Dickson (2005) and DelValls and Dickson (1998). The emf (electromotive force) measurements for the two batches of buffer were conducted along with emf measurements of a batch of HCl 0.01 M standardized according to Dickson (1987) and Dickson (1990).

Cell preparation

Six cells, each composed of a hydrogen electrode and a silver/silver chloride (Ag/AgCl) electrode, were run in parallel. Half of the cells were prepared with HCl

0.01 M, and the other half with the TRIS buffer solution. The results obtained with the two batches of buffer were compared with results from previous studies in order to check the quality of the buffer (DelValls and Dickson 1998; Nemzer and Dickson 2005).

The hydrogen electrodes used to calibrate the buffer were platinized just before use. For this purpose, two clean hydrogen electrodes are set up perpendicularly to each other in a beaker containing a platinizing solution (chloroplatinic acid hexahydrate $H_2PtCl_6.6H_2O$ in 100 ml Milli-Q water), and connected to a power source with a current of 40 mA for 10 minutes until the apparition of an evenly distributed black deposition (Figure 2.1).

Figure 2.1. Platinization of the hydrogen electrodes.

The Silver/Silver Chloride electrodes were designed and prepared according to Bates (1964). The silver oxide used for the preparation of the electrodes was dried in a vacuum oven at 100 ºC before use. The silver oxide paste was applied on the platinum helix at the end of the electrode to form a small ball. The electrodes were then heated for 15 minutes at 100 ºC, and finally heated at 495 ºC for 15 minutes. The same procedure was followed five times, until the silver ball formed at the end of the electrodes (Figure 2.2) had a smooth aspect (with no visible cracks). The electrodes were let to stand in Milli-Q water overnight and then chloridized with 1 M

HCl using a current of 10 mA for 10 minutes. The electrodes were stored in 0.01 M HCl for two days before use.

Figure 2.2. Preparation of the silver/silver chloride electrodes.

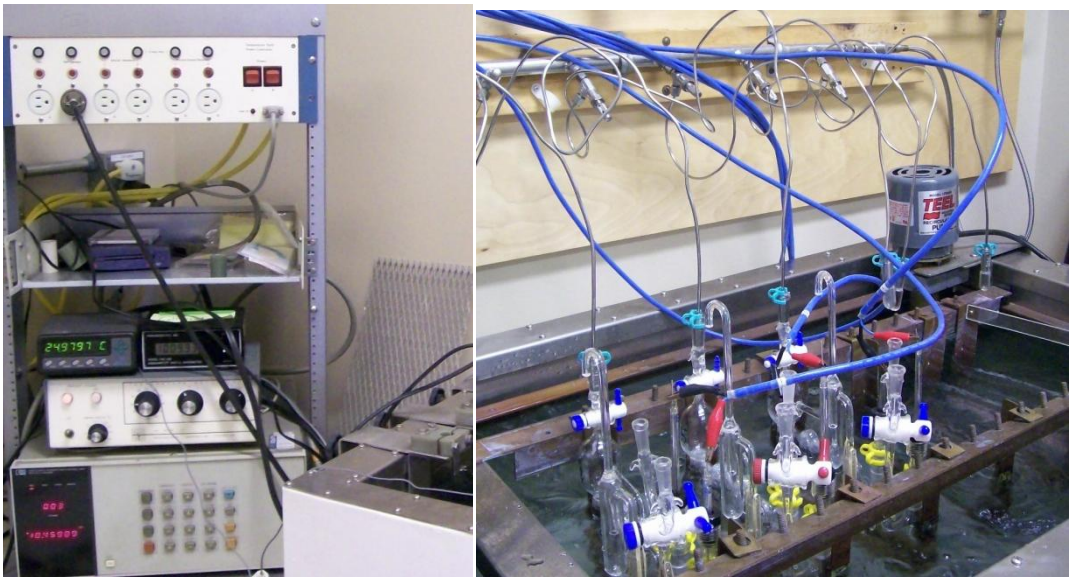

Figure 2.3. Bath instrumentation (left) composed of a voltmeter (Hewlett-Packard data acquisition system), a digital quartz barometer, and a platinum resistance thermometer; and cell bath (right).

The custom-made cells were filled with the solutions to analyze (TRIS buffer or HCl), previously degassed with H_2, and placed in the temperature controlled bath (Figure 2.3) thermostated at 25 ºC (298.15 ± 0.01 K). The voltage E (V), temperature (ºC) and pressure (hPa) were carefully monitored every 30 minutes until the voltage had stabilized within ±0.00001 V (equivalent to an error in the pH calculation of 0.0002).

Calculation

The emf readings of the cells containing the HCl and TRIS solutions were corrected for standard pressure according to Dickson (1987) (equation 2.12):

$$E(p^0) = E(\text{observed}) - \left(\frac{RT}{2F}\right) \ln\left\{\frac{f(H_2,g)}{p^0}\right\} \qquad (2.12)$$

Where p° is the standard pressure = 101.325 kPa

R is the gas constant = 8.314472 J K^{-1} mol^{-1}

T is the temperature in Kelvin = T (°C) +273.15

F is the Faraday constant = 96485.3399 C mol^{-1}

$f(H_2,g)$ is the fugacity of hydrogen gas (equation 2.13):

$$f(H_2,g) = p(\text{atm}) + 0.4\rho gh - p(H_2O) \qquad (2.13)$$

Where p(atm) is the measured barometric pressure at the time and place of the experiment

0.4 ρgh is the empirical bubbler-depth correction factor (0.196 kPa for HCl; 0.200 for TRIS)

$p(H_2O)$ is the vapor pressure of water in the solution (3.1676 kPa for HCl; 3.1050 for TRIS)

The pressure corrected voltage of the HCl cells was then standardized at the temperature of 298.15 K (equation 2.14):

$$E^0(T) = E(p^0) + \frac{2RT}{F} \ln(m_{HCl} * \gamma_{\pm}) \qquad (2.14)$$

Where m_{HCl} is the molality of hydrochloric acid in mol kg^{-1}

$\gamma_{\pm}$ is the mean activity coefficient of hydrochloric acid (0.904 at 298.15 K) (Dickson 1987)

The E° (T) standardized values obtained for the HCl cells were corrected to those of Bates and Bower (1954) according to Nemzer and Dickson (2005) and DelValls and Dickson (1998) (equation 2.15):

$$E^0(T) = E^0(T, BB) + \Delta E^0(298.15\ K) \qquad (2.15)$$

Where E°(T,BB) is the calculated smoothed value of the emf using the Bates and Bower function at the temperature of the measurement (0.22240 at 298.15 K).

The pressure corrected E(p°) of the TRIS cells were corrected to the Bates and Bower (1954) values (equation 2.16) using the correction obtained with the HCl cells in equation 2.15:

$$E(p^0, BB) = E(p^0) - \Delta E^0(298.15\ K) \qquad (2.16)$$

The pH of the buffer was calculated according to DelValls and Dickson (1998) and Nemzer and Dickson (2005) (equation 2.17):

$$pH = \frac{E(p^0,BB) - E_m^*}{\frac{RT\ln 10}{F}} + \log(m_{Cl^-}) + 0.01642 \qquad (2.17)$$

Where E_m^* is the standard potential of the ($AgCl_{(s)} + H_{2(g)} = Ag_{(s)} + HCl_{(aq)}$) reaction (Dickson 1990; Campbell et al. 1993)

R is the gas constant = 8.314472 J K^{-1} mol^{-1}

T is the temperature in Kelvin

F is the Faraday constant = 96485.3399 C mol^{-1}

m_{Cl-} (mol kg^{-1} H_2O) = $m_{NaCl} + m_{KCl} + m_{HCl} + 2m_{CaCl2} + 2m_{MgCl2}$ (obtained from the exact composition of the TRIS buffer, as shown in Table 2.1)

0.01642 is the pH conversion factor (from mol kg^{-1} H_2O to mol kg^{-1} solution; Nemzer and Dickson 2005)

Buffer certification

The corrected E (p°) values obtained with the batch of 0.01 mol kg^{-1} HCl in June 2008 (average of 0.46429 and 0.46435 V for each run of 3 cells; σ = 0.00004 and

0.00003) ranged within the values previously reported in the literature (Dickson 1987). The corrected E(p°) values obtained with the TRIS buffer cells also showed good agreement with the values of Nemzer and Dickson (2005) and DelValls and Dickson (1998); with an average value of 0.73847 and 0.73858 for each batch of buffer (σ = 0.00003 and 0.00001 respectively) compared to literature values ranging from 0.73853 to 0.73864 (DelValls and Dickson 1998) and from 0.73847 to 0.73860 (Nemzer and Dickson 2005). The certified pH values obtained for the two batches of TRIS buffers at 25 ºC were within the range reported by Nemzer and Dickson (2005):

pH = 8.0933 ± 0.0002 (1σ) for the 20 liters batch (first batch)

pH = 8.0917 ± 0.0004 (1σ) for the 5 liters batch (second batch)

2.2.3. Potentiometric system

2.2.3.1. System description

The potentiometric method is based on the measurement of the emf of a cell composed of a silver/silver chloride reference electrode and a glass pH electrode. In order to obtain high quality measurements, a reproducible liquid junction (forming the junction between the sample and the bridge solution of the reference electrode) is necessary (Culberson 1981). The system (Ruthern Instruments) used in this study (Figure 2.4) creates a free-diffusion liquid junction which has been shown to reduce liquid junction potential errors encountered with the conventional pH electrode systems (Whitfield et al. 1985; Covington and Whitfield 1988). The free-diffusion liquid junction is obtained by forming a capillary liquid junction between the reference reservoir (containing the silver/silver chloride electrode) and the pH cell containing the pH electrode and the sample. The bridge solution (2.5 M potassium chloride) introduced below the sample via a solenoid pump allows the ionic contact between the hydrogen (Russell pH Ltd SW79) and the reference electrode (Russell pH Ltd CRR/DWG1575). The instrument was powered using a 12 V power supply and operated with a LabVIEW program.

The system, when used in continuous data logging mode, provided pH and temperature readings every minute. The flow-through pH cell was composed of a Platinum Resistance Thermometer (PRT; precision better than 0.1 ºC), two glass hydrogen electrodes, and a glass capillary for the free diffusion liquid junction. A difference in the temperature measurement of 0.1 ºC is equivalent to a difference of 0.003 pH unit in the calculation of the TRIS buffer pH (equation 2.18) and consequently in the pH of the sample (equation 2.19). No calibration of the PRT was done, but the difference between the in situ temperature and the pH system temperature (PRT reading) was checked and any measurements with a difference above 0.1 °C were rejected.

Two glass pH electrodes were used in the system in order to check for any faulty electrode. The measurements were conducted at the in-situ temperature, which eliminates any further temperature correction usually necessary with temperature-controlled systems (Hunter 1998). In order to avoid errors from electrode drift, calibration using TRIS buffer was undertaken at regular intervals (every 8 to 12 hours) and the buffer was brought to a temperature close to that of the sample before each calibration (Wedborg et al. 1999). The theoretical value of the pH of the TRIS buffer (pH_B) was calculated from equation (2.18) (Dickson et al. 2007; DelValls and Dickson 1998):

$$pH_B = \frac{(11911.08 - 18.2499 \times S - 0.039336 \times S^2)}{T} - 366.27059 + 0.53993607 \times S + 0.00016329 \times S^2 + (64.52243 - 0.084041 \times S)\ln(T) - 0.11149858 \times T \qquad (2.18)$$

Where S is the salinity and T is the temperature (in K)

The pH of the sample (pH_S) was determined according to equation (2.19) (Dickson et al. 2007):

$$pH_S = pH_B + \frac{E_B - E_S}{\left(\frac{RT \ln 10}{F}\right)} \qquad (2.19)$$

Where E_B is the emf of the TRIS buffer (in mV)

E_S is the emf of the sample (in mV)

T is the temperature of the sample (in K)

F is the Faraday constant (96485.3399 C mol^{-1})

R is the gas constant (8.314472 J K^{-1} mol^{-1})

2.2.3.2. System preparation and operation

The potassium chloride solution used for the liquid junction (2.5 M KCl, Fisher Scientific analytical reagent grade) was introduced in a blood bag placed on top of the system in order to allow a gravity-fed liquid junction. The reference electrode cell was filled with the KCl solution and the solenoid valve (075P2NC12-02B, Bio-Chem Valve) controlling the liquid junction (Figure 2.4) was activated manually in order to remove any air left in the reference cell. The liquid junction was then automatically flushed every 10 minutes via the solenoid valve while the system was in operation in order to renew the liquid junction (Figure 2.4). The pH cell was wrapped in foam in order to minimize heat transfer and to reduce any drift in pH measurement due to changes in the cell temperature.

A calibration was performed before each set of measurements after selecting the appropriate buffer from the instrument program. As the TRIS buffer was used in this study, the seawater buffer was selected (as opposed to the NaCl buffer). The water flow going through the pH cell needed to be sufficiently strong to prevent bubbles forming in the pH cell which would create a drift in pH with time (between 1 and 2 l min^{-1}). A flow too slow would also increase the temperature in the cell, creating an offset in the pH measurement. The electrodes were left in the cell filled with buffer when not in use.

The data was retrieved from the pH system using the MS-DOS Interlink software (Interlink/Interserver). For this purpose a custom-made null modem adapter serial cable (7-wire) was used to connect the pH system and the computer on which the data was being transferred (client computer).

A drift observed on one of the electrode readings might indicate coating on the glass membrane of the electrodes due to algae, biological material and other particles present in the water. To prevent this fouling, the hydrogen electrodes were regularly cleaned with a non-acidic solution such as Decon 90 (10%) or Neutricon (10%) and rinsed with Milli-Q water. The electrodes were wiped dry and stored in TRIS buffer

solution. The reference silver/silver chloride (Ag/AgCl) electrode was stored in 2.5 M KCl. The pH cell and tubing were cleaned in Decon 90 (10%) or Neutricon (10%).

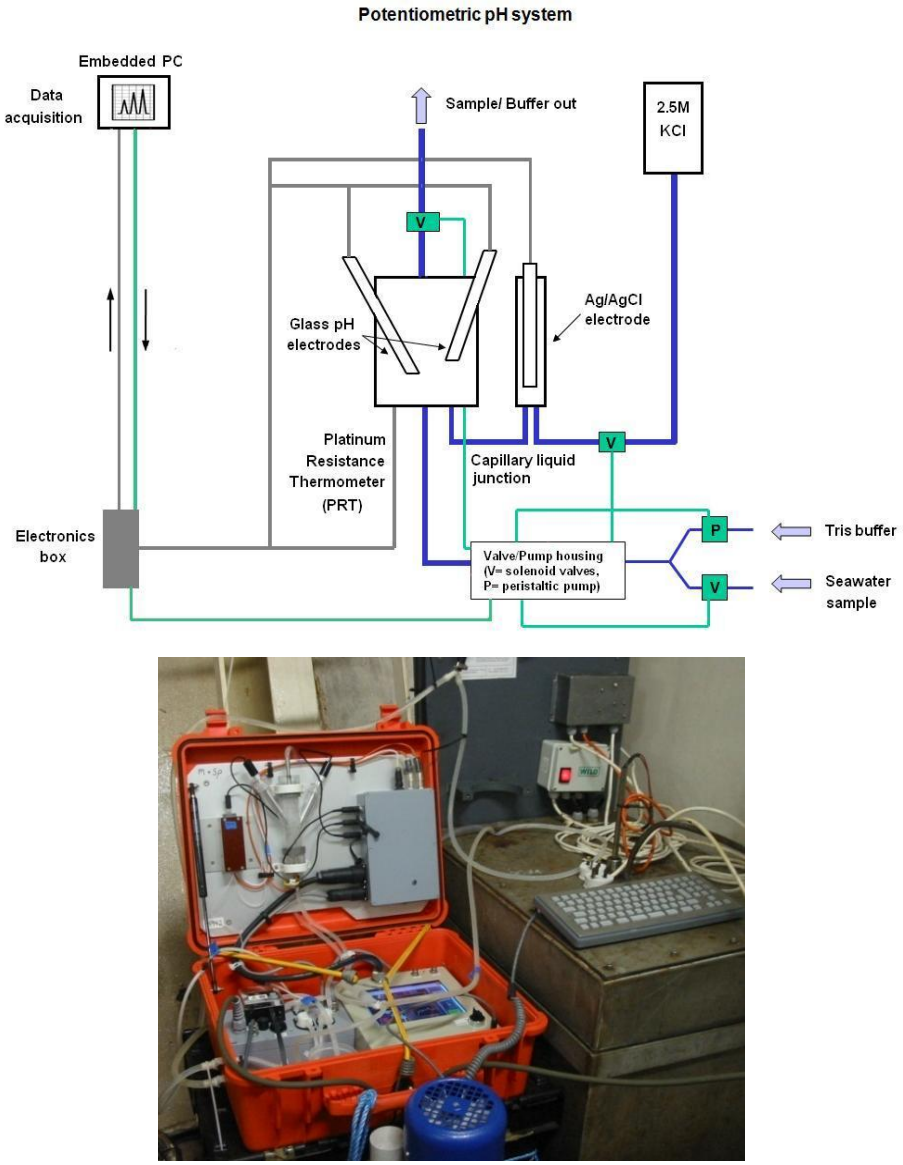

Figure 2.4. Drawing of the potentiometric pH system used in this study (top); and potentiometric pH system installed on the *MV Pride of Bilbao* (bottom). The grey lines on the drawing represent the data acquisition, the blue lines represent the solutions (seawater sample, buffer and liquid junction), and the green lines represent the valves and pump system.

2.2.3.3. Accuracy and precision

The accuracy of a pH measurement is difficult to determine and strongly depends on the accuracy of the buffer used to calibrate the system (Wedborg et al. 1999), as there

are at this time no Certified Reference Materials available for oceanic pH measurements. The two batches of buffer prepared and certified at the Scripps Institution of Oceanography were run on the potentiometric system in order to compare them with the buffer solutions prepared at NOCS. The tests were performed at room temperature and showed good agreement (0.003 ±0.003) between the certified buffers and the buffer solutions prepared at NOCS. The precision of the system as well as the drift of the instrument between calibrations were estimated to be within 0.004 (peak to peak difference) from repeated measurements on the same batch of seawater (Figure 2.5).

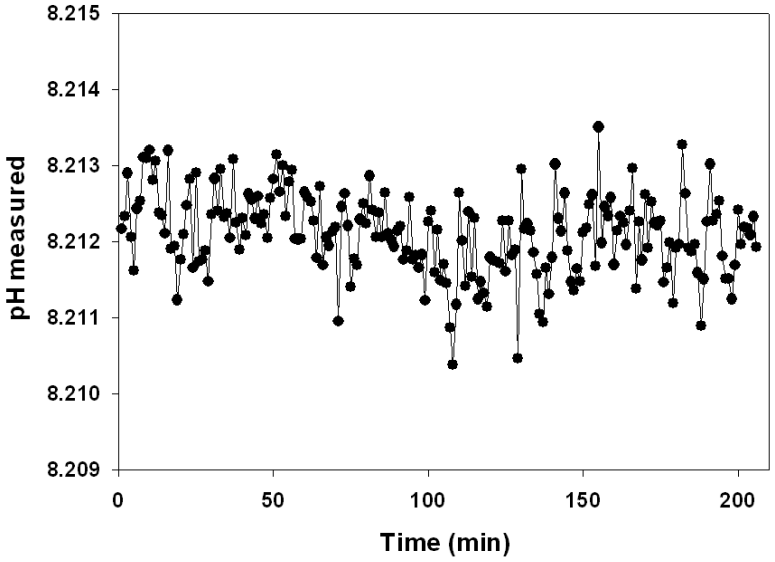

Figure 2.5. Continuous pH measurements obtained on the same batch of seawater with the potentiometric system. The measurements were conducted at sea for several hours while the ship was on station in order to estimate the drift of the instrument.

2.2.3.4. System performance

The system used in this study has been shown to produce high quality and high resolution data (Figure 2.6) following careful electrode handling and TRIS buffer preparation. The preliminary results obtained with the potentiometric pH system showed strong correlation with the pCO_2 data ($r^2 = 0.87$; n = 834) measured on the *Pride of Bilbao* (Figure 2.6; pCO_2 data courtesy of Charlene Bargeron).

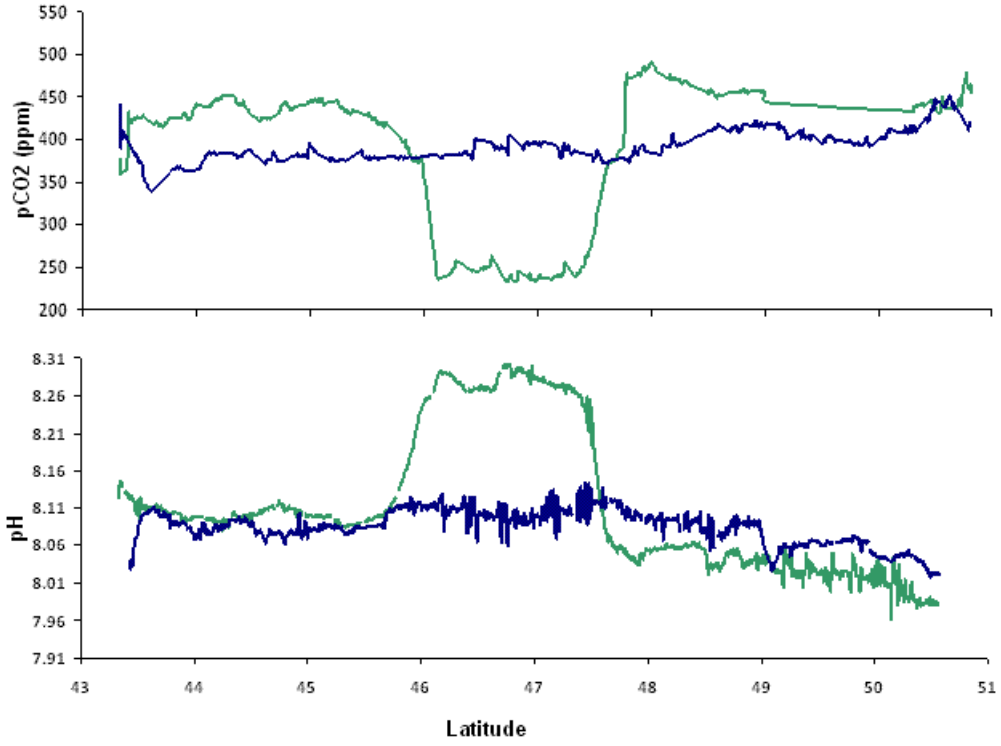

Figure 2.6. Comparison of pCO_2 (ppm; courtesy of Charlene Bargeron) and potentiometric pH data obtained on the Pride of Bilbao (April 2007) between Portsmouth and Bilbao (green) and Bilbao-Portsmouth (blue). These results were obtained during a trial crossing.

2.2.4. Spectrophotometric measurement

2.2.4.1. Overview

In order to determine the inter-annual variability of oceanic pH, spectrophotometric measurements are highly recommended. Global annual decrease in surface ocean pH has been estimated to be between -0.0017 and -0.0019 y^{-1} from the Bermuda Atlantic Time-Series and the Hawaii Ocean Time-Series, respectively (Bates 2007; Doney et al. 2009a). The required accuracy and precision for pH measurements should hence be of the same order. Spectrophotometric measurements have been shown to provide pH data with a minimum accuracy of ±0.005 and precision of ±0.001 pH unit, which fulfills the requirements for studying changes in the ocean (Clayton and Byrne 1993; Bellerby et al. 2002; Seidel et al. 2008)

Spectrophotometric measurements are based on the use of a sulfonephthalein dye indicator. These acid-base indicators exist in three chemical forms: H_2I, HI^-, and I^{2-}, each form having substantially different absorption properties. The reaction of interest in the determination of oceanic pH is the one associated with the second dissociation constant of the indicator (equation 2.20 and 2.21):

$$HI^-(aq) = H^+(aq) + I^{2-}(aq) \qquad (2.20)$$

$$K_2 = \frac{[H^+][I^{2-}]}{[HI^-]} \qquad (2.21)$$

Where K_2 is the second dissociation constant of the indicator

The choice of the dye used depends on the expected range of pH (the pK_2 of the indicator must be close to the pH of the sample). For surface water pH measurements, the indicator thymol blue has been recommended (Ohline et al. 2007; Bellerby et al. 2002; Zhang and Byrne 1996; Byrne 1987).

The absorbance of the solution containing the sample and the indicator is measured at three different wavelengths: 435, 596 and 730 nm. The two wavelengths 435 and 596 nm correspond to the maximum absorbance of the protonated (HI^-) and unprotonated (I^{2-}) form of the thymol blue indicator, respectively. The measurement at a non-absorbing wavelength (730 nm) is necessary to correct for any instrument drift or error with the cell repositioning. A flow cell with a 10 cm path length is recommended to ensure optimum results (Dickson et al. 2007). The temperature of the sample should also be accurately measured and recorded to better than 0.1 ºC (a difference in temperature of 0.1 ºC is equivalent to an error of 0.001 pH unit in the calculation using the thymol blue indicator; equation 2.22 to 2.26).

2.2.4.2. Indicator solution

The thymol blue indicator solutions were regularly prepared at NOCS for the development of the spectrophotometric system and its trial at sea. Thymol blue ($C_{27}H_{30}O_5S$) is insoluble in water, and therefore a stock solution (2 mM) was made up in 0.7 M NaCl (Seidel et al. 2008), with a few drops of alkaline solution (NaOH 1 M) in Milli-Q water. The solution was left to dissolve overnight and stored in the

dark. The pH of the thymol blue solution was adjusted to the pH of the sample (about 8.2 for surface waters measurements) with hydrochloric acid 1 M HCl (Seidel et al. 2008; Bellerby et al. 2002) on the day of analysis. The final concentration of the indicator in the sample should range between 2.10^{-6} and 2.10^{-5} M (Zhang and Byrne 1996) and should give an absorbance between 0.4 and 1.0 for each wavelength (Dickson et al. 2007).

2.2.4.3. Calculation

The pH of the sample was calculated on the total hydrogen ion scale using the following equations (2.22 to 2.26) (Dickson et al. 2007; Clayton and Byrne 1993):

$$pH = pK_2 + \log\left[\frac{(R - e_1)}{(e_2 - Re_3)}\right] \quad (2.22)$$

Where $R = A_{596}/A_{435}$

$pK_2 = -\log K_2$

e_i are the extinction coefficient ratios:

$e_1 = \varepsilon_{596}(HI^-) / \varepsilon_{435}(HI^-)$

$e_2 = \varepsilon_{596}(I^{2-}) / \varepsilon_{435}(HI^-)$

$e_3 = \varepsilon_{435}(I^{2-}) / \varepsilon_{435}(HI^-)$

With for the thymol blue indicator (Zhang and Byrne 1996):

$$pK_2 = 4.706\frac{S}{T} + 26.3300 - 7.17218\log T - 0.017316S \quad (2.23)$$

$$e_1 = -0.00132 + 1.600 \times 10^{-5}T \quad (2.24)$$

$$e_2 = 7.2326 - 0.0299717T + 4.600 \times 10^{-5}T^2 \quad (2.25)$$

$$e_3 = 0.0223 + 0.0003917T \quad (2.26)$$

The pK_2 equation (2.23) (Zhang and Byrne 1996) was determined for the salinity range 30-40 and temperature range 5-35 °C. The equations for the extinction coefficient ratios (e_i) of the thymol blue (2.24 to 2.26) used in this study were the ones reported by Zhang and Byrne (1996). It is however strongly recommended to determine them for in-situ applications (i.e. when temperature is not controlled) or for each particular spectrophotometric pH system (Seidel et al. 2008).

For an accurate calculation of the pH of the sample prior to the indicator dye addition, a correction is required for the addition of another acid-base system. For this purpose, a measurement of the solution with dye and without dye is undertaken at each wavelength (Dickson et al. 2007; Clayton and Byrne 1993). Another correction is necessary in order to remove the background absorbance and this is done by subtracting the baseline absorbance (at 730 nm) for each of the obtained peaks (Dickson et al. 2007; Mojica Prieto and Millero 2002). Finally, the absorbance ratio (R) needs to be corrected from the dilution occurring after the dye addition according to equation 2.27 (Dickson et al. 2007):

$$R_{corrected} = R - V\,(0.125 - 0.147R) \qquad (2.27)$$

Where V is the volume of indicator added to the sample (in cm^3)

2.2.4.4. Discussion

The development of a spectrophotometric pH system at NOCS would allow pH measurements in the range of precision expected to investigate annual surface ocean acidification (precision and accuracy better than ±0.002).The first prototype of the spectrophotometric system in development at NOCS was tested at sea in April 2008. Despite some promising results, mixing problems were observed, leading to large drifts in the results over a short period of time. However, due to the ongoing aspect of the spectrophotometric system in development at NOCS, no further trial was conducted for the present study.

2.3. DIC and TA measurements

2.3.1. The VINDTA 3C

The instrument used for the determination of DIC and TA is the VINDTA 3C (Versatile INstrument for the Determination of Titration Alkalinity), from Marianda (Germany), connected with a coulometer (5011, UIC). The titration and calculation are controlled by LabVIEW software. All samples are measured at 25 ºC following temperature regulation using a water-bath (F12, Julabo). Repeated measurements on the same batch of seawater ($n \geq 3$) were run every day of analysis, prior to the

samples, in order to assess the precision of the method. Certified Reference Materials (CRM) from A.G. Dickson (Scripps Institution of Oceanography) were used as standards to calibrate the system at the beginning of each day of analysis (batches 71, 75, 81, 90 and 91 were used in this study). A CRM is also run at the end of each day of analysis to check for any instrument drift. The replicate analysis on the CRMs showed good precision for both DIC and TA, with a precision within bottle of 2.2 ± 1.5 and 1.9 ± 1.5 μmol kg^{-1} (1σ) for DIC and TA, respectively; and a precision between bottles of 2.4 ± 1.7 and 2.9 ± 1.6 μmol kg^{-1} (1σ) for DIC and TA, respectively (within the same batch of CRM and within the same batch of acid). A correction factor was applied to all measured values (Millero et al. 1998b) in order to normalize the measured values (for both TA and DIC, equation 2.28):

$$\text{Corrected Value} = \text{Measured Value} \times (CRM_{cert}/CRM_{meas}) \qquad (2.28)$$

Where CRM_{cert} corresponds to the certified value of the CRM used.

2.3.2. Dissolved Inorganic Carbon

All the DIC samples were analyzed using a coulometric titration. Prior to the analysis, the sample (20 ml) was acidified with phosphoric acid (10%) which resulted in the conversion of all species of total dissolved inorganic carbon into CO_2 gas. The generated CO_2 was carried into the coulometric cell (containing ethanolamine $HOCH_2CH_2NH_2$, and a thymolphtalein indicator) using an inert gas (N_2); and the hydroxyethylcarbamic acid ($HOCH_2CH_2NHCOOH$) formed was titrated coulometrically with the hydroxide ions generated (equations 2.29 to 2.32).

$$CO_2 + HOCH_2CH_2NH_2 = HOCH_2CH_2NHCOOH \qquad (2.29)$$

$$Ag° = Ag^+ + e^- \qquad (2.30)$$

$$2H_2O + 2e^- = H_{2(gas)} + 2OH^- \qquad (2.31)$$

$$HOCH_2CH_2NHCOOH + OH^- = HOCH_2CH_2NHCOO^- + H_2O \qquad (2.32)$$

The purged CO_2 causes the indicator to fade and the percentage of transmittance (%T) of the thymolphtalein indicator to increase, automatically activating the titration current. The end of the titration is determined spectrophotometrically when

the final transmittance of the solution is kept at a constant value (29%T). In order to remove any water vapor from the carrier gas, a condenser is placed before the coulometric cell and connected to a Peltier cooler (custom-made) set to a temperature just above freezing (ideally between 1 and 2 °C). The titration can last for up to 20 min, or until 4 endpoints are found. The endpoint is defined as an increment lower than the blank determined at the beginning of each day (blank ideally comprised between 50-70 counts per min, with an upper limit set to 100 counts per min).

The VINDTA 3C system used in this study is similar to the SOMMA (Single-Operator Multi-Metabolic Analyzer) system in terms of procedure and performance. The latter is however calibrated with known volumes of pure CO_2 gas (Johnson et al. 1993), allowing for an extra calibration of the system (in addition to CRMs measurements).

2.3.3. Total Alkalinity

Total Alkalinity of the samples was determined using a closed-cell titration (Dickson et al. 2007). The sample of seawater (100 ml) was titrated with 0.1 M hydrochloric acid (HCl) prepared in 0.7 M sodium chloride (NaCl) in order to maintain the ionic strength in the titration cell close to the ionic strength of the sample. The acid was added in small increments (150 µl) until the carbonic acid equivalence point was reached (protonation of carbonate and bicarbonate ions). A glass electrode/reference electrode system monitored the titration (measurement of the electromotive force). The end-point is determined using the change in pH, measured with the emf (Nernst slope not E_0 adjusted), against the volume of acid added to the sample. The emf and the total volume of acid added allow the calculation of total alkalinity based on a non-linear curve fitting (least-squares) approach (Dickson et al. 2007).

2.4. Calculation of the carbonate system

The measurement of any two parameters of the carbonate system allows the calculation of the other ones (including the saturation state of calcite and aragonite, the carbonate and bicarbonate ion concentrations, etc…) through the use of the appropriate thermodynamic constants. Although several programs are available for

the calculation of the carbonate system parameters, only the CO_2 SYS program (Lewis and Wallace 1998) was used in this study.

As mentioned in chapter 1, the carbonate system is characterized by its complex equations and associated thermodynamic constants. Reliable equilibrium constants of carbonic acid (first and second acidity or dissociation constants, K_1^* and K_2^*; equations 2.33 and 2.34) are needed to determine accurately the carbonate system and these dissociation constants are highly dependent on temperature, salinity and pressure (Zeebe and Wolf-Gladrow, 2001; Lee et al. 2000). The dissociation constants K_1^* and K_2^* are associated with equations 1.6 and 1.5, respectively (chapter 1).

$$K_1^* = \frac{[H^+][HCO_3^-]}{[CO_2]} \qquad (2.33)$$

$$K_2^* = \frac{[H^+][CO_3^{2-}]}{[HCO_3^-]} \qquad (2.34)$$

Several sets of constants are available in the literature (Hansson 1973; Mehrbach et al. 1973; Goyet and Poisson 1989; and Roy et al. 1993), and the calculation of the carbonate system parameters associated with the different sets of constants can lead to large differences (Table 2.2). However, only the Mehrbach et al. (1973) constants have been determined in sea water, whereas the other ones have been determined in artificial sea water (Mojica Prieto and Millero 2002; Lee et al. 2000).

The constants of Mehrbach et al. (1973), refitted by Dickson and Millero (1987) are therefore recognized as the most reliable for studies in sea water (Mojica Prieto and Millero 2002; Lee et al. 2000; Lueker et al. 2000; Lamb et al. 2002; McElligott et al. 1998; Ohline et al. 2007), while the other sets of constants have been shown to be suitable for artificial sea water (Mojica Prieto and Millero 2002).

The CO_2SYS.EXE program was used to calculate the carbonate system parameters from any two variables measured (Lewis and Wallace 1998; Pierrot et al. 2006), along with the equilibrium constants of CO_2 (K_1 and K_2) of Mehrbach et al. (1973), refitted by Dickson and Millero (1987). The salinity, temperature and nutrients data

of the sample at the time of collection are required in order to recalculate the CO_2 system parameters.

Constants	pH_{SWS}	pCO_2 (μatm)	$CO_2(aq)$ ($\mu mol\ kg^{-1}$)	HCO_3^- ($\mu mol\ kg^{-1}$)	CO_3^{2-} ($\mu mol\ kg^{-1}$)
Roy et al. 1993	8.08	353	10.0	1735	255
Hansson 1973	8.10	343	9.7	1739	251
Mehrbach et al. 1973	8.11	327	9.3	1742	249

Table 2.2. Calculated carbonate parameters using the different sets of constants (DIC = 2000 µmol kg^{-1}, TA = 2350 µmol kg^{-1}, S = 35, T = 25 °C) (Zeebe and Wolf-Gladrow 2001).

Amongst the different pairs used for the calculation, however, some pairs have been shown to be more reliable than others (Table 2.3) and to lead to better precision. The results of the recalculation will hence depend on the precision and accuracy of the two parameters measured or used for the calculation.

Reference	*Pair used*	*Error observed*
McElligott et al. (1998)	pH-DIC	ΔfCO_2 = ±1%
	pH-TA	ΔfCO_2 = ±1%
	DIC-TA	ΔfCO_2 = -2% to +10%
Lee et al. (2000)	pH-DIC	ΔTA = ±3 µmol kg^{-1}
	TA-DIC	ΔfCO_2 = ±1%
Lueker et al. (2000)	TA-DIC	ΔfCO_2 = 0-3% below 500 µatm
Lamb et al. (2002)	fCO_2-DIC	ΔTA = 6 µmol kg^{-1}
	pH-DIC	ΔTA = 4-5 µmol kg^{-1}
Ohline et al. (2007)	pH-TA	ΔpCO_2 = ±1.15%

Table 2.3. Errors found in the literature from recalculation using the Mehrbach et al. (1973) constants and different pairs of the carbonate system parameters.

2.5. Conclusion

In order to understand and quantify the impact of ocean acidification on marine organisms and biogeochemical cycles, the requirement to obtain high frequency and quality oceanic pH measurements is getting more and more important. While spectrophotometric pH measurements are recommended to investigate the inter-

annual variability in oceanic pH, the potentiometric pH method was shown to be highly efficient for observations of seasonal changes in pH (during periods of high biological activity) and mesoscale activity. Despite a precision and accuracy inferior to what is reported for spectrophotometric measurements, both spatial and temporal high resolution data can be achieved using the potentiometric method which will help provide a better understanding of the natural processes driving changes in pH. In addition to high precision pH measurements, the determination of DIC and TA in sea water will allow the calculation of the other parameters of the carbonate system through the use of the appropriate thermodynamic constants. This combined effort is necessary in order to determine the contribution of physical and biological processes to the variability of the carbonate system.

Chapter 3

Contrasting effects of temperature and winter mixing on the seasonal and interannual variability of the carbonate system in the Northeast Atlantic Ocean

This chapter is a reproduction of the article published in *Biogeosciences* as:

Dumousseaud, C., Achterberg, E.P., Tyrrell, T., Charalampopoulou, A., Schuster, U., Hartman, M., Hydes, D.J, 2010. Contrasting effects of temperature and winter mixing on the seasonal and inter-annual variability of the carbonate system in the Northeast Atlantic Ocean. *Biogeosciences* **7,** 1481-1492 (doi:10.5194/bg-7-1481-2010).

This article was written up by Cynthia Dumousseaud, with significant intellectual input and comments from Eric Achterberg, Toby Tyrrell, Ute Schuster (UEA) and David Hydes. The coccolithophore data was provided by Anastasia Charalampopoulou as well as some of the DIC and TA data for 2005/2006, and the *Santa Maria f*CO_2 data was provided by Ute Schuster.

Abstract

Future climate change as a result of increasing atmospheric CO_2 concentrations is expected to strongly affect the oceans, with shallower winter mixing and consequent reduction in primary production and oceanic carbon drawdown in low and mid-latitudinal oceanic regions. Here we test this hypothesis by examining the effects of cold and warm winters on the carbonate system in the surface waters of the Northeast Atlantic Ocean for the period between 2005 and 2007. Monthly observations were made between the English Channel and the Bay of Biscay using a ship of opportunity program. During the colder winter of 2005/2006, the maximum depth of the mixed layer reached up to 650 meters in the Bay of Biscay, whilst during the warmer (by 2.6 ±0.5 °C) winter of 2006/2007 the mixed layer depth reached only 300 meters. The inter-annual differences in late winter concentrations of nitrate (2.8 ±1.1 µmol l^{-1}) and dissolved inorganic carbon (22 ±6 µmol kg^{-1}), with higher concentrations at the end of the colder winter (2005/2006), led to differences in the dissolved oxygen anomaly and the chlorophyll *a*-fluorescence data for the subsequent growing season. In contrast to model predictions, the calculated air-sea CO_2 fluxes (ranging from +3.7 to -4.8 mmol m^{-2} d^{-1}) showed an increased oceanic CO_2 uptake in the Bay of Biscay following the warmer winter of 2006/2007 associated with wind speed and sea surface temperature differences.

3.1. Introduction

Since the late 1700s, the atmospheric concentration of CO_2 has increased from 280 to 380 ppm and the oceans have absorbed about half of the anthropogenic CO_2 emitted to the atmosphere (Sabine et al. 2004). While some oceanic regions act as a source of CO_2 to the atmosphere, the North Atlantic Ocean is reported as one of the strongest sinks in the world (Takahashi et al. 2009; Takahashi et al. 2002; Gruber et al. 2002). The uptake of atmospheric CO_2 by the oceans is however lowering oceanic pH and the saturation state of calcium carbonate (Orr et al. 2005; Feely et al. 2004; Caldeira and Wickett 2003). Coccolithophores, coral reefs and other major calcifiers are expected to be affected by future changes in the oceanic carbonate chemistry and pH (Fabry 2008).

Climate change is predicted to reduce the capacity of the oceans to absorb CO_2 through a decrease in winter mixing and a consequent reduced nutrient supply to surface layers and lower primary productivity during the following spring bloom (Sarmiento et al. 1998; Bopp et al. 2001; Doney et al. 2009b). The North Atlantic sink of CO_2 has been in decline during the last few decades, related to changes in the North Atlantic Oscillation (NAO), surface circulation, vertical winter mixing, inorganic carbon chemistry, and/or sea surface warming (Schuster et al. 2009; Doney et al. 2009b; Schuster and Watson 2007; Corbière et al. 2007; Thomas et al. 2008).

However, the natural small-scale variability of the carbonate system observed in the oceans on a seasonal and inter-annual basis often makes the prediction of long-term impacts more difficult (Bates et al. 1996a), and highlights the importance of understanding the variability of the carbonate system on a regional and global scale. Time-series programs such as the Bermuda Atlantic Time-Series (BATS), the European Station for Time-series in the Ocean, Canary Islands (ESTOC), and the Hawaii Ocean Time-Series (HOTS) have improved our understanding of the processes affecting the carbonate system (e.g. Bates 2007; González-Dávila et al. 2003a; Dore et al. 2009). A significant number of other high-resolution observational programs are now operational (Doney et al. 2009b), including observations from

ships of opportunity as part of the FerryBox program (Hydes et al. 2003) and the CarboOcean project.

The FerryBox route presented in this study covers about 1000 km from the highly productive and well-mixed waters of the English Channel, to the deep oligotrophic and seasonally stratified waters of the Bay of Biscay (Borges et al. 2006). Due to a complex physical context, the carbonate system and primary production in the English Channel and adjacent areas are subject to large seasonal and spatial variability (Frankignoulle et al. 1996a and b; Wollast and Chou 2001; Bargeron et al. 2006).

The observations made on a ship of opportunity, the MV *Pride of Bilbao*, constitute a unique dataset of carbonate chemistry measurements in the Northeast Atlantic Ocean surface waters, for two consecutive years. The aim of this work was to observe the natural processes affecting the seasonal and inter-annual variability of the carbonate system and the air-sea CO_2 flux in the English Channel and the Bay of Biscay. These observations, linked with the changes in winter mixing observed within the two years of our study, will provide a better understanding on how this ocean region may be affected by future climate change.

3.2. Methods

3.2.1. Area of study

The sample collection was undertaken on the ship of opportunity MV *Pride of Bilbao*, a passenger ferry undertaking weekly crossings between Portsmouth (UK) and Bilbao (Spain). The route covers the area between the Portsmouth harbour and the Iberian shelf (Figure 3.1), crossing eight regions of different oceanographic characteristics (Bargeron et al. 2006). However, only the section between the Central English Channel and the Southern Bay of Biscay will be taken into account in this study (zones 2 to 7 in Figure 3.1), as no samples were collected in the harbour regions. Thirteen crossings were occupied by researchers between September 2005 and July 2007 (Table 3.1).

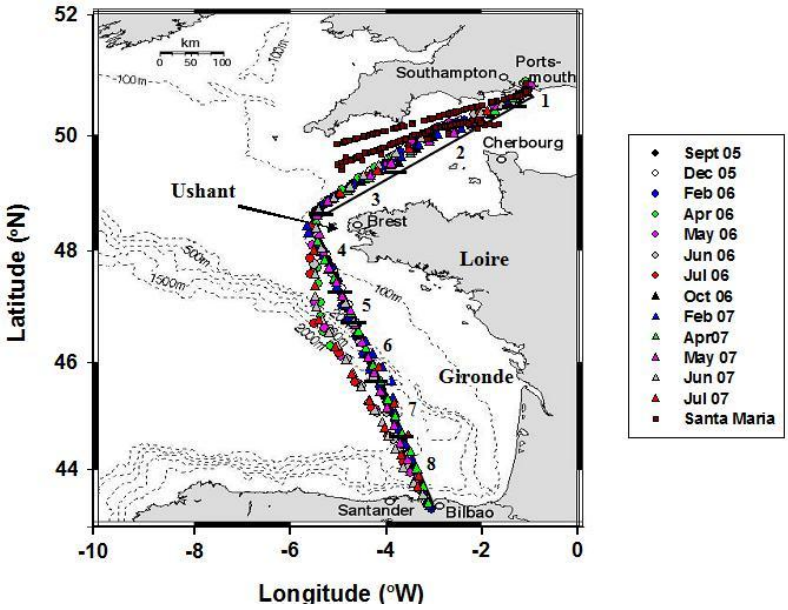

Figure 3.1. Location of the FerryBox route and sub-regions associated: (1) Portsmouth Harbour; (2) Central English Channel; (3) Western English Channel; (4) Ushant region; (5) Shelf break; (6) Northern Bay of Biscay; (7) Southern Bay of Biscay; (8) Iberian Shelf. The sampling positions for each crossing are shown as well as the MV *Santa Maria* track (Figure adapted from Kelly-Gerreyn et al. 2006).

3.2.2. Sampling

All samples were collected from the ship's underway supply (intake at about 5 m depth). Samples for Dissolved Inorganic Carbon (DIC) and Total Alkalinity (TA) were drawn, unfiltered, in 250 ml borosilicate glass bottles (Schott Duran), with a head space of 1% (2.5 ml) allowed for water expansion, and immediately poisoned with 50 µl saturated solution of mercuric chloride to prevent further biological activity (Dickson et al. 2007). Samples were collected every four hours and stored for later analysis in the laboratory.

Date	*DIC and TA samples*	*Date*	*DIC and TA samples*
26 Sep – 29 Sep 05	34 (DIC only)	18 Oct – 19 Oct 06	39
14 Dec – 15 Dec 05	33	10 Feb – 11 Feb 07	34
28 Feb – 02 Mar 06	40	04 Apr – 05 Apr 07	33
10 Apr – 11 Apr 06	21	10 May – 11 May 07	28
10 May – 12 May 06	15	04 Jun – 06 Jun 07	32
12 Jun – 15 Jun 06	27	10 Jul – 12 Jul 07	19
09 Jul – 11 Jul 06	16		

Table 3.1. Crossing dates (Portsmouth to Bilbao) between 2005 and 2007.

Continuous temperature, conductivity and chlorophyll *a*-fluorescence measurements were obtained from a MINIpack system (Chelsea Technologies Group, UK) installed on the ship (Hydes et al. 2003). The salinity data was calibrated using samples taken every two hours on each researcher-occupied crossing, and analysed at the NOCS calibration laboratory using a salinometer (8400 B Autosal, Guildline, Canada). The precision and accuracy of the salinity measurements were ±0.1.

Nutrient samples were collected every half hour during the occupied crossings and analysed at NOCS using standard methods on an auto-analyser for silicate, total nitrate (nitrate plus nitrite) and phosphate (Grasshoff 1983). The precision and accuracy of the nutrient concentrations were ±0.1 µmol l^{-1} for nitrate and silicate, and ±0.02 µmol l^{-1} for phosphate. Dissolved oxygen concentrations were obtained using an optode (3930, Aanderaa, Norway) installed on the ship, and calibrated with discrete samples collected every hour and analysed on board by Winkler titration (Hydes et al. 2009). The precision and accuracy of the oxygen measurements were ±1 mmol m^{-3} (Hydes et al. 2009).

3.2.3. DIC and TA measurements

The analysis of DIC and TA was undertaken using the VINDTA 3C (Marianda, Germany). The DIC samples were analysed using a coulometric titration (coulometer 5011, UIC, USA) and TA was determined using a closed-cell titration according to Dickson et al. (2007). The cell (100 ml) for the TA determination was equipped with a pH half cell electrode (glass bodied Orion 8101SC, Ross, USA) and an Ag/AgCl reference electrode (model 6.0729.100, Metrohm, Switzerland). The calculation of TA was based on a non-linear curve fitting (least-squares) approach (Dickson et al. 2007). All samples were analyzed at 25 ºC (±0.1 ºC) with temperature regulation using a water-bath (Julabo F12, Germany).

Repeated measurements on the same batch of seawater ($n \geq 3$) were undertaken every day prior to sample analysis, in order to assess the precision of the method which was estimated for the whole dataset to be 1.1 ± 0.5 µmol kg^{-1} for DIC and 1.1 ± 0.6 µmol kg^{-1} for TA. The analytical precision hence was within the previously reported precision range for TA and DIC measurements (Bates et al. 1996a and b; Millero et

al. 1998a). Certified Reference Materials (from A.G. Dickson, Scripps Institution of Oceanography) were analysed as standards to calibrate the instrument at the beginning and end of each day of analysis. A daily correction factor was applied to all measured values according to Millero et al. (1998b), in order to standardize the results. To remove the influence of salinity on the distribution of DIC and TA, the data was normalized (nDIC and nTA) to a salinity of 35 (Millero et al. 1998a):

$$nDIC = DIC*(35/S) \quad (3.1)$$

$$nTA = TA*(35/S) \quad (3.2)$$

Where S is the salinity observed.

The fugacity of CO_2 (fCO_2) measurements available for the English Channel for the period 2006 and 2007 from the ship of opportunity MV *Santa Maria* (Schuster et al. 2009; Figure 3.1) were used along with our TA, temperature, salinity and nutrient data to corroborate values of DIC. The in situ fCO_2 measured was corrected for the difference between in situ and equilibrator temperature (Schuster et al. 2007). The time and position of measurements in the English Channel by the MV *Santa Maria* and *Pride of Bilbao* matched well (Figure 3.1). The calculation was done using the CO_2SYS program (Pierrot et al. 2006), and the equilibrium constants of CO_2 from Mehrbach et al. (1973), refitted by Dickson and Millero (1987), were used for the calculation (Wanninkhof et al. 1999). The uncertainty in the calculation of DIC from TA and fCO_2 measurements was estimated to ± 3.4 µmol kg^{-1} (Zeebe and Wolf-Gladrow 2001).

The DIC values calculated using the MV *Santa Maria* fCO_2 data and our TA measurements showed good agreement with our DIC measurements (*Pride of Bilbao*) for the months of December 2005, February 2006, April 2006, October 2006, and July 2007 (11 ±8 µmol kg^{-1}; Appendix 1). The data for February, April, May and June 2007 showed however large differences between the calculated and the measured DIC values (42 ±5 µmol kg^{-1}; Appendix 1). From these comparisons it became apparent that some of the 2007 DIC data from the *Pride of Bilbao* required correction. The calculated DIC concentrations for the English Channel were used where direct comparison with the MV *Santa Maria* data was possible, and a monthly

correction factor (calculated from the ratio between the measured and the calculated DIC concentrations) was applied to the February (2.3%), April (2.1%), May (2.1%) and June (1.7%) 2007 DIC data from the *Pride of Bilbao*.

3.2.4. Coccolithophore abundance

Up to 2 l of seawater were pre-filtered through a 200 µm mesh to prevent zooplankton grazing during the filtration. The samples (collected at the same time as the DIC and TA samples) were filtered onto 0.4 µm membrane filters of 47 mm diameter (Isopore, Millipore, USA) using a vacuum of 400-500 mm Hg (reduced to 100 mm Hg towards the end of the filtration). A glass fibre filter (GF/F, Whatman, UK) was placed underneath the filters to ensure an even distribution of the material on the filter. Filters were rinsed with an ammonium hydroxide solution (approximate pH 9 to 10) to remove seawater salts, left to air-dry and stored in dark and dry conditions. Before analysis, a small piece of each filter was cut radially, placed on a stub and gold-coated. A Scanning Electron Microscope (Leo 1450VP, Carl Zeiss, Germany) and automated software (SmartSEM, V05.01, Carl Zeiss, Germany) were used to capture and store all images (Tyrrell et al. 2008). The number of coccospheres in each sample was counted on each scanning electron micrograph (SEM) taken (225 per filter, equivalent to an area of 1 mm^2) at 5000x magnification.

3.2.5. Air-Sea CO_2 flux calculation

The air-sea CO_2 fluxes (F, in mmol m^{-2} d^{-1}) were calculated as follows (Wanninkhof 1992) for the three day period of each crossing:

$$F = k\alpha\Delta pCO_2 \qquad (3.3)$$

Where ΔpCO_2 (µatm) is the difference between oceanic partial pressure of CO_2 (pCO_2) and atmospheric pCO_2 (a negative flux would hence correspond to a net transfer of CO_2 from the atmosphere to the ocean), k is the gas transfer velocity (m s^{-1}), and α is the solubility coefficient of CO_2 (mol atm^{-1} m^{-3}). The atmospheric pCO_2 data was obtained from the Mace Head (53.33 ºN; RAMCES/LSCE monitoring network) and the Azores meteorological stations (38.77 ºN; NOAA/ESRL Global

monitoring division) and averaged for each crossing. The average difference in atmospheric pCO_2 observed between the two stations was 1.1 ±0.5 µatm (r = 0.988; n= 92). The oceanic pCO_2 data were calculated from the DIC and TA data obtained in this study and averaged for each crossing and each region. The solubility coefficient of CO_2 (α) was calculated according to Weiss (1974). The equation of Nightingale et al. (2000), based on an extensive data set of tracer release experiments over a wide range of wind speed measurements (Schuster et al. 2009), was used for the calculation of the gas transfer velocity (k). The equation from Sweeney et al. (2007) was used for comparison and the fluxes calculated following these two equations agreed within 0.05 ±0.04 mmol m^{-2} d^{-1}. The wind speed data used for the calculation of the gas transfer velocity were obtained from the daily QuikSCAT satellite data (Physical Oceanography DAAC Ocean ESIP Tool (POET) http://poet.jpl.nasa.gov/), monthly averaged for each of the six regions studied. The wind speed data were obtained for 10 m height on a 0.25° spatial resolution.

3.2.6. External sources of data

In addition to the chlorophyll *a*-fluorescence data obtained from the MINIpack, the 8-days averaged SeaWIFS chlorophyll-*a* data (OBPG SeaWIFS 8-day 9-km products http://reason.gsfc.nasa.gov/OPS/Giovanni/ocean.swf8D.shtml; NASA Ocean Color Time-Series) from the Bay of Biscay and the English Channel for the period between 2005 and 2007 were used to investigate the inter-annual variability.

In order to determine the mixed layer depth (MLD) we used data from four Argo floats located in the Bay of Biscay for the period of our study (4900557, 6900359, 6900360, and 6900362; http://www.coriolis.eu.org/cdc/argo.htm). The MLD was estimated according to the temperature and density criteria which defines the MLD as the shallowest depth corresponding to a temperature or density difference with the surface waters of more than $\Delta T = 0.5$ °C and $\Delta\sigma_t = 0.125$, respectively (Monterey and Levitus 1997).

3.3. Results and discussion

3.3.1. Salinity, temperature and nitrate

A decrease in salinity and temperature with increasing latitude was observed for each crossing (Figure 3.2a and 3.2b). The salinity distribution did not show a strong variation throughout the year and ranged for the whole study between 35.2 in the Central English Channel and 35.8 in the Southern Bay of Biscay. Lower salinities of approximately 34.8 were observed in the Ushant region in April 2006 due to freshwater inputs from the French rivers Loire and Gironde (Kelly-Gerreyn et al. 2006). Surface waters in February 2007 were warmer than in February 2006 by 2.6 ±0.5 °C for all regions; whereas July 2007 surface water temperatures were lower than July 2006 by 2.0 ±0.7 °C.

Enhanced nitrate concentrations were observed during the winter months, with depleted levels in summer (Figure 3.2c). Surface nitrate concentrations were higher during the 2005/2006 winter than during the 2006/2007 winter, whilst summer nitrate concentrations were below 0.05 µmol l^{-1} for both years and all regions. In the Bay of Biscay, surface nitrate concentrations were higher (up to 8.0 µmol l^{-1}) during the winter 2005/2006 than the values reported for the 2003/2004 winter (up to 4.5 µmol l^{-1} in February 2004) by Bargeron et al. (2006), whilst in winter 2006/2007 they were comparable (up to 4.1 µmol l^{-1}) to those of the 2003/2004 winter (Bargeron et al. 2006). From the English Channel to the Shelf Break, nitrate concentrations in the 2005/2006 winter were similar to the 2003/2004 winter (Bargeron et al. 2006) with an average winter concentration of 7.3 µmol l^{-1}, whilst during the 2006/2007 winter they were lower than during the winter 2003/2004 (Bargeron et al. 2006) with an average concentration of 5.4 µmol l^{-1}.

3.3.2. Dissolved oxygen anomaly and chlorophyll *a*-fluorescence

The dissolved oxygen anomaly at standard pressure ($\Delta[O_2]^o$) was calculated from the measured dissolved oxygen concentration ($[O_2]_{obs}$) and the saturation oxygen concentration ($[O_2]^o_{sat}$) according to Bargeron et al. (2006); a positive value indicating supersaturation:

$$\Delta[O_2]^o = [O_2]_{obs} - [O_2]^o_{sat} \qquad (3.4)$$

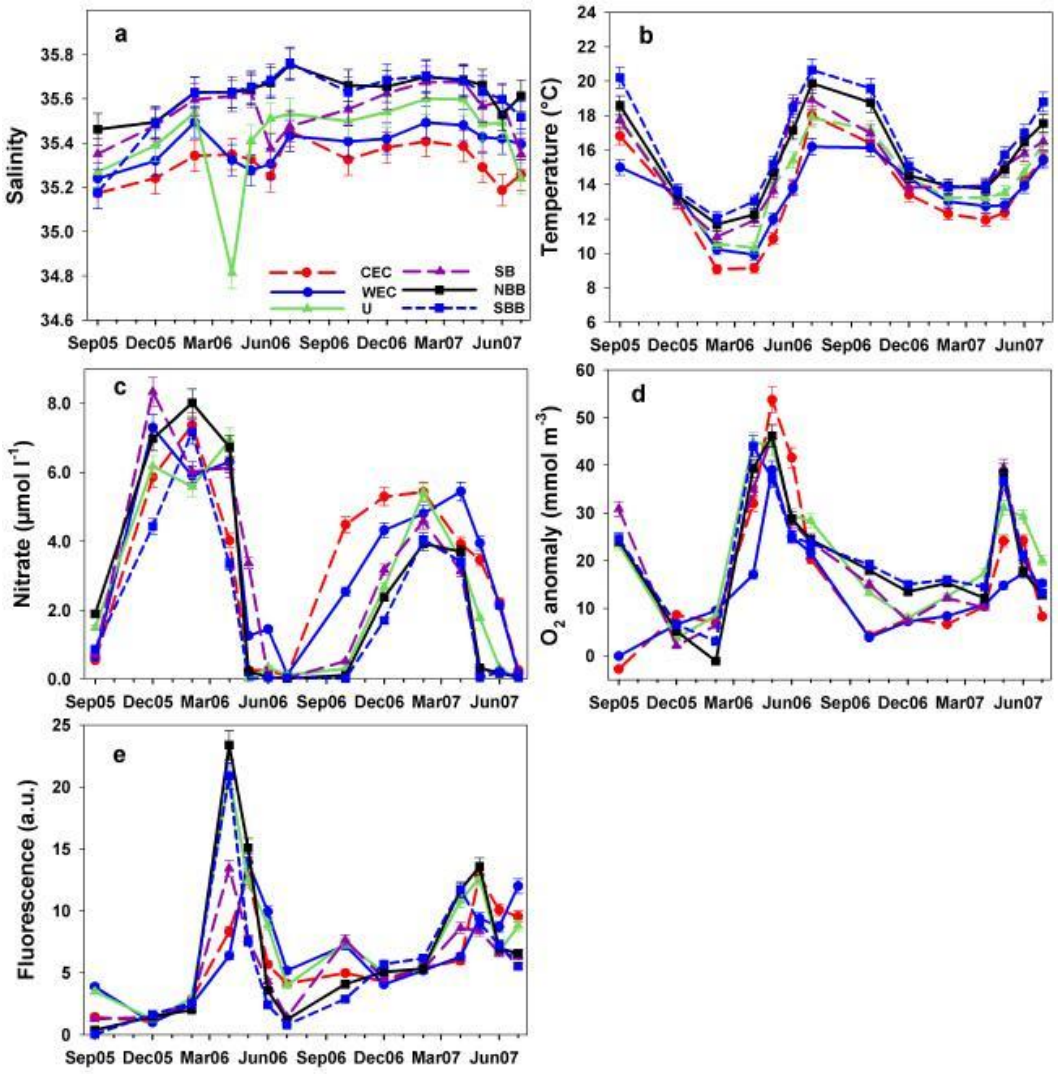

Figure 3.2. Monthly mean of (a) sea surface salinity, (b) sea surface temperature (°C), (c) surface nitrate concentration (µmol l^{-1}), (d) dissolved oxygen anomaly (mmol m^{-3}) and (e) chlorophyll *a*-fluorescence (arbitrary units) distribution averaged for each region: Central English Channel (dashed red line; circles); Western English Channel (blue line; circles); Ushant (green line; triangles); Shelf Break (dashed purple line; triangles); Northern Bay of Biscay (black line; squares); Southern Bay of Biscay (short dashed blue line; squares). The error bars represent the standard deviation for each mean. Data points are linearly interpolated between sampling points to allow a clear distinction of observations between regions. It should not be assumed that the interpolation provides an accurate estimate of the missing data.

The oxygen anomaly distribution (Figure 3.2d) showed maxima during periods of high primary production in spring times, and minima during the winter months when oxygen-depleted waters were brought to the surface due to winter mixing (Hydes et al. 2008), resulting in oxygen supersaturated surface waters in spring and undersaturated waters in winter. During spring 2006, dissolved oxygen anomalies were higher than in spring 2007 (up to 53.7 and 39.3 mmol m^{-3}, respectively), whilst during the 2005/2006 winter, they were lower than during the 2006/2007 winter (-2.8 and 3.9 mmol m^{-3}, respectively). This suggested a shallow winter mixing in 2006/2007, supported by the lower nitrate concentrations (Figure 3.2c) observed in the winter of 2006/2007 compared to 2005/2006.

The chlorophyll *a*-fluorescence data (Figure 3.2e) provide an indication of the timing of peaks in primary production and of phytoplankton biomass present in the water. The data showed a similar temporal distribution to the oxygen anomaly, with maximum values during spring (23.4 and 13.6 arbitrary units for spring 2006 and 2007, respectively) and minimum values during winter. The spring chlorophyll *a*-fluorescence maximum in the Northern and Southern Bay of Biscay was almost twice as high (1.7 and 1.8 times higher, respectively) in 2006 compared to 2007 (23.4 and 20.9 arbitrary units in 2006 as opposed to 13.6 and 11.7 in 2007 for the two regions), in agreement with the SeaWIFS time-series chlorophyll-*a* distributions (Figure 3.3).

The chlorophyll *a*-fluorescence data for the Shelf Break and Ushant regions also indicated enhanced biomass (1.6 times higher) in 2006 compared to 2007 (20.9 and 13.4 arbitrary units in 2006 as opposed to 12.7 and 8.6 in 2007 for the two regions). The English Channel waters have been described as optically-complex case 2 waters (Vantrepotte et al. 2007; Morel and Prieur 1977) and the interpretation of the optical signal can therefore be difficult and subject to errors. However, the SeaWIFS time-series chlorophyll-*a* distributions (Figure 3.3) appeared to agree well with the temporal trend of the chlorophyll *a*-fluorescence data (Figure 3.2e), with little or no inter-annual variability observed in the Central and Western English Channel regions between the two years of our study (12.8 and 13.9 arbitrary units in 2006 and 12.8 and 12.0 in 2007 for the two regions).

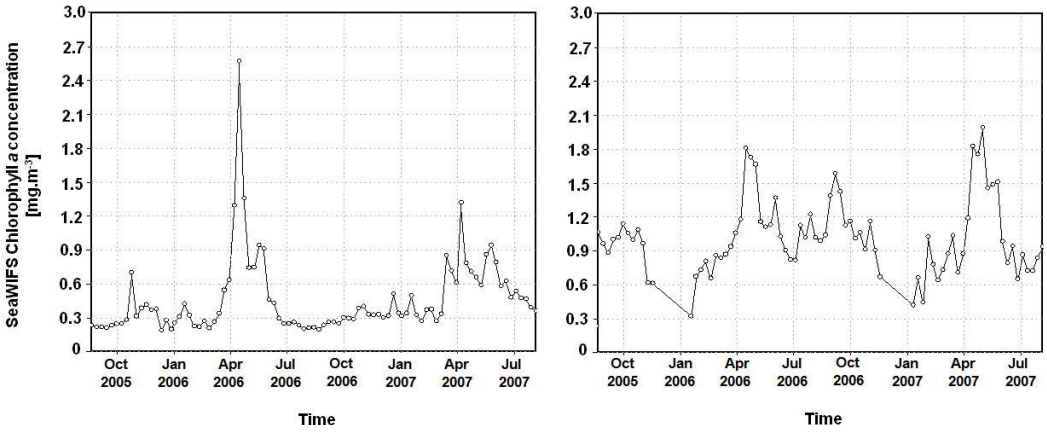

Figure 3.3. SeaWIFS chlorophyll-*a* distribution (8-days average) for the Bay of Biscay area (left) and the English Channel area (right) between September 2005 and July 2007. Graphs generated by NASA's Giovanni (giovanni.gsfc.nasa.gov).

3.3.3. Total Alkalinity

The TA concentrations ranged between 2319 µmol kg^{-1} and 2363 µmol kg^{-1} (Figure 3.4a). The normalized TA ranged from 2286 µmol kg^{-1} to 2329 µmol kg^{-1} (Figure 3.4b), with the exception of the Ushant anomaly in April 2006 (nTA = 2354 µmol kg^{-1}) where a salinity anomaly was observed due to the influence of riverine inputs (Figure 3.2a). Corbière et al. (2007) reported similar values of nTA ranging between 2327 µmol kg^{-1} (winter 2002) and 2289 µmol kg^{-1} (summer 2003) for the Northwest Atlantic subpolar gyre. A drawdown in nTA was observed in most of the regions during the crossings of May and July 2006 and corresponded with the highest cell abundances (up to $0.9x10^6$ cells l^{-1} and $0.4x10^6$ cells l^{-1}, respectively) of *Emiliana huxleyi*, which was the dominant coccolithophore species observed on each crossing. All other crossings showed *E. huxleyi* abundances of less than $0.1x10^6$ cells l^{-1}, which was about an order of magnitude lower than values reported during intense coccolithophore blooms in the North Atlantic (Holligan et al. 1993; Robertson et al. 1994).

The seasonal distribution of TA is controlled by production and dissolution of calcium carbonate, uptake and supply of nitrate (Brewer and Goldman 1976; Wolf-Gladrow et al. 2007), and freshwater inputs or removal such as mixing, precipitation,

evaporation or river inputs (Tseng et al. 2007; Bates et al. 1996b). However, due to the low coccolithophore abundances observed in this study, it is expected that the production and dissolution of calcium carbonate was not the principal factor controlling the seasonal distribution of TA.

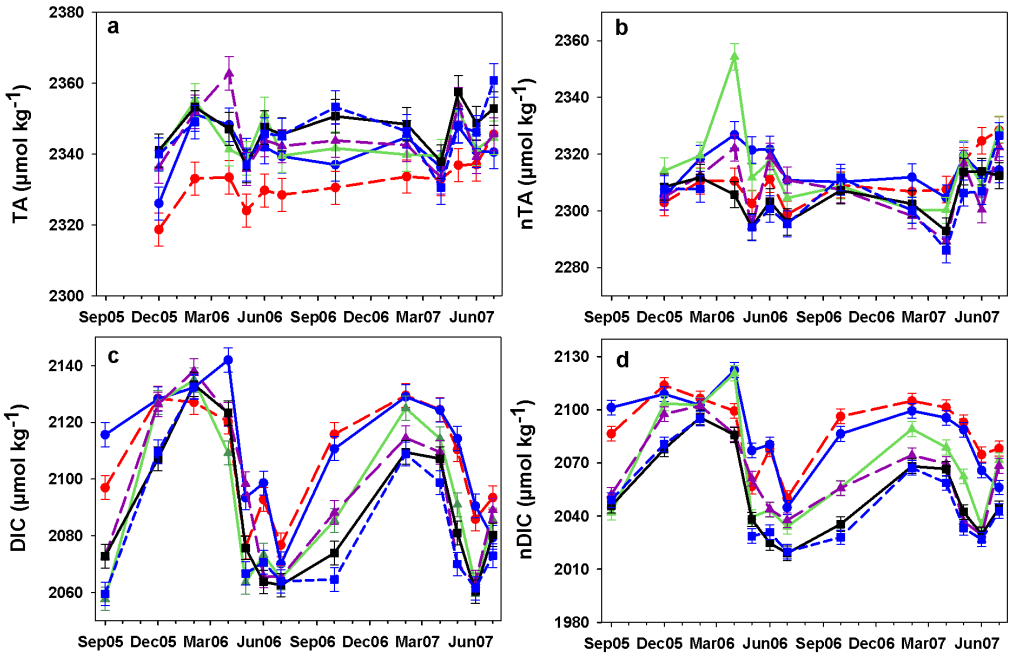

Figure 3.4. Monthly mean concentrations (µmol kg^{-1}) of (a) TA, (b) nTA, (c) DIC and (d) nDIC: Central English Channel (dashed red line; circles); Western English Channel (blue line; circles); Ushant (green line; triangles); Shelf Break (dashed purple line; triangles); Northern Bay of Biscay (black line; squares); Southern Bay of Biscay (short dashed blue line; squares). Each data point represents the average of several measurements made within one part of the transect (Figure 3.1). The error bars represent the standard deviation of each mean. Data points are linearly interpolated between sampling points to allow a clear distinction of observations between regions. It should not be assumed that the interpolation provides an accurate estimate of the missing data.

The nTA distribution showed little variability, with the exception of the April 2006 data in the Ushant region, which indicated limitation of the normalization procedure when dealing with riverine inputs into coastal waters. The Lee et al. (2006) algorithm for the North Atlantic Ocean was used to calculate TA from sea surface salinity and sea surface temperature (SST) data during the winter months. The measured TA

showed good consistency with the calculated data, with a mean difference of 5.9 ±4.3 μmol kg^{-1} (n=128), in agreement with the uncertainty reported by Lee et al. (2006).

3.3.4. Dissolved Inorganic Carbon

The DIC concentrations showed an overall increase with latitude for all crossings (Figure 3.4c), ranging from 2058 μmol kg^{-1} (September 2005, Ushant and Southern Bay of Biscay) to 2142 μmol kg^{-1} (April 2006, Western English Channel). The salinity-normalized DIC (nDIC) concentrations (Figure 3.4d) ranged from 2020 μmol kg^{-1} (July 2006, Southern Bay of Biscay) to 2122 μmol kg^{-1} (April 2006, Western English Channel). Our DIC observations were in agreement with values previously reported for the North Atlantic by Corbière et al. (2007) and Robertson et al. (1994), where DIC values ranged from 2070 μmol kg^{-1} in summer to 2140 μmol kg^{-1} in winter. This also agrees with the range reported for the Norwegian Sea, with DIC values ranging between 2140 μmol kg^{-1} in winter and 2050 μmol kg^{-1} to 2080 μmol kg^{-1} in summer (Findlay et al. 2008).

The spring chlorophyll *a*-fluorescence maxima corresponded with periods of DIC drawdown (Figure 3.2e and 3.4c). The DIC values increased during the winter months corresponding to the decrease in the SST (Figure 3.2b) and the minimum in O_2 anomaly (Figure 3.2d). During the winter of 2006/2007, however, the nitrate concentrations and the O_2 anomaly suggested that the winter mixing was shallower than during the 2005/2006 winter for all regions except the Central and Western English Channel (Figure 3.2c and 3.2d), leading to a smaller increase in the DIC concentration during the winter of 2006/2007 for the same regions.

3.3.5. Seasonal variability of DIC and nitrate

Surface DIC and nitrate concentrations were higher in winter than in summer as a result of carbon and nutrient enriched deep waters being brought to the surface due to deep winter mixing (Tseng et al. 2007; Bates et al. 1996b). The increase in phytoplankton biomass observed during spring and early summer (as indicated by the chlorophyll *a*-fluorescence data in Figure 3.2e) resulted in a decrease in DIC

concentrations (Figure 3.4c), with a DIC minimum of 2063 µmol kg^{-1} observed in the Bay of Biscay in July 2006 and June 2007. The average seasonal amplitude for DIC and nitrate concentrations, respectively, from winter to spring was 62 µmol kg^{-1} and 7.4 µmol l^{-1} in 2005/2006, and 35 µmol kg^{-1} and 4.7 µmol l^{-1} in 2006/2007. From late summer to early winter, an increase in surface water DIC was observed, resulting from the enhanced oceanic CO_2 uptake from the atmosphere due to increasing CO_2 solubility in seawater with decreasing air and sea surface temperature (Zeebe and Wolf-Gladrow 2001). Entrainment by autumn storms of deep waters with higher DIC content also increased surface water DIC concentrations.

Year	*Region*	*ΔNitrate observed*	*ΔDIC observed*	*ΔDIC from Redfield*	*ΔDIC from 8.0*	*Observed DIC:NO3⁻*
	CEC	7.3	50	***48***	58	6.8
	WEC	7.2	58	47	***57***	8.1
2005/	Ushant	6.2	63	41	***49***	10.2
2006	Shelf Break	8.3	61	55	***67***	7.3
	NBB	8.0	71	53	***64***	8.9
	SBB	7.2	68	47	***57***	9.4
Average 2005/2006		*7.4*	*62*	*49*	*59*	*8.4*
	CEC	5.2	36	***34***	41	7.0
2006/	WEC	5.3	45	35	***42***	8.5
2007	Ushant	5.4	39	***36***	43	7.3
	Shelf Break	4.5	25	***30***	36	5.7
	NBB	3.9	29	26	***31***	7.5
	SBB	4.0	36	26	***32***	9.0
Average 2006/2007		*4.7*	*35*	*31*	*38*	*7.5*

Table 3.2. Observed (differences based on the nitrate and DIC winter maximum and spring minimum) and estimated (from the DIC:NO_3^- molar ratio) seasonal amplitude of DIC for the periods September 2005 to July 2006 and October 2006 to July 2007 (CEC = Central English Channel; WEC = Western English Channel; NBB = Northern Bay of Biscay; SBB = Southern Bay of Biscay).

We used a DIC:NO_3^- molar ratio (calculated from the seasonal depletion of DIC and nitrate) to estimate the seasonal DIC amplitude expected due to nitrate drawdown (Table 3.2). This ratio ranged from 5.7 to 10.3 (Table 3.2), indicating strong carbon over-consumption in this region compare to nitrate consumption. An averaged ratio of 8.0 was shown to give a better estimate of the seasonal carbon consumption

between winter and summer than the Redfield ratio of 6.6. This disagreement with the standard Redfield C:N ratio is often observed in coastal waters due to a more efficient recycling of nitrogen compared to carbon (Sambrotto et al. 1993). A similar discrepancy was observed in separate studies of the Northeast Atlantic (Körtzinger et al. 2001) and the Norwegian Sea (Findlay et al. 2008), where the use of data on nitrate consumption and a Redfield C:N ratio (6.6) was also shown to significantly underestimate the carbon consumption.

3.3.6. Influence of winter mixing on the carbonate system variability

The cold winter of 2004/2005 in the Bay of Biscay with dry and cold north and northeasterly winds had a strong effect on the surface layer characteristics due to a decrease in SST and enhanced winter mixing (Somavilla et al. 2009). The heat losses from the ocean to the atmosphere for this winter in the Bay of Biscay resulted in the highest accumulated flux on record since the 1960s (Somavilla et al. 2009). The SST anomaly extended into the following winter (2005/2006), resulting in a second winter of deep winter mixing. The air temperature during the subsequent winter of 2006/2007 was estimated to be the warmest on record for about 500 years (Luterbacher et al. 2007), causing warming of the surface ocean and a reduction in winter mixing.

The winter MLD in the Bay of Biscay was estimated from the Argo floats temperature data to be between 450 and 650 meters in 2005/2006, and between 200 and 300 meters in 2006/2007 (Figure 3.5). The MLD observed for 2006/2007 corresponded to the average MLD observed between 2002 and 2004 (approximately 200 m) for the Bay of Biscay (Padin et al. 2008). The deeper MLD during the 2005/2006 winter resulted in higher surface winter concentrations of nutrients and DIC, and an enhancement of the spring bloom in the Bay of Biscay in 2006 (Figure 3.2e and 3.3). The intensity of the spring bloom was reduced in 2007 as a result of a reduced winter mixing in 2006/2007. The inter-annual differences in DIC and nitrate concentrations were similarly affected by the difference in winter mixing in the Bay of Biscay, with winter nitrate concentrations 1.6 times higher in 2005/2006 compared with 2006/2007. This agreed with the differences in phytoplankton biomass, derived

from the chlorophyll *a*-fluorescence data, observed between the two years (ratio of 1.7 between the two years).

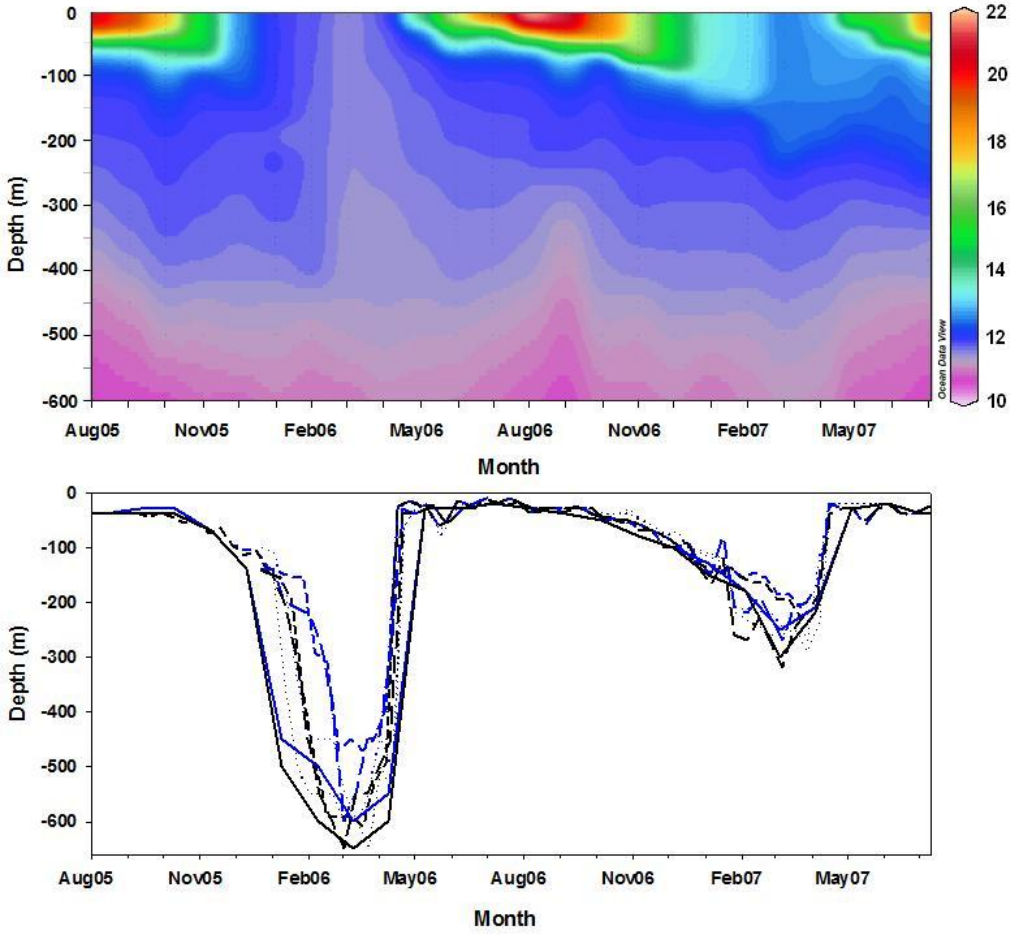

Figure 3.5. Argo float 6900362 temperature data for the Bay of Biscay for the period between August 2005 and July 2007 in the upper 600 meters (top panel), and mixed layer depths (MLD) calculated for the Argo floats 4900557 (short dashed line), 6900359 (dotted line), 6900360 (long dashed line) and 6900362 (solid line) data (bottom panel) with ΔT (depth-surface) of -0.5 °C (blue line) and $\Delta\sigma_t$ (depth-surface) of 0.125 (black line) for the period between August 2005 and July 2007 (http://www.coriolis.eu.org/cdc/argo.htm).

Inter-annual and seasonal variations in DIC concentrations in the North Atlantic Ocean have been reported to be dependent on the winter MLD and SST anomalies (Gruber et al. 2002; Bates 2001). The NAO has been shown to relate to changes in the MLD associated with anomalies in SST and convection (Dickson et al. 1996; Gruber et al. 2002). In this region, a more negative phase of the NAO is associated with stronger winter mixing, negative SST anomalies, higher winter DIC

concentrations (due to the deep supply from vertical mixing) and lower spring/summer DIC concentrations (due to increased primary production); whereas a more positive NAO phase is accompanied by warmer SSTs, less intense winter mixing, and a less pronounced seasonal cycle of DIC (Gruber et al. 2002).

3.3.7. Air-Sea CO_2 fluxes

The calculated air-sea CO_2 fluxes (F_{CO2}) showed significant differences between the various regions (Figure 3.6). The English Channel acted as a seasonal source of CO_2 to the atmosphere during autumn and winter months and as a sink during spring and summer months (from +3.7 mmol m^{-2} d^{-1} in winter, to -4.4 mmol m^{-2} d^{-1} in summer). This is in agreement with other studies in this area (Frankignoulle et al. 1996a; Borges and Frankignoulle 2003; Padin et al. 2007). Heterotrophic processes involving degradation of the enhanced organic matter levels in the well-mixed waters of the English Channel explain the oversaturation of CO_2 with the consequent CO_2 flux out of the water column during autumn and winter (Borges and Frankignoulle 2003; Borges et al. 2006). In contrast, the Bay of Biscay acted as a sink of CO_2 during all seasons, with the exception of July 2006 for the Southern Bay of Biscay. Fluxes ranged between +0.2 and -3.9 mmol m^{-2} d^{-1}, consistent with the results of Padin et al. (2008 and 2009) and Frankignoulle and Borges (2001).

Despite a few gaps in the monthly data available for the flux estimates, a good coverage of the seasonal cycle was available for the two years. The air-sea fluxes showed clear differences between similar months in 2005/2006 compared with 2006/2007, apart from the Central English Channel, the Western English Channel and the Ushant regions. The latter regions did not show a significant difference between the two years (paired *t*-test, $p = 0.14$, $n = 18$). In all other regions, May, June and July 2007 showed an increase in the oceanic CO_2 sink, with the air-sea fluxes between 1.3 and 7.9 times larger compared with May, June and July 2006 (paired *t*-test, $p = 0.0004$, $n = 11$; $p = 0.009$ for all months, $n = 17$).

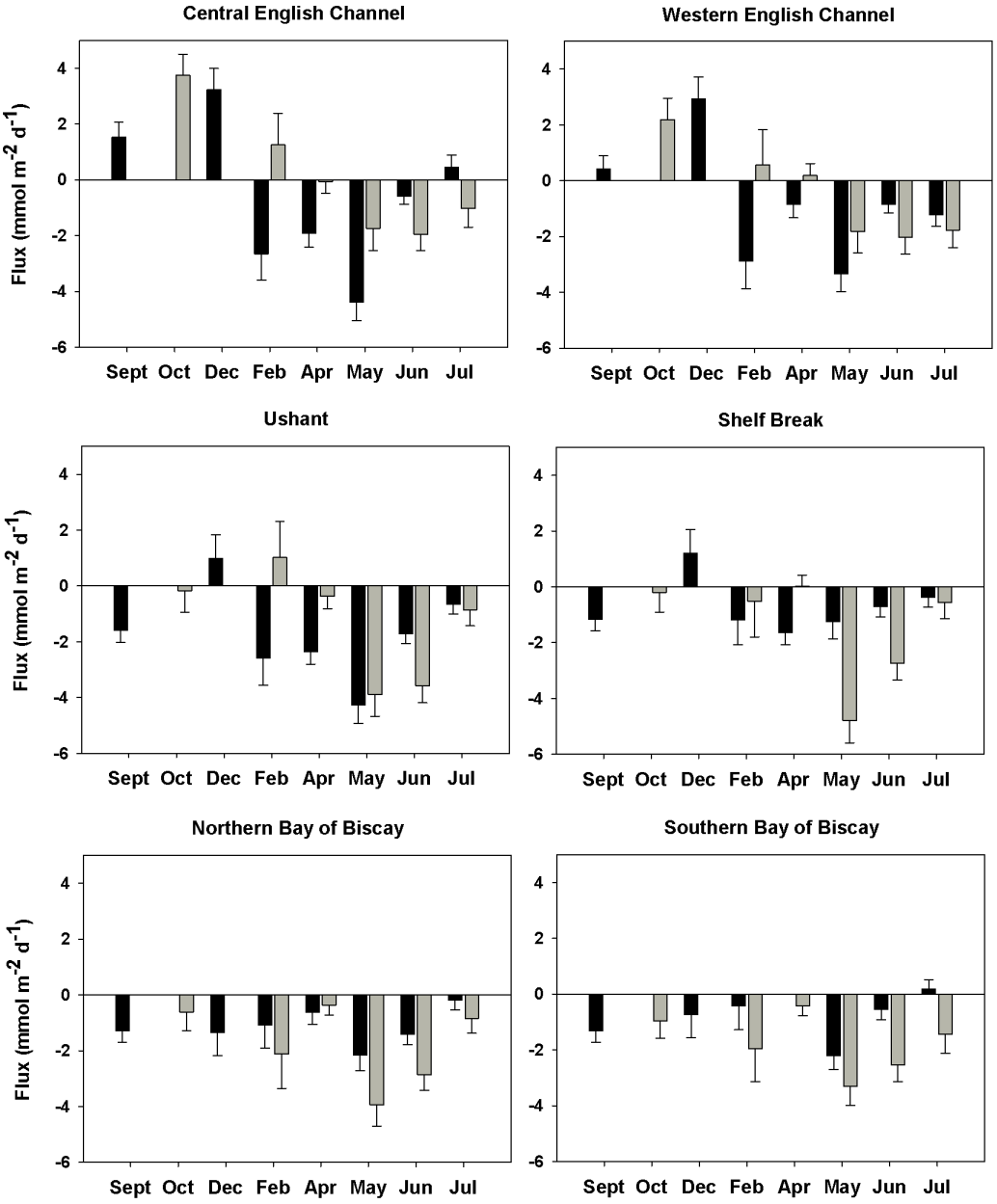

Figure 3.6. Calculated monthly air-sea CO_2 fluxes (mmol m^{-2} d^{-1}; negative values indicate a net flux into the sea) for each region in 2005/2006 (dark grey) and 2006/2007 (light grey).

The wind speeds (Figure 3.7) were higher in February, May, June and July 2007 compared to 2006, which may have influenced the air-sea CO_2 flux differences observed in the Bay of Biscay and the Shelf break regions between the two years. The winter 2005/2006 was colder than winter 2006/2007 by 2.6 ºC, while the

summer of 2005/2006 was warmer than the summer of 2006/2007 by 2 ºC (Figure 3.2b). This resulted in winter to summer SST differences of about 7.8 ºC in 2005/2006 and 3.4 ºC in 2006/2007, leading to enhanced solubility of CO_2 in the summer of 2007 compared to 2006.

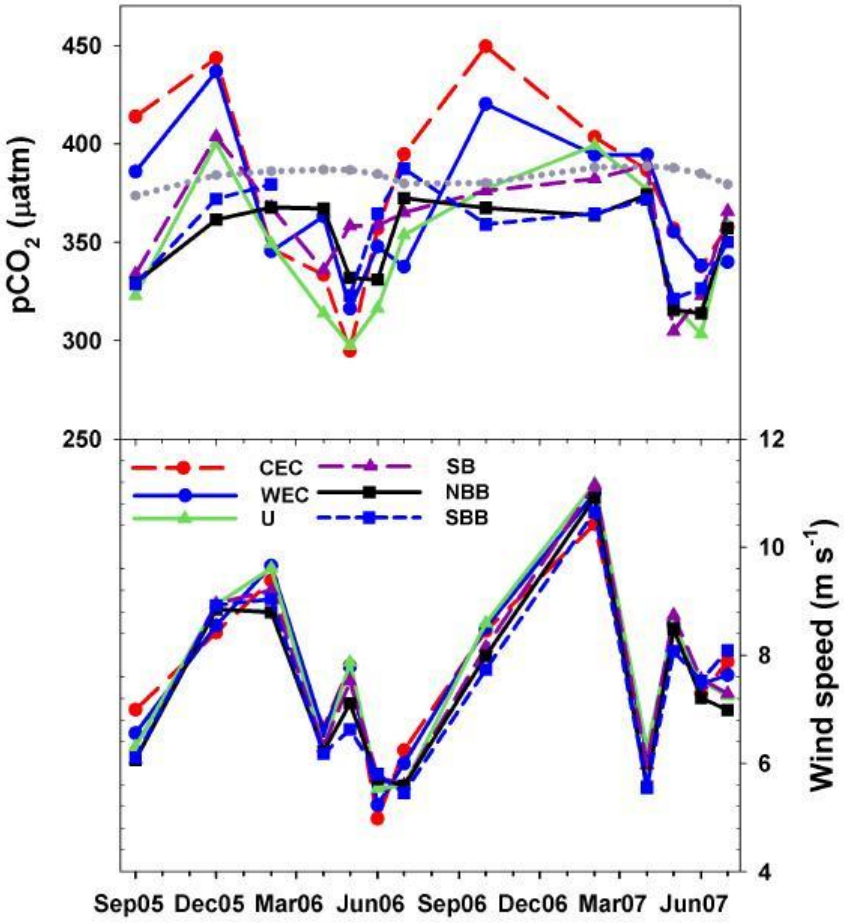

Figure 3.7. Monthly mean calculated sea surface pCO_2 (µatm) for each region (upper plot with left axis), atmospheric pCO_2 data (µatm; dotted grey line in upper plot with left axis), and QuikSCAT wind speed data (m s^{-1}; lower plot with right axis). Central English Channel (dashed red line; circles); Western English Channel (blue line; circles); Ushant (green line; triangles); Shelf Break (dashed purple line; triangles); Northern Bay of Biscay (black line; squares); Southern Bay of Biscay (short dashed blue line; squares). Data points are linearly interpolated between sampling points to allow a clear distinction of observations between regions. It should not be assumed that the interpolation provides an accurate estimate of the missing data.

Varying parameter	*Season*	*Value*	*Flux calculated*	*Seasonal difference*	*Flux difference*
Wind speed (m s^{-1})	Winter 2005/2006	10	-1.5		
	Summer 2006	6	-0.6	4	+0.9
	Winter 2006/2007	11	-1.8		
	Summer 2007	8	-1.0	3	+0.8
Temperature (ºC)	Winter 2005/2006	10.8	-4.2		
	Summer 2006	18.6	+1.5	7.8	+5.7
	Winter 2006/2007	13.4	-2.4		
	Summer 2007	16.8	+0.1	3.4	+2.5
DIC (µmol kg^{-1})	Winter 2005/2006	2131	+2.7		
	Summer 2006	2064	-3.5	67	-6.2
	Winter 2006/2007	2111	+0.5		
	Summer 2007	2062	-3.7	49	-4.0

Table 3.3. Effect of varying wind speed (m s^{-1}), temperature (ºC) and DIC concentration (µmol kg^{-1}) on the air-sea CO_2 flux calculation in mmol m^{-2} d^{-1}. Fluxes were calculated according to equation 3.3. The oceanic pCO_2 values were calculated from DIC, TA, salinity, and temperature data using the CO_2SYS program. The calculation considered only one varying parameter at a time while all other parameters were considered constant: TA = 2350 µmol kg^{-1}; S = 35; T = 16; wind speed = 8 m s^{-1}; DIC = 2100 µmol kg^{-1}; and atmospheric pCO_2 = 380 µatm.

After the colder winter (2005/2006), the following seasonal changes occurred upon transition to summer (with their estimated impacts on the air-sea CO_2 flux, in mmol m^{-2} d^{-1}, given in brackets, see Table 3.3 for method of calculation): wind speed decreased by 4 m s^{-1} (+0.9); temperature increased by 7.8 ºC (+5.7); and DIC decreased by 67 µmol kg^{-1} (-6.2). After the warmer winter of 2006/2007 however, the following seasonal changes occurred: wind speed decreased by 3 m s^{-1} (+0.8); temperature increased by 3.4 ºC (+2.5); and DIC decreased by 49 µmol kg^{-1} (-4.2).

The seasonal changes in DIC and SST both had important impacts on air-sea flux of CO_2 (Table 3.3). In terms of differences between years, it appears that the effects on air-sea CO_2 flux of the greater seasonal warming following the colder winter (+3.2) and lower wind speed (+0.1) outweighed the effect of stronger spring blooms in 2006 (-2.0). According to our analysis, the effect of the difference in winter mixing between the two years was therefore counteracted and in fact overwhelmed by the greater amount of warming of the surface waters. It was this latter factor, we

calculate, which led to a stronger CO_2 sink in summer 2007 compared to summer 2006. Our observations for the Bay of Biscay are consequently in contrast to recent model results for the stratified northern North Sea, where biological production, and not temperature, was emphasized as the main driver for the air-sea flux of CO_2 (Prowe et al. 2009).

3.4. Conclusions

The changes in winter mixing and SST observed between the two consecutive years of our study period showed lower-amplitude seasonal cycles of nitrate and DIC and an associated decrease in primary production following the warmer winter of 2006/2007. While no particular changes were observed in the English Channel regions, elsewhere an enhanced carbon uptake from the atmosphere to the ocean was observed in the summer of 2007 compared to the summer of 2006. This occurred despite more intense phytoplankton blooms in spring 2006 compared with 2007. We attribute the surprisingly lower ocean carbon uptake in summer 2006 to a greater amount of warming from winter to summer (SST increase of 8 °C between February and July in 2006, compared with only 3.4 °C in 2007). This greater degree of warming tended to increase surface ocean pCO_2 towards higher values in summer 2006, and was sufficiently strong to offset the effects of the stronger phytoplankton blooms in that year. Stronger winds in summer 2007 compared with summer 2006 also contributed to an increased carbon uptake in summer 2007. While upper ocean stratification is expected to increase due to further CO_2 emissions, with the prediction that this will lead to decreased oceanic CO_2 uptake, we show in this study that a decrease in winter mixing can be followed by an increase in oceanic CO_2 uptake during the following summer. Our study highlights the importance of winter to summer temperature differences in controlling the annual CO_2 sink in temperate waters. These results are therefore important in order to understand how the oceans might respond to future climate change and accompanying changes in stratification and storm frequency in this oceanic region.

Chapter 4

Control of the carbonate system by upwelling and respiration in the sub-tropical Northeast Atlantic Ocean

Abstract

The distributions of four oceanic carbonate system parameters (Dissolved Inorganic Carbon, Total Alkalinity, partial pressure of CO_2 and pH_T) were determined in January and February 2008 in the sub-tropical Northeast Atlantic Ocean (12 to 29 ºN; 16 to 36 ºW) as part of the UK SOLAS program. Spatial variability was observed for all the chemical parameters and was associated with the different water masses present in the area, the coastal upwelling associated with the Eastern Boundary Current, and the Northeast Atlantic oxygen minimum zone. A strong correlation was observed in the surface waters between the carbonate system parameters and hydrographic properties, which explained 64% of the observed variability. The air-sea CO_2 fluxes also showed large regional variations and ranged from +1.9 to -4.0 mmol m^{-2} d^{-1}. The northern part of the study area acted as a source of CO_2 to the atmosphere, attributable to the coastal upwelling and the strong north-easterly trade winds observed north of the Cape Verde Islands, while the waters in the southern part acted as a CO_2 sink. Enhanced DIC concentrations (> 2150 µmol kg^{-1}) and low calcite and aragonite saturation states ($\Omega_{Ca} < 3$ and $\Omega_{Ar} < 2$) were observed just below 50 m depth in the southern part (south of 19 ºN). The DIC concentrations showed a strong correlation with the AOU (r = 0.97), associated with the remineralization of organic matter in the oxygen minimum zone. These results suggest that the carbonate chemistry in the sub-tropical Northeast Atlantic Ocean was controlled by both coastal upwelling and respiration.

4.1. Introduction

Atmospheric CO_2 concentrations are showing a continuous increase, with current values at approximately 390 ppm (Hofmann et al. 2009). Ocean uptake of anthropogenic CO_2 is resulting in an annual decrease in surface ocean pH, which was recently estimated for the North Pacific Sub-tropical Gyre to -0.0019 y^{-1} (Dore et al. 2009; Doney et al. 2009a); and a decrease in the saturation state of calcium carbonate (Feely et al. 2004; Orr et al. 2005). The ability of marine calcifying organisms to build and maintain their calcite and aragonite shells is thought to be compromised by the changes in the oceanic carbonate system (Orr et al. 2005). Superimposed on the gradual changes of the oceanic carbonate system due to anthropogenic CO_2 uptake, is the natural spatial and temporal variability resulting from physical and biological processes, including wind stress, deep water mixing, ocean boundary upwelling, photosynthesis and respiration and ocean warming or cooling (Doney et al. 2009b and c; Dumousseaud et al. 2010; Gruber et al. 2002).

The region of the sub-tropical northeast Atlantic Ocean is strongly influenced by the highly productive coastal upwelling system off the Northwest African coast and the oxygen minimum zone south of the Cape Verde Islands (Pérez et al. 2001; Stramma et al. 2008a and b; Stramma et al. 2005; Fisher et al. 2007; Carr 2002). The upwelling system is bounded by the flow of the Canary Current and the North Equatorial Current (Fisher et al. 2007; Tomczak and Godfrey 2003).

Coastal upwelling processes can determine short and long term variability of the carbonate system and regional CO_2 fluxes, and can be of particular importance to the global carbon cycle (Santana-Casiano et al. 2009; Feely et al. 2008; Torres et al. 1999). Moreover, competing effects can be observed in upwelling regions due to the high supply of nutrients leading to enhanced biological activity and consequent entrainment of anthropogenic CO_2; while low-pH and CO_2 supersaturated waters are brought to the surface leading to CO_2 outgassing from the ocean to the atmosphere. This was recently reported for the upwelling system along the US West Coast where entrainment of anthropogenic CO_2 resulted in low pH waters (< 7. 75) and undersaturation with respect to aragonite ($\Omega_{Ar} < 1$) (Feely et al. 2008).

The sub-tropical northeast Atlantic Ocean is characterized by complex current and water mass systems (Stramma et al. 2005; Stramma et al. 2008a; Mittelstaedt 1983). The water masses in the upper 800 m characterized in this region include the Tropical Surface Waters (TSW), the sub-surface Central Waters (CW) and the Antarctic Intermediate Waters (AAIW). The Central Waters are composed of the North Atlantic Central Waters (NACW) and the South Atlantic Central Waters (SACW), themselves delimited by the Cape Verde Frontal Zone located north of the Cape Verde Islands (around 21 ºN) and which acts as a frontier between the more saline NACW and the less saline SACW (Pierre et al. 1994; Fisher et al. 2007). The distribution of the water masses is strongly affected by the near-surface current system (Figure 4.1), composed of the Canary Current, the North Equatorial Current (NEC), and the North Equatorial Counter Current (NECC) (Stramma et al. 2005, Stramma and Müller 1989).

Hydrographic properties have been described in detail for the sub-tropical northeast Atlantic, but the observations of the carbonate system distribution reported for this oceanic region have mainly focused on the northern part, west of Spain (González-Dávila et al. 2003b; Álvarez et al. 1999), and north of the Canary Islands (Pérez et al. 2001). In addition, carbonate system measurements have been reported since 1994 for the ESTOC (European Station for Time-series in the Ocean, Canary Islands) station, located north of the Canary Islands (29 °N, 15 °W; Santana-Casiano et al. 2007).

The understanding of the physical and biological processes that determine the carbonate system variability in the present ocean is of particular importance in order to predict future changes associated with climate change, including enhanced ocean temperatures, stratification and increased storminess (Lovenduski et al. 2008; Le Quéré et al. 2007; Bopp et al. 2001). The aim of this study was to determine the key processes controlling the carbonate chemistry in the sub-tropical northeast Atlantic Ocean. Simultaneous measurements of the four measurable parameters of the carbonate system were undertaken (Dissolved Inorganic Carbon (DIC), Total Alkalinity (TA), partial pressure of CO_2 (pCO_2) and pH_T). A comparison of the relative changes of these carbonate parameters will be discussed as well as their

variability with regard to the influence of the coastal upwelling, the oxygen minimum zone, and the water masses present in the area.

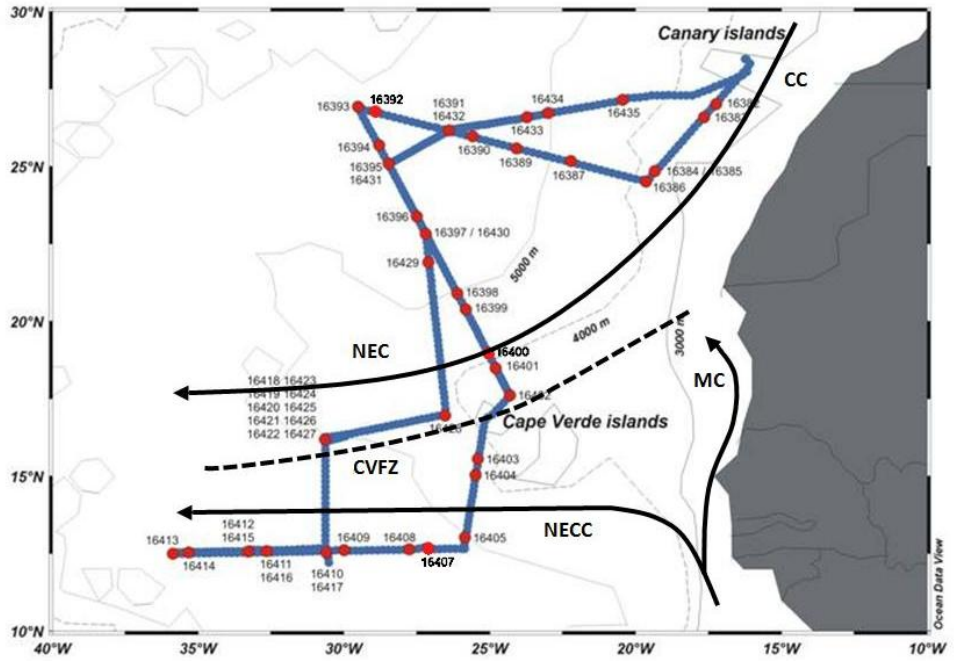

Figure 4.1. D326 cruise track (blue) and stations location (red dots). The black arrows represent the near-surface currents found in the region: the Mauritania Current (MC); the Canary Current (CC); the North Equatorial Current (NEC); and the North Equatorial Counter Current (NECC). The location of the Cape Verde Frontal Zone (CVFZ) is represented by a black dashed line (adapted from Mittlestaedt 1983; Stramma et al. 2005 and 2008).

4.2. Methods

The cruise D326 took place in the period between January 5th and February 5th 2008 in the sub-tropical Northeast Atlantic (Figure 4.1) aboard the RRS *Discovery* as part of the UK SOLAS (Surface Ocean – Lower Atmosphere Study) program. Continuous sea surface temperature (SST) and sea surface salinity (SSS) data were obtained every minute from the ThermoSalinoGraph (TSG; FSI temperature and conductivity sensor), while continuous surface chlorophyll-*a* fluorescence data were obtained from a fluorometer (WETStar, WET Labs, USA). Both instruments were installed on the ship's underway supply (intake depth at approximately 7 m). The accuracy and precision of the temperature data from the TSG were ±0.003 °C. Salinity samples were collected on a daily basis from the CTD casts and from the

underway supply and analyzed on the on-board salinometer (8400B Autosal) for calibration of the TSG and CTD salinity measurements. Samples for dissolved oxygen concentrations were collected from each CTD cast (approximately 6 samples per cast) in order to calibrate the oxygen sensor (Seabird SBE 43) installed on the stainless steel CTD frame, and analyzed by Winkler titration following Holley and Hydes (1995) with a precision of 1%. The Apparent Oxygen Utilization (AOU) was calculated from the measured oxygen concentration (O_2) and the oxygen concentration at saturation (O_2^*) which was calculated according to Garcia and Gordon (1992) with the solubility coefficients from Benson and Krause (1984).

$$AOU = [O_2^*] - [O_2] \qquad (4.1)$$

Samples for chlorophyll-*a*, DIC, TA and nutrients were collected from the CTD casts using Niskin bottles to generate depth profiles (24 casts, 8 depths); and from the ship's underway sea water supply at 2 hours interval between CTD stations to obtain surface water distributions. Chlorophyll-*a* concentrations were determined in duplicate following the method of Welschmeyer (1994) with a standard error of 0.006 ± 0.007 µg l^{-1} (1σ) on average. The determination of nanomolar phosphate and total nitrate concentrations was undertaken following Patey et al. (2008) with a precision of ±0.27 nmol l^{-1} for phosphate and ±0.20 nmol l^{-1} for nitrate. The accuracy of the method for nanomolar nutrients was estimated for the whole cruise between 0.27 and 2.6 nmol l^{-1} for phosphate (1.3 nmol l^{-1} on average) and between 0.4 and 5.0 nmol l^{-1} for nitrate (1.4 nmol l^{-1} on average).

The DIC and TA samples were analyzed on a VINDTA 3C instrument (Marianda, Germany). The DIC samples were analyzed using a coulometric titration (UIC coulometer 5011) and TA was determined using a closed-cell titration according to Dickson et al. (2007). The precision of the method, assessed daily from repeated measurements on the same batch of seawater and from replicate samples, was estimated for the whole dataset to be 1.0 ± 0.6 µmol kg^{-1} for DIC and 1.4 ± 0.6 µmol kg^{-1} for TA (±1σ). Certified Reference Materials (from A.G. Dickson, Scripps Institution of Oceanography) were analyzed as standards to calibrate the instrument at the beginning and end of each day of analysis.

The TA measurements were compared against the TA calculated from the sub-tropical regional algorithm of Lee et al. (2006) based on temperature and salinity measurements. The two TA values (measured and calculated) were in good agreement, with a mean difference of 7.9 ± 5.6 μmol kg^{-1} (n = 193; Appendix 2). To remove the influence of salinity on the distribution of DIC and TA, the data was normalized (nDIC and nTA) to a salinity of 35 (Millero et al. 1998a).

The DIC and TA measurements were used to calculate other parameters of the carbonate system using the CO_2SYS program (Pierrot et al. 2006) using the constants of Mehrbach et al. (1973) refitted by Dickson and Millero (1987). In order to determine the forcing factors associated with the carbonate system variability and the percentage of variance explained by them, a principal component analysis (PCA; Pearson 1901) was applied to the carbonate system (TA and DIC) and other variables (SSS, SST, latitude, nutrients).

Surface underway pH_T (total scale) was measured every minute using a potentiometric system (Ruthern Instruments, UK) according to the potentiometric method described in Dickson et al. (2007). The pH cell was composed of a reference silver/silver chloride electrode (Russell pH Ltd CRR/DWG1575), a glass pH electrode (Russell pH Ltd SW79) and a free-diffusion capillary liquid junction (2.5 M KCl) connecting these electrodes. The calibration of the system was undertaken every 8 to 12 hours with TRIS buffer made up in artificial sea water according to Dickson et al. (2007). The precision of the method and drift of the instrument were estimated to be within 0.005 from continuous measurement on the same batch of seawater. The measured pH showed good agreement with the pH calculated from DIC and TA, with an average difference of 0.01 ± 0.01 (1σ; Appendix 3).

The oceanic and atmospheric pCO_2 values were determined continuously during the cruise on an hourly basis using an equilibrator based (combined glass-bead and showerhead equilibrator) pCO_2 system with a non-dispersive infrared analyzer (Live pCO_2, CASIX and Dartcom, UK; Hardman-Mountford et al. 2008). Seawater was drawn from the underway supply and marine air was sampled from approximately 10 m above the surface. The pCO_2 measurements were calibrated hourly with CO_2 standard gases of 0, 250 and 450 ppm and the in situ pCO2 measured was corrected for the difference between in situ and equilibrator temperature.

The air-sea CO_2 flux F (mmol m^{-2} d^{-1}) was calculated as follows (Wanninkhof 1992):

$$F = k \alpha (pCO_2^{sea} - pCO_2^{air}) \qquad (4.2)$$

Where k is the gas transfer velocity (m s^{-1}), and α is the solubility coefficient of CO_2 (mol atm^{-1} m^{-3}). The solubility coefficient of CO_2 (α) was calculated according to Weiss (1974). The gas transfer velocity (k) was calculated from the equation of Nightingale et al. (2000). The wind speed data used for the calculation of the gas transfer velocity were obtained from the ship's foremast anemometer, located at 10 m above the surface.

4.3. Results and discussion

The cruise track covered the region from the oligotrophic waters located west of 30 °W to near the upwelling zone located along the African coast (Pierre et al. 1994), as well as the Cape Verde and the Canary Islands regions. These particular conditions resulted in large spatial variations in salinity, temperature, nutrients and carbonate system parameters, and can be related to the presence of the different water masses in the upper 800 m (Pierre et al. 1994).

4.3.1. Surface distributions of hydrographic, biological and chemical properties

The SSS showed an overall decrease towards the equator due to enhanced rainfall, and ranged between 35.5 and 37.6 for the study region (Figure 4.2a). The SST increased from the northern to the southern parts of the study region and ranged between 19.4 and 25.3 ºC (Figure 4.2b). The surface water nitrate concentrations remained very low along the cruise track and ranged between 3 and 25 nmol l^{-1}, with the exception of enhanced concentrations of up to 260 nmol l^{-1} in the vicinity of the Cape Verde Islands (Figure 4.2c). The surface water phosphate concentrations ranged from 2 to 100 nmol l^{-1}, with higher concentrations near the Cape Verde Islands (Figure 4.2d). The sea water density distribution (Figure 4.2e) showed a strong variation along the cruise track, due to the presence of different water masses,

and ranged between 23.9 and 26.4 kg m^{-3} (σ_t). The chlorophyll-*a* concentrations were relatively low in the study region (Figure 4.2f), ranging between 0.1 and 0.7 µg l^{-1}, with the highest values in the vicinity of the Canary and Cape Verde Islands.

The surface water DIC concentrations ranged between 1943 and 2076 µmol kg^{-1} and TA between 2337 and 2470 µmol kg^{-1}. Surface water DIC and TA concentrations both increased with increasing latitude (Figures 4.3a and b). Our surface water TA measurements in the vicinity of the Canary Islands (between 2416 and 2438 µmol kg^{-1}) were in relatively good agreement with values reported for the ESTOC station (Santana-Casiano et al. 2007), which ranged between 2400 and 2420 µmol kg^{-1}. The highest DIC values observed in the northern part of the study region (up to 2076 µmol kg^{-1}) were however lower than the minimum seasonal values reported for the ESTOC station (2085 µmol kg^{-1}). Overall, the ranges of surface DIC and TA concentrations observed in this study agreed well with values reported between 10 and 30 °N (~30 °W) by the Global Data Analysis Project (GLODAP) (Key et al. 2004), which ranged between 1970 and 2104 µmol kg^{-1} (DIC) and between 2330 and 2452 µmol kg^{-1} (TA). The surface water nDIC concentrations ranged between 1900 and 1980 µmol kg^{-1} along the cruise track with enhanced concentrations in the vicinity of the Cape Verde and Canary Islands (Figure 4.3c). The surface water nTA distribution did not show any distinctive spatial patterns and ranged between 2275 and 2320 µmol kg^{-1} (Figure 4.3d).

A strong correlation was observed between the surface TA and DIC distributions ($r = 0.96$, $n = 71$, $p < 0.0001$). Surface water DIC and TA concentrations correlated closely with the SSS distribution ($r = 0.93$ and 0.97; $n = 95$ and 72 for DIC and TA, respectively; $p < 0.0001$; Appendix 4), and with the SST distribution ($r = -0.84$ and -0.92; $n = 72$ and 95 for TA and DIC respectively; $p < 0.0001$; Appendix 4). The PCA performed on the underway data indicated a first Principal Component (PC) which explained 64% of the variability in the dataset from the co-variation of SSS, SST, DIC and TA surface distributions ($p < 0.0001$). A second PC, related to gradients in nitrate and phosphate, explained 19% of the dataset variability ($p < 0.0001$).

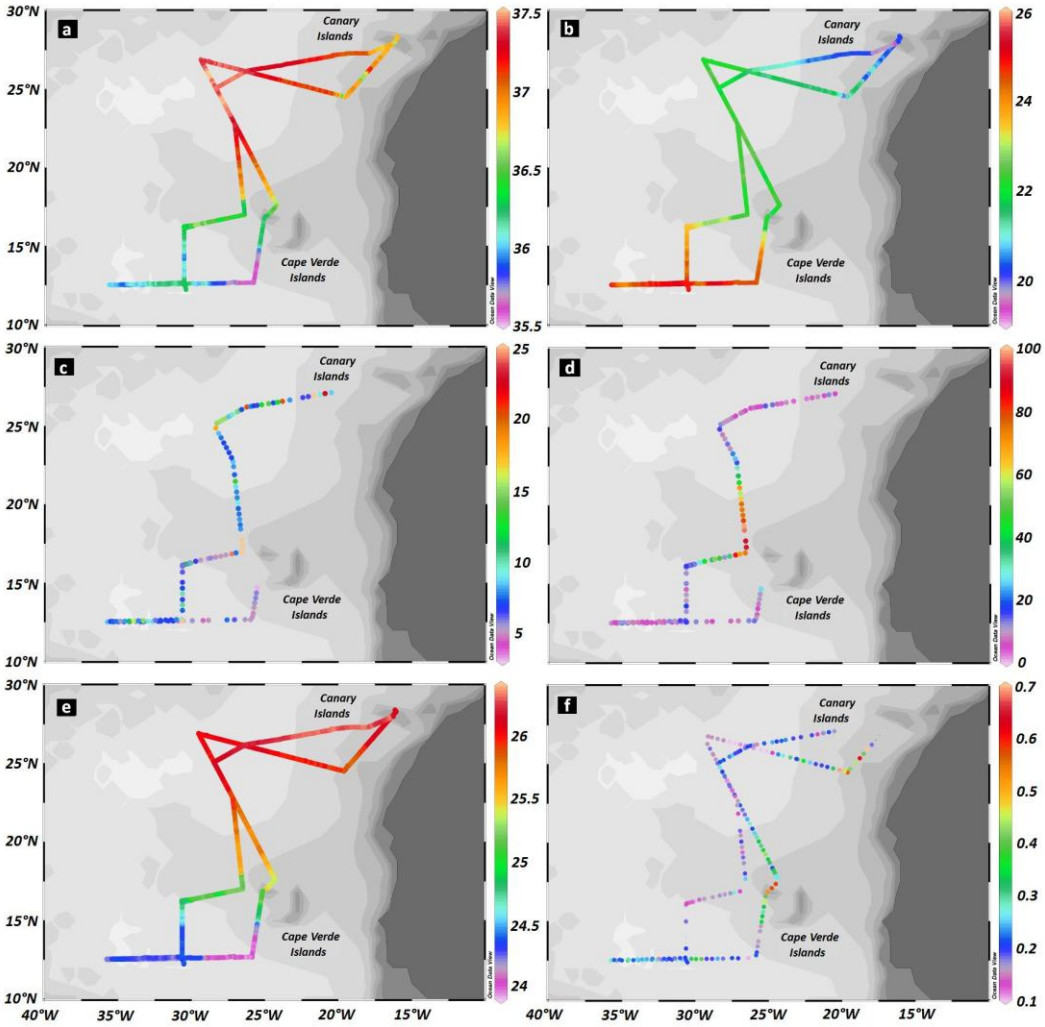

Figure 4.2. Surface distributions of (a) salinity, (b) temperature (ºC), (c) nitrate concentrations (nmol l^{-1}), (d) phosphate concentrations (nmol l^{-1}), (e) density σ_t (kg m^{-3}), and (f) chlorophyll-*a* concentrations (µg l^{-1}).

The high spatial resolution measurements of surface water pH_T for the study region showed values ranging between 8.13 and 8.22, whereas pCO_2 measurements ranged between 335 and 405 µatm. The range of oceanic pCO_2 observed was hence in agreement with previously reported pCO_2 values in this oceanic region, ranging between 300 and 450 µatm (Copin-Montégut and Avril 1995). Enhanced surface water pH_T and lower pCO_2 were observed in the southern part of the study region, with lower pH_T and higher pCO_2 in the north-eastern part of the study region, south of the Canary Islands (around 25 ºN and 20 ºW; Figure 4.4a and b). The distributions of surface water pH_T and pCO_2 showed a negative correlation along the cruise track ($r = -0.87$; $n = 322$; $p < 0.0001$).

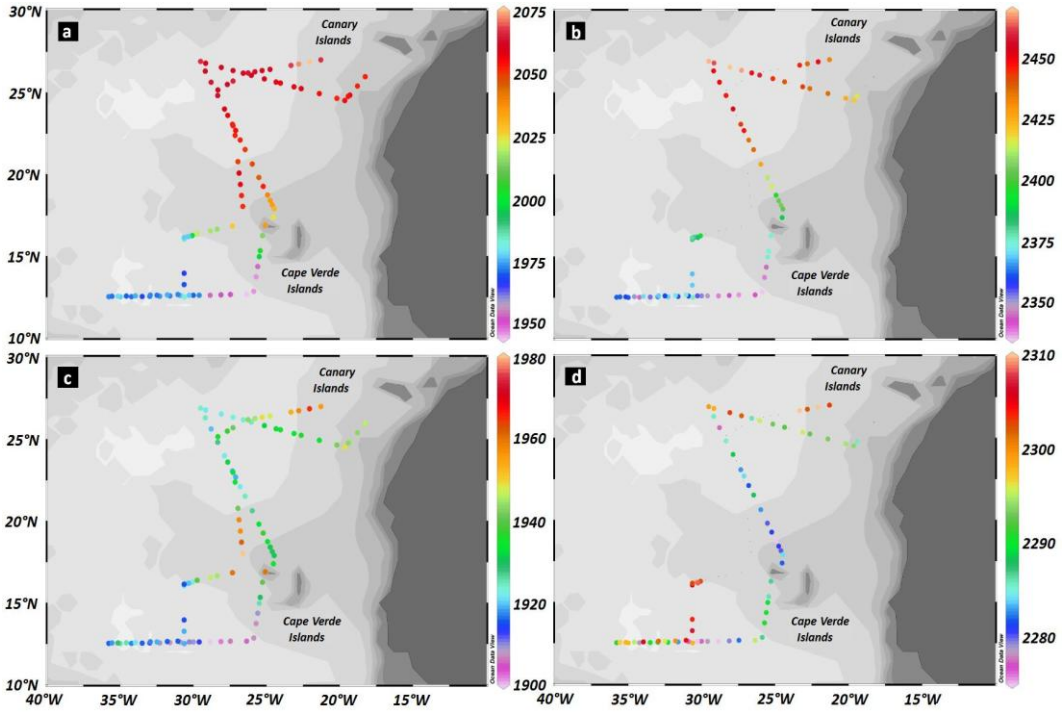

Figure 4.3. Surface distributions of (a) DIC, (b) TA, (c) salinity normalized (S=35) nDIC, and (d) salinity normalized (S=35) nTA (all expressed in µmol kg^{-1}).

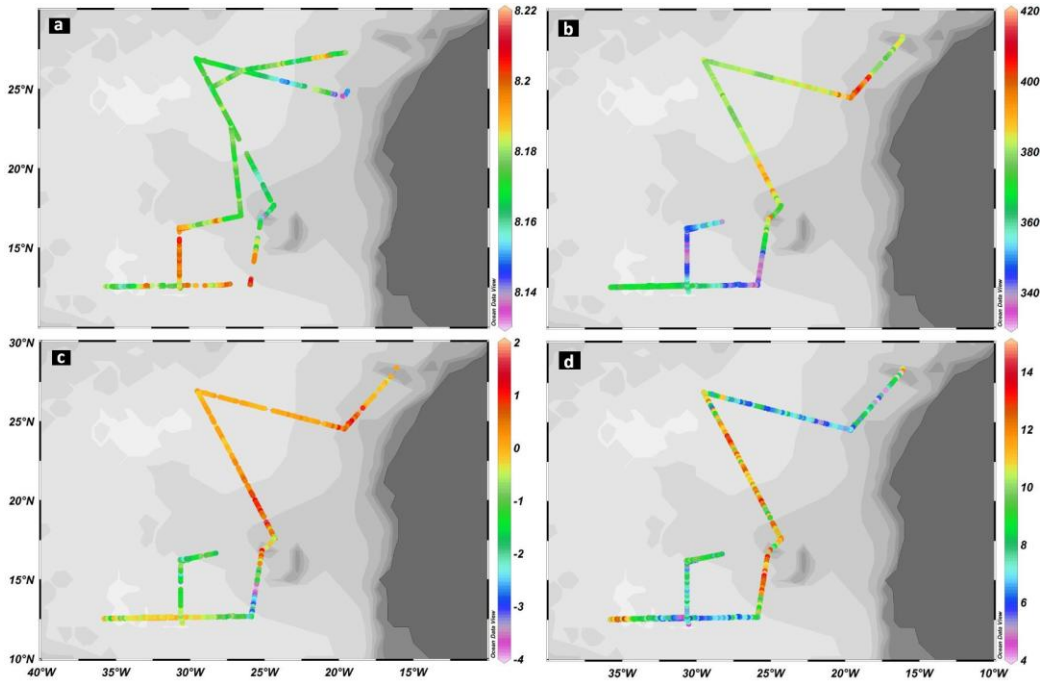

Figure 4.4. Surface distributions of (a) pH, (b) oceanic pCO_2 (µatm), (c) air-sea CO_2 flux (mmol m^{-2} d^{-1}; a positive flux indicates oceanic source of CO_2 to the atmosphere), and (d) wind speed (m s^{-1}).

4.3.2. Meridional distributions of hydrographic, biological and chemical properties

The meridional depth distributions showed strong correlations between the various physical, biological and chemical variables (Figure 4.5). The TA distribution closely followed the salinity distribution ($r = 0.97$; $n = 130$; $p < 0.0001$; Appendix 5) whilst the temperature and DIC distributions showed a strong negative correlation ($r = -0.80$; $n = 199$; $p < 0.0001$; Appendix 5). The temperature and salinity data were also strongly correlated ($r = 0.79$; $n = 201$; $p < 0.0001$; Appendix 5), except for the SST maximum in the southern part of the study region. This corresponded with the equatorial temperature maximum where a decoupling was observed between the salinity and temperature data due to freshwater inputs. The strong relationships between the carbonate system and the hydrographic properties have also been reported for the region north of the Canary Islands by Pérez et al. (2001). These workers showed that the physical properties of the various water masses observed north of the Canary Islands explained more than 93% of the carbonate system variability. Similar observations were reported by González-Dávila et al. (2003b) in the Gulf of Cadiz where 96% of the variability in the distribution of chemical parameters was attributed to the presence of different water masses through the use of a mixing model.

The hydrographic properties of the different water masses in the study area have been described in detail by Stramma et al. (2005; 2008a), and are principally composed of the TSW and the sub-surface CW. The presence of AAIW is indicated by salinity and TA minima, and DIC and nitrate maxima (Stramma et al. 2008a; 2005; Goyet et al. 1998; Table 4.1). The isopycnals on the density distributions in Figure 4.5f indicate the density fronts between the different water masses (Stramma et al. 2005). The maximum influence of the TSW was in the upper 80 m in the region south of 19 ºN (Figure 4.5) according to the density criterion of $\sigma_t \leq 25.8$ kg m^{-3} (Stramma et al. 2005; Table 4.1). The CW showed a maximum influence in the upper 180 m with densities between 25.8 and 27.1 kg m^{-3} (Figure 4.5, Table 4.1). The influence of the AAIW was observed below 150 to 200 m (12 ºN and 27 ºN respectively). The density ($\sigma_t > 27.1$ kg m^{-3}) and salinity ($S < 35.4$) criteria were used

to determine the maximum influence and the chemical properties of the AAIW (Stramma et al. 2005; Pierre et al. 1994).

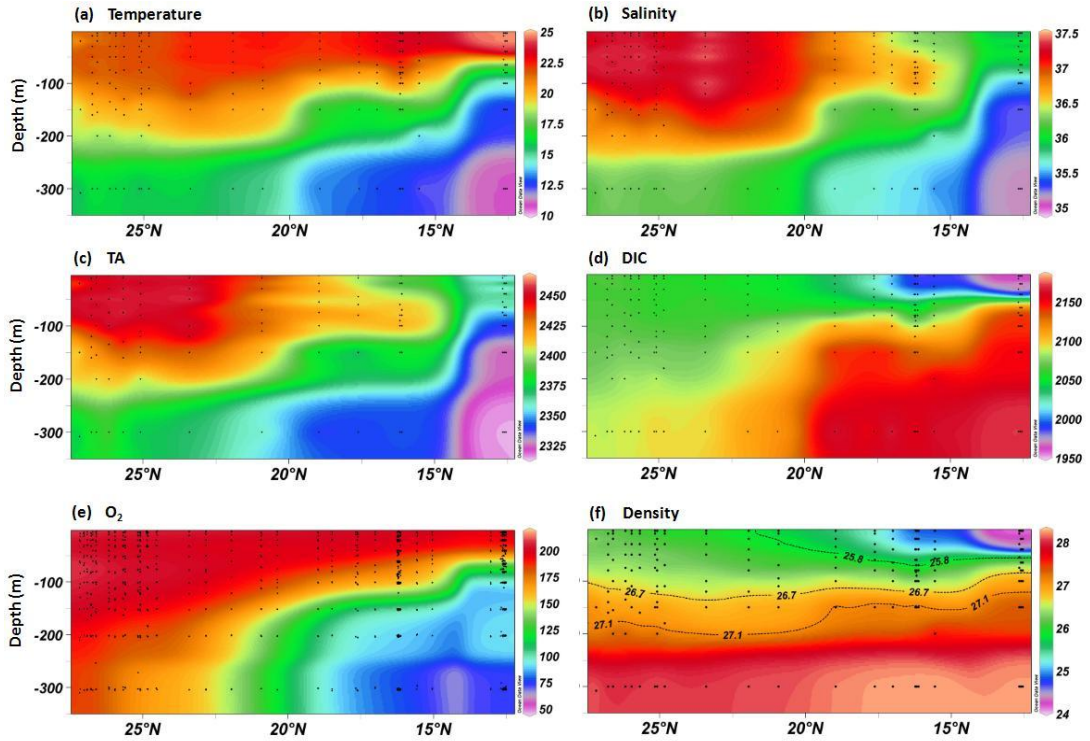

Figure 4.5. Latitudinal depth distributions in the range 0 to 350 m of (a) temperature (ºC), (b) salinity, (c) TA (µmol kg^{-1}), (d) DIC (µmol kg^{-1}), (e) dissolved oxygen (µmol kg^{-1}), and (f) density σ_t (kg m^{-3}). Data in these latitudinal plots were taken from all casts in a longitudinal zone between 20 °W and 32 °W.

The carbonate system properties of each water mass present were identified from reported hydrographic properties, along with our observations (Table 4.1). The TSW were characterized by TA and DIC concentrations ranging between 2340 and 2440 µmol kg^{-1}, and between 1950 and 2060 µmol kg^{-1}, respectively. The TA and DIC concentrations observed in the CW were consistent with the values observed by Pérez et al. (2001) and ranged between 2330 and 2460 µmol kg^{-1} for TA, and between 2050 and 2170 µmol kg^{-1} for DIC. The TA and DIC concentrations in waters influenced by AAIW (below 150 m) ranged respectively between 2310 and 2350 µmol kg^{-1}, and between 2130 and 2180 µmol kg^{-1}. This was consistent with the low TA and high DIC values previously observed in the tropical Atlantic Ocean at approximately 1000 m depth, where a stronger influence of the AAIW was observed (Goyet et al. 1998).

	T (ºC)	*Salinity*	*Density σ_t (kg m^{-3})*	*DIC (µmol kg^{-1})*	*TA (µmol kg^{-1})*
TSW	21-25[6]	35.6-37.1[6]	<25.8[1]	1950-2060[6]	2340-2440[6]
CW	18.5[2]	36.675[2]		2090[2]	2397[2]
			25.8 -27.1[1]		
	15.25-18.65[3]	35.7-36.8[3]			
	13.5-22.9[6]	35.4-37.5[6]		2050-2170[6]	2330-2460[6]
AAIW	2.4-18.6[6]	<35.4[4]	27.1-32.15[1]	2130-2180[6]	2310-2350[6]
				2230[5]	2280[5]

Table 4.1. Hydrographic and chemical characteristics of the different water masses observed from the literature and from this study: [1]Stramma et al. (2005); [2]Pérez et al. (2001); [3]Tomczak and Godfrey (2003); [4]Pierre et al. (1994); [5]Goyet et al. (1998) ; [6]This study.

Three distinctive regions were hence apparent in the surface water (Figure 4.2, 4.3 and 4.4) and depth distributions (Figure 4.5). The Canary Islands region (between 29 and 23 ºN) was characterized by higher salinity and TA distributions. The Cape Verde Islands region (between 22 and 20 ºN) was associated with higher surface water nutrient and chlorophyll-*a* concentrations. The region south of 19 ºN was associated with lower salinity and TA levels in the water column; enhanced SST and surface O_2 concentrations with lower surface DIC; low temperature and O_2 concentrations and enhanced DIC concentrations below 50 m.

4.3.3. Influence of coastal upwelling on air-sea CO_2 fluxes

The calculated air-sea CO_2 fluxes (F) showed a strong spatial variability along the cruise track and ranged from -4.0 to +1.9 mmol m^{-2} d^{-1} (Figure 4.4c). The region between the Canary Islands and the Cape Verde Islands mainly acted as a source of CO_2 to the atmosphere, with fluxes ranging between -0.5 and +1.9 mmol m^{-2} d^{-1}. The region south and west of the Cape Verde Islands acted overall as a sink of CO_2, with fluxes ranging between +0.3 and -4.0 mmol m^{-2} d^{-1}. The strongest CO_2 sink (-4.0 mmol m^{-2} d^{-1}) was observed in the southern part of the study area (13 ºN; 26 ºW) where lower surface water pCO_2 (335 µatm) and higher pH_T values (8.22) were observed. The strongest fluxes of CO_2 from the ocean to the atmosphere (+1.9 mmol m^{-2} d^{-1}) were observed in the low pH-high pCO_2 regions, and in the central part of

the cruise track where enhanced wind speeds (Figure 4.4d) of up to 15 m s^{-1} were observed.

This spatial variability in the CO_2 flux distribution was attributed to the trade-wind driven coastal upwelling off the coast of NW Africa affecting the north-eastern part of the study region (Fisher et al. 2007; Carr 2002; Mittelstaedt 1983) and to the stronger winds observed in the central part of the study region. A positive correlation was observed between the surface DIC concentrations and the air-sea CO_2 flux ($r = 0.61$; $n = 66$; $p < 0.0001$) while almost no relationship was observed between the air-sea CO_2 fluxes and the fluorescence data ($r = 0.35$; $n = 503$; $p < 0.0001$) or the temperature data ($r = -0.50$; $n = 503$; $p < 0.0001$).

Santana-Casiano et al. (2009) observed a high variability in the air-sea CO_2 fluxes associated with the complex environment of the Benguela upwelling system in the southeast Atlantic Ocean (14 to 33 ºS), with surface oceanic pCO_2 ranging between 340 and 460 µatm during the austral winter (compared with 350 to 440 µatm in this study), and the highest values associated with the influence of the coastal upwelling.

This agrees with the observations in this study where high pCO_2 and low pH_T were observed in the area affected by the coastal upwelling. Similar observations were reported for the Peruvian coastal upwelling system which exhibited high DIC (up to 2180 µmol kg^{-1}) and fCO_2 (up to 700 µatm) values in the active upwelling regions (Goyet et al. 2009). The values of fCO_2 and DIC observed in waters adjacent to the Peruvian upwelling system (430 µatm and 2080 µmol kg^{-1}, respectively) were however similar to the maximum values reported in this present study (440 µatm and 2075 µmol kg^{-1}, respectively). Extremely high pCO_2 values (1100 µatm) have also been observed along the coast in the Californian upwelling system (Feely et al. 2008), with values rapidly decreasing to 350-400 µatm away from the coast.

4.3.4. Oxygen minimum zone

Clear regional differences were apparent in dissolved oxygen and DIC profiles from casts from the three distinctive regions in our study area (Figure 4.6a and b). Cast 16392 in the northern part of the study area (see Figure 4.1 for locations of the casts) showed small variations in dissolved O_2 and DIC with depth, while cast 16407

sampled south of 13 ºN showed large differences in dissolved O_2 and DIC concentrations with depth. Cast 16400 was sampled near to the Cape Verde Islands and showed a depth distribution for DIC which appeared transitional with respect to casts 16392 and 16407.

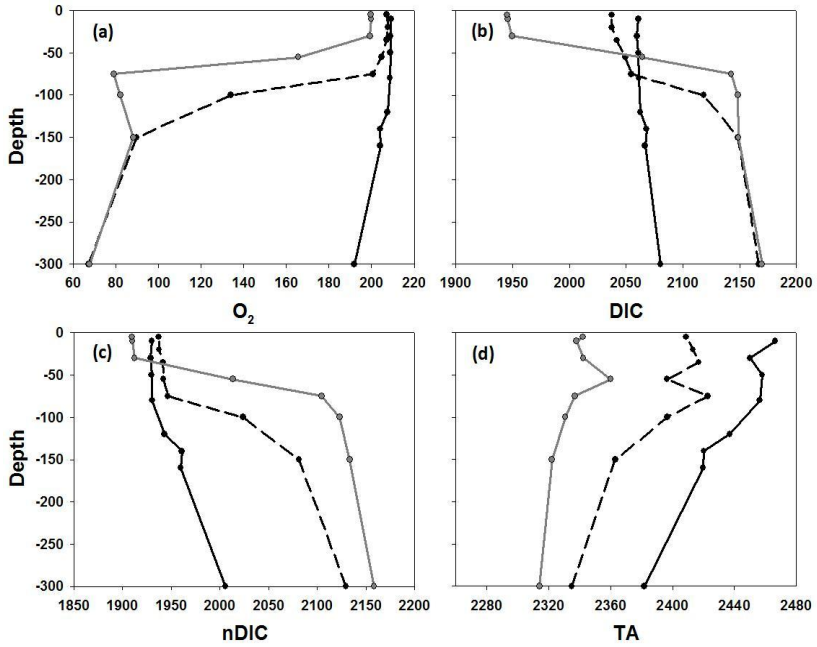

Figure 4.6. Depth profiles of (a) dissolved oxygen (µmol kg^{-1}); (b) DIC; (c) nDIC (normalized to a salinity of 35); (d) TA in µmol kg^{-1} for the casts 16392 (solid black line, North of Cape Verde Islands at 26.8 °N, 29 °W), 16400 (black dashed line, near to Cape Verde Islands at 19 °N, 25 °W) and 16407 (grey line, South of Cape Verde Islands at 12.7 °N, 27 °W).

The nDIC distribution (Figure 4.6c) showed similar surface values for the three regions, but a much sharper increase with depth around the Cape Verde Islands (cast 16400) and in the south (cast 16407), as observed for the dissolved O_2 distributions. The depth profiles of TA did not show a marked change with depth for the different regions, but showed a decrease in TA with decreasing latitude associated with the decrease in salinity and the influence of the different water masses described earlier (Figure 4.6d).

The low dissolved O_2 values (< 100 µmol kg^{-1}) observed south of 19 ºN at depths between 100 and 1000 m (Figure 4.6a and 4.7) are characteristic of the oxygen minimum zone (OMZ) located in this region (Stramma et al. 2005; 2008a and b;

2009). The OMZ observed in the sub-tropical northeast Atlantic results from slow ocean ventilation south of the Cape Verde Islands and from degradation of sinking organic matter below the euphotic zone (Stramma et al. 2008a and b; Karstensen et al. 2008). The OMZ is found along the frontier between the CW and the AAIW at depths between 200 and 800 m. The Cape Verde Frontal Zone (CVFZ) located around 21 ºN also marks the boundary between well ventilated waters north of the CVFZ and OMZ waters to the south (Stramma et al. 2005).

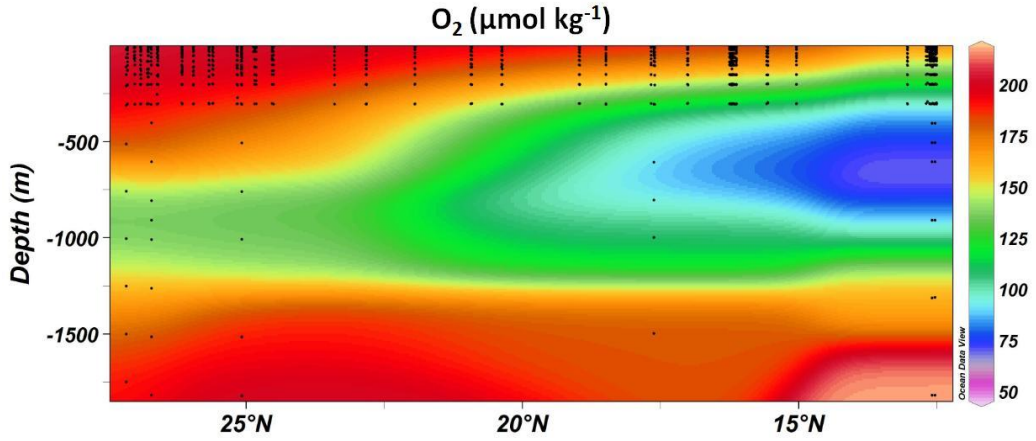

Figure 4.7. Latitudinal depth distribution of dissolved oxygen (µmol kg^{-1}) in the range 0 to 1800 m (Data from all casts in a longitudinal zone between 20 °W and 32 °W).

High DIC concentrations (> 2150 µmol kg^{-1}) were observed in the OMZ below 100 m (Figure 4.5 and 4.6b). A strong positive correlation was observed between AOU and DIC concentrations in the whole study region for depths between 100 and 4000 m (Figure 4.8), with DIC = 0.565 AOU + 2057.8 ($r = 0.97$; $p < 0.0001$; $n = 106$). Changes in DIC are strongly related to changes in AOU, as both are affected by remineralization of organic matter below the euphotic zone (Matear and Hirst 2003; Peng et al. 2003). A $\Delta DIC:\Delta AOU$ ratio of 0.56 (Figure 4.8) is fairly close to the $C:O_2$ ratio of 0.69 (Anderson and Sarmiento 1994), suggesting that remineralization of organic matter strongly influenced the DIC distribution in this area, with slow ocean ventilation being responsible for this presumably permanent low dissolved O_2/high DIC zone.

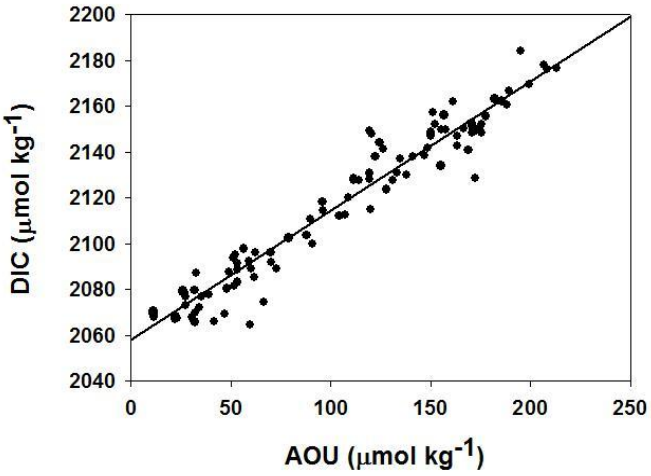

Figure 4.8. DIC and AOU relationship for samples collected at depth between 100 m and 4000 m. The least-squares regression line is shown ($r = 0.97$; $p < 0.0001$; $n = 106$). The low AOU surface values observed in the upper 100 m were not taken into account.

Our observations agree with findings for the OMZ waters of the eastern South Pacific Ocean (Goyet et al. 2009) with DIC concentrations of up to 2200 µmol kg^{-1} at 500 m (compared with 2175 µmol kg^{-1} at 300 m in this study) associated with the degradation of organic matter and TA concentrations below 2300 µmol kg^{-1} (compared with 2325 µmol kg^{-1} at 300 m in this study).

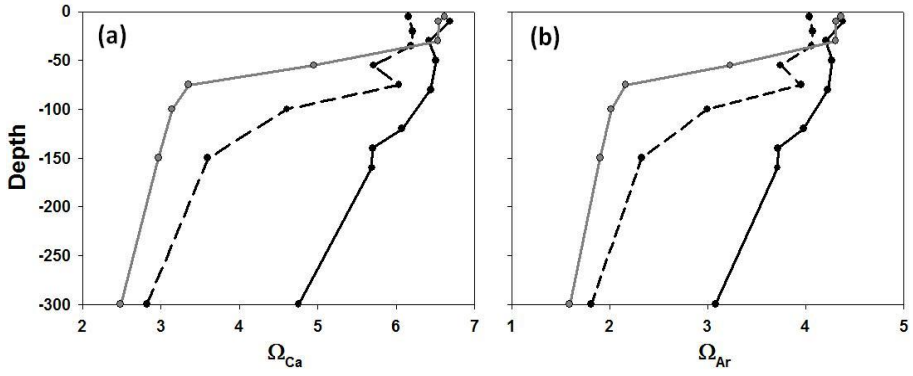

Figure 4.9. Depth profiles of (a) omega calcite (Ω_{Ca}); and (b) omega aragonite (Ω_{Ar}) for the casts 16392 (solid black line, North of Cape Verde Islands at 26.8 °N, 29 °W), 16400 (black dashed line, near to Cape Verde Islands at 19 °N, 25 °W) and 16407 (grey line, South of Cape Verde Islands at 12.7 °N, 27 °W).

Finally, low calcite and aragonite saturation states (calculated from DIC and TA, together with temperature, salinity and nutrient data) were observed in the OMZ (Ω_{Ca}

< 3 and Ω_{Ar} < 2) just below 50 m (Figure 4.9) and associated with the high DIC and low O_2 waters. An expansion of the OMZs has been observed and is expected to further increase due to future warming of the oceans with strengthened stratification and reduced ventilation (Stramma et al. 2009 and 2008b; Matear and Hirst 2003). It can be expected that this will consequently increase the DIC concentrations of the OMZs and decrease the aragonite and calcite saturation states. This process will most likely lead to sub-surface waters becoming increasingly undersaturated over time with respect to calcium carbonate, in addition to the continuing decline in saturation caused by invasion into the ocean of anthropogenic CO_2. These processes may also have a considerable impact on the nitrogen cycle due to enhanced denitrification with consequent N_2O production, and therefore on the carbon cycle through a reduction in new production (Oschlies et al. 2008; Bange et al. 2005).

4.4. Conclusions

The sub-tropical northeast Atlantic Ocean was found to exhibit regional variability of the four carbonate chemistry parameters. Strong correlations were observed between the carbonate system and hydrographic properties of the regional water masses. The spatial variability of the carbonate system was also associated with coastal upwelling off the northwest African coast and the OMZ. More particularly, the air-sea CO_2 fluxes were influenced by the coastal upwelling and high winds, resulting in CO_2 outgassing in the northern parts of the study region, in contrast to the region south of the Cape Verde Islands which was a net sink of CO_2. The carbonate system in sub-surface waters within the OMZ was strongly related to the AOU. This study showed the potential impact of the OMZ on the carbonate system due to reduced ocean ventilation and increased remineralization of organic matter, leading to an increase in DIC and a decrease in the saturation state of calcium carbonate. As observed for other systems, this study showed that upwelling-influenced marine environments are subject to low pH and low calcium carbonate saturation states and can be of particular interest for the study of the impact of ocean acidification on marine ecosystems.

Chapter 5

Mesoscale variability of the carbonate system in the Iceland Basin

5.1. Introduction

The Iceland Basin is characterized by strong mesoscale (i.e. of the order of 10 to 10^2 km) activity associated with the presence of large eddy structures (Read and Pollard 2001; Martin et al. 1998; Holligan et al. 1993). Oceanic eddies are developed due to ocean current instabilities running opposite to the main current. These mesoscale eddy structures can penetrate deep below the ocean surface waters and hence can have an important influence on primary productivity and the intensity of the spring bloom due to their role in the supply of new nutrients to the euphotic zone (Allen et al. 2005). More particularly, the North Atlantic Current (NAC; Figure 5.1) has been shown to affect the structure of the water masses and the stratification of the water column in the Iceland Basin due to complex circulation pathways (Pollard et al. 2004; Figure 5.1).

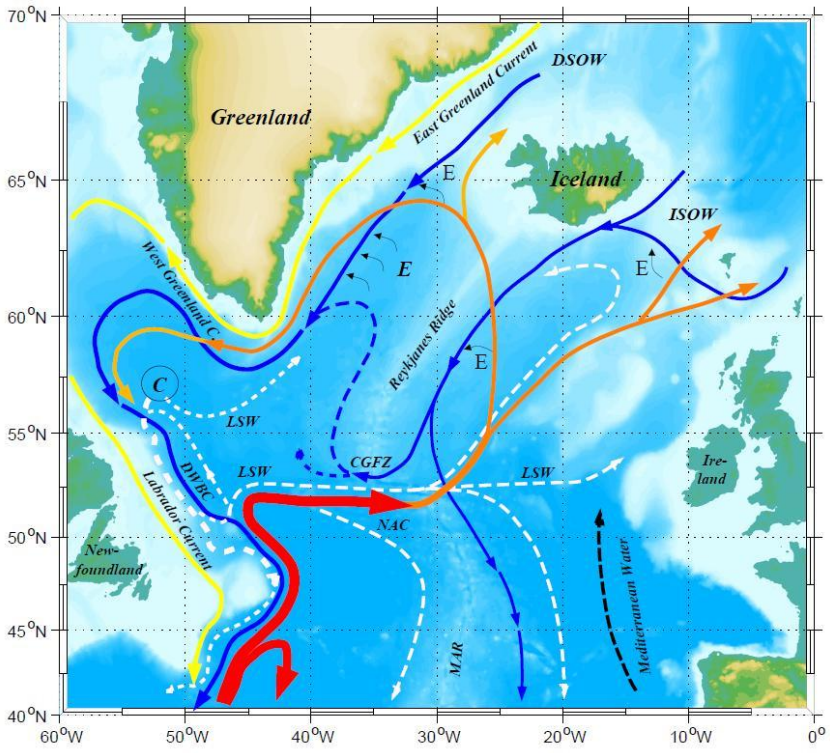

Figure 5.1. Diagram of surface and deep circulation in the North Atlantic Sub-polar Gyre, indicating locations of the North Atlantic Current (NAC), the Iceland Scotland Overflow Water (ISOW), the Denmark Strait Overflow Water (DSOW), the Deep Western Boundary Currant (DWBC), the Mid-Atlantic Ridge (MAR), and the Charlie Gibbs Fracture Zone (CGFZ) (figure obtained from the IFM-GEOMAR website at: http://www.ifm-geomar.de/index.php?id=575&L=1).

Observations have shown enhanced primary productivity associated with mesoscale eddies, resulting from the significant supply of nutrients to the surface waters associated with local upwelling within the eddy structures (Falkowski et al. 1991; McGillicuddy et al. 1998; Martin and Richards 2001; Sweeney et al. 2003; McGillicuddy et al. 2007; Bibby et al. 2008). However, little is known about the effect of mesoscale eddies on the carbonate system and more particularly on air-sea CO_2 fluxes and carbon export, due to the different effects of upwelling and enhanced biological activity on Dissolved Inorganic Carbon (DIC) concentration (Williams and Follows 1998; González-Dávila et al. 2006; Chen et al. 2008).

The objective of this study was to investigate the spatial distribution of the carbonate system parameters and their changes associated with mesoscale activity in the Iceland Basin during a post-bloom period. For this purpose, continuous high resolution potentiometric pH_T measurements were undertaken, along with DIC and Total Alkalinity (TA) measurements. An inter-comparison of the observed carbonate parameters will be discussed, as well as their relative variations associated with changes in physical and biogeochemical variables.

5.2. Methods

5.2.1. Area of study

The BIB (Biophysical Interaction in the Iceland Basin) cruise D321 took place between the 24th July and the 23rd August 2007 on the RRS *Discovery*. The aim of the cruise was to investigate the biophysical interactions taking place on an eddy-scale surface during a post-bloom period. The cruise was conducted in a box-type survey area of 100 x 100 km length scale (58.5 °N to 60 °N; 18.5 °W to 21 °W), in which four repeated surveys were conducted (Figure 5.2).

5.2.2. Sampling

The surface water sampling for discrete DIC, TA, nutrients and chlorophyll-*a* measurements was undertaken approximately every 4 hours from the underway supply of the ship (intake at about 7 m depth). Continuous sea surface temperature and salinity data were obtained from a ThermoSalinoGraph (TSG), and the

chlorophyll *a*-fluorescence data were obtained from a fluorometer (WETStar, WET Labs, USA). Both instruments were installed on the ship's underway supply. The underway temperature data from the TSG was used as it better represents the water sampled (temperature measured in the stream of sea water sampled for the carbonate system measurements), and no correction was made for warming from intake to sensor. Fifteen depth profiles were sampled for DIC, TA, chlorophyll-*a* and nutrients from 20 L Niskin bottles fitted on a stainless steel rosette frame equipped with a CTD system (Seabird) and fluorescence and oxygen sensors. Regular salinity samples were collected from the CTD casts and the underway supply and analysed on a salinometer (8400B Autosal) in order to calibrate the continuous CTD and TSG measurements. The concentrations of nitrate, phosphate and silicate were measured on-board using an auto-analyser (Skalar SanPlus) according to Kirkwood (1996). Chlorophyll-*a* concentrations were analysed on-board following the Welschmeyer (1994) method.

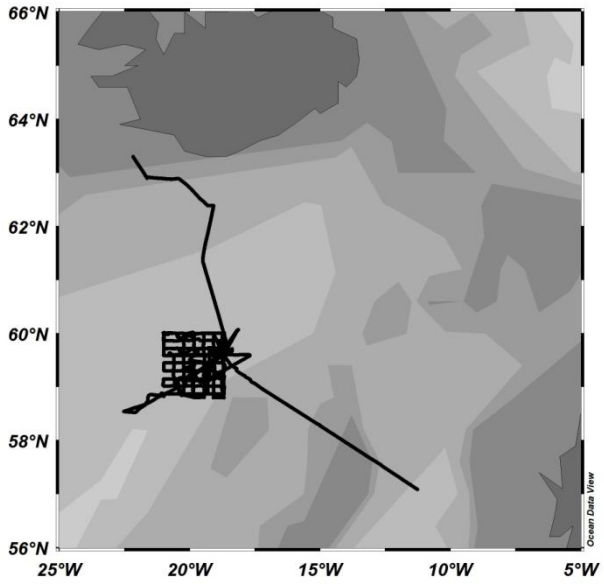

Figure 5.2. D321 cruise track and associated survey area.

5.2.3. DIC and TA measurements

The instrument used for the determination of DIC and TA was a VINDTA 3C (Marianda, Germany). DIC measurements were conducted using a coulometric titration (UIC coulometer 5011) and TA was determined using a closed-cell titration, as described in Dickson et al. (2007). Repeated measurements on the same batch of

seawater ($n \geq 3$) were undertaken at the start of every day of analysis in order to assess the precision of the method. The overall precision for the whole dataset was estimated as 1.4 ± 0.4 µmol kg^{-1} for DIC and 1.2 ± 0.5 µmol kg^{-1} for TA. Certified Reference Materials (from A.G. Dickson, Scripps Institution of Oceanography) were analysed as standards to calibrate the VINDTA system at the beginning and end of each day of analysis.

5.2.4. Underway pH measurements

During the cruise, surface underway pH_T (total scale) was measured at a frequency of one analysis per minute using a potentiometric method (Dickson et al. 2007). The pH system (Ruthern Instruments) used in this study employed a free-diffusion capillary liquid junction (2.5 M KCl) which allowed ionic contact between the hydrogen and the reference electrode. The pH cell was composed of a reference silver/silver chloride electrode (Russell pH Ltd CRR/DWG1575) and a glass pH electrode (Russell pH Ltd SW79). The calibration of the system was undertaken with TRIS buffer made up in artificial sea water according to Dickson et al. (2007). The precision of the method and drift of the instrument were estimated to be within 0.005 (estimated from the drift observed in pH from continuous measurement on the same batch of seawater, Figure 2.5). Further details of the analytical method are provided in chapter 2.

5.3. Inter-consistency of the carbonate system measurements

The measurement of three of the four parameters of the carbonate system allowed the re-calculation of the other parameters in order to test the inter-consistency of the measurements (c.f. chapter 2). The calculations were undertaken using the CO_2SYS program (Lewis and Wallace 1998; Pierrot et al. 2006). The equilibrium constants of CO_2 from Mehrbach et al. (1973), refitted by Dickson and Millero (1987) were used for the calculation. The measured pH_T was compared to the pH_T calculated from the TA and DIC data, and the two values agreed within 0.04 ± 0.02 (n = 41).

The TA measurements were compared with the TA calculated using the temperature and salinity data from the Lee et al. (2006) equation for the North Atlantic Ocean. The measured TA showed a relatively good consistency with the calculated data,

with absolute differences between the two data sets ranging between 0.2 and 17.6 µmol kg^{-1}, and with an average difference of 5.8 ± 4.1 µmol kg^{-1} (n = 165). The high differences observed between the two data sets can possibly be explained by the delay between the sample collection and the analysis. Due to some technical problems mainly involving electrode failure of the TA part of the VINDTA, the analysis of the TA samples was delayed for about a year. This could also explain the larger differences observed between the measured pH and the calculated pH when compared to the sub-tropical Northeast Atlantic dataset presented in chapter 4. However, some problems with the calibration resulting from the preparation of the TRIS buffer cannot be excluded.

5.4. Results and discussion

5.4.1. Surface distribution of the parameters

The sea surface temperature (SST) ranged between 12.4 and 14.2 °C within the survey area (Figure 5.3a). The sea surface salinity (SSS) distribution was relatively constant for the whole cruise and ranged between 35.2 and 35.5 (Figure 5.3b). The surface density distribution σ_t ranged from 26.4 to 26.8 kg m^{-3} (Figure 5.3c). The surface nitrate concentrations ranged from 1.1 to 5.4 µmol l^{-1} (Figure 5.3d). Surface pH_T ranged between pH 8.14 and 8.20 (Figure 5.3e) and chlorophyll-*a* concentrations ranged between 0.1 and 0.9 µg l^{-1} (Figure 5.3f).

Surface water concentrations of TA and nTA ranged between 2305 to 2335 µmol kg^{-1} and 2280 to 2310 µmol kg^{-1}, respectively, and surface DIC concentrations ranged between 2055 to 2085 µmol kg^{-1} for the whole cruise. The spatial resolution of surface water DIC and TA data was however too low to observe any spatial variability associated with mesoscale activity (not shown). The DIC and TA values were in the range reported by Corbière et al. (2007) for the North Atlantic sub-polar gyre (58 to 61 ºN) for the period between 1993 and 2003, with summer DIC concentrations ranging between 2060 and 2100 µmol kg^{-1} and summer TA concentrations ranging between 2290 and 2320 µmol kg^{-1}. Robertson et al. (1994) reported similar concentrations during the summer of 1991 in the Iceland Basin, with

TA ranging between 2320 and 2340 µmol kg^{-1} and DIC ranging between 2065 and 2095 µmol kg^{-1}.

A Principal Component Analysis (PCA) was conducted on the underway sampled variables and showed that 33% of the dataset variability was due to gradients in SST, salinity, DIC, nitrate, and silicate. The TA distribution did not show co-variance with any parameters according to the PCA analysis. The second and third principal components showed that the gradients in longitude and surface water density explained 20% of the variance, while latitude and temperature explained 17% of the dataset variability.

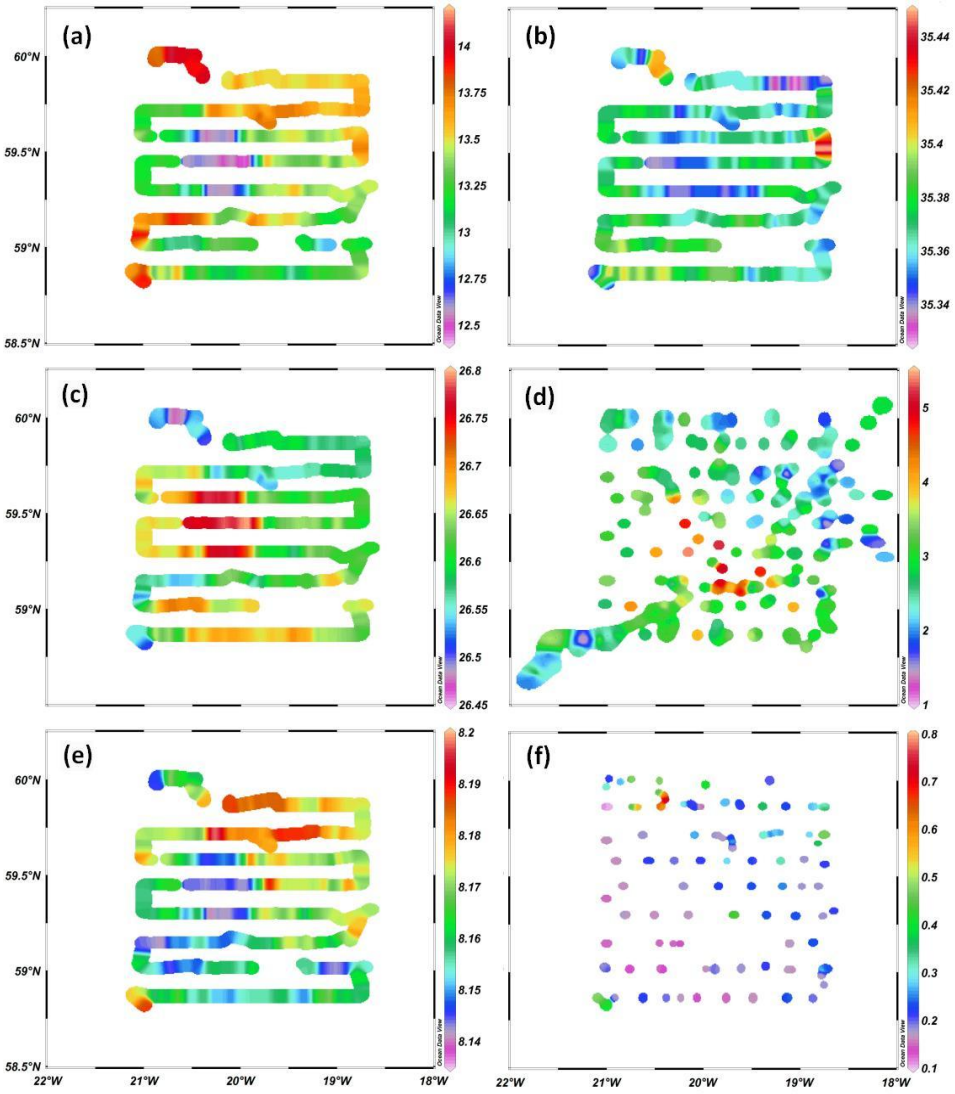

Figure 5.3. Underway surface water distributions of (a) T (°C); (b) S; (c) density σ_t (kg m^{-3}); (d) nitrate (µmol l^{-1}); (e) pH_T; and (f) chlorophyll-*a* (µg l^{-1}) for the second survey (5 - 10th August 2007).

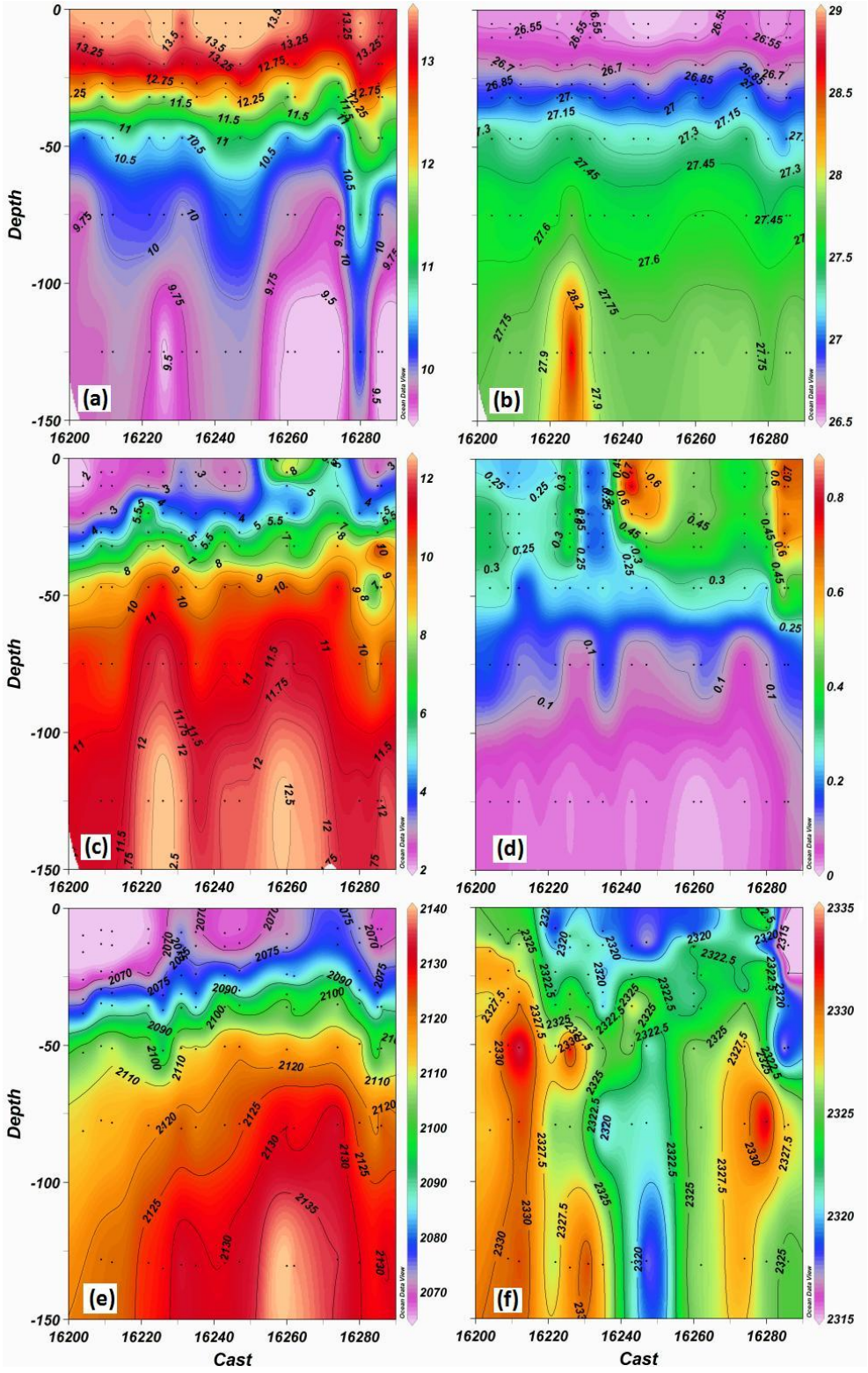

Figure 5.4. Depth profile measurements (0 to 150 m) of (a) temperature (°C); (b) density σ_t (kg m^{-3}); (c) nitrate concentrations (µmol l^{-1}); (d) chlorophyll-*a* concentrations (µg l^{-1}); (e) DIC concentrations (µmol kg^{-1}); and (f) TA concentrations (µmol kg^{-1}). The graphs are not representative of the spatial distribution in the study region, but of the temporal distribution.

5.4.2. Depth distributions of the parameters

The temperature in the water column ranged between 8 °C and 14 °C (Figure 5.4a). The salinity was relatively constant for the whole cruise and ranged between 35.2 and 35.5 (not shown). The σ_t density distribution ranged between 26.4 and 28.5 kg m^{-3} (Figure 5.4b), and nitrate between 1.1 and 12.5 µmol l^{-1} (Figure 5.4c). The chlorophyll-*a* concentrations ranged for the whole cruise between 0.01 and 0.88 µg l^{-1} (Figure 5.4d). The DIC concentrations in the water column ranged between 2060 and 2160 µmol kg^{-1} (Figure 5.4e) and were strongly correlated with temperature ($r = -0.875$; $p < 0.0001$; $n = 140$; Appendix 6) and nutrients ($r = 0.936$ for nitrate and 0.818 for phosphate; $p < 0.0001$; $n = 130$; Appendix 6). The TA concentrations in the water column showed a weak vertical gradient and ranged for the whole dataset between 2310 and 2340 µmol kg^{-1} (Figure 5.4f). TA showed a strong correlation with salinity ($r = 0.709$; $p < 0.0001$; $n = 120$; Appendix 6).

A PCA of the variables sampled on the CTD casts showed that 72% of the depth distribution variability could be explained by gradients in DIC, density, depth, temperature, salinity, nitrate and silicate. The second principal component showed that 20% of the dataset variability could be explained by gradients in TA, salinity and nitrate; which confirmed the correlation observed between TA and salinity.

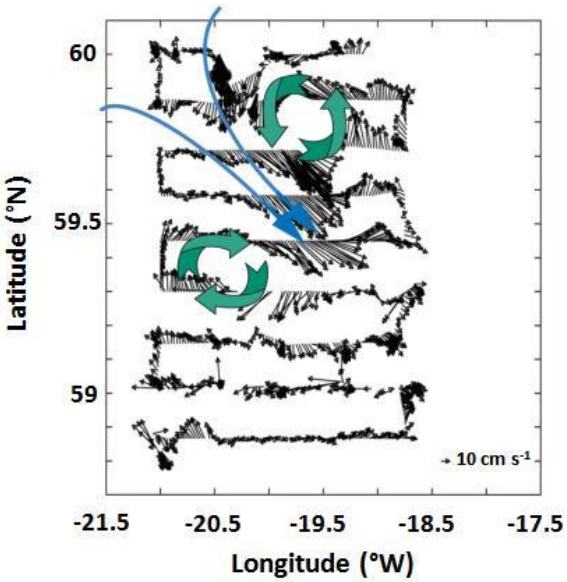

Figure 5.5. ADCP vector plot (30 m) of the second survey (5th – 10th August 2007) and approximate location of the two eddies and the central jet (from Pidcock et al. 2007).

5.4.3. Mesoscale variability associated with an eddy dipole

The development of an eddy dipole structure was observed early in the cruise in the survey area and its movement and position followed through satellite observations and use of a Vessel-Mounted Acoustic Doppler Current Profiler (VM ADCP) data (Pidcock et al. 2007). The eddy dipole was composed of an anti-cyclonic mode water eddy (AC) located in the south-western part of the survey area (position of the core during the second survey: 59.8 °N; 19.6 °W), and a cyclonic eddy (C) in the north-eastern part (59.3 °N, 20.4 °W). The approximate position of the two eddy cores and the central jet flowing in a southeasterly direction between them is shown on the ADCP vector-plot (30 m) obtained for the second survey in Figure 5.5.

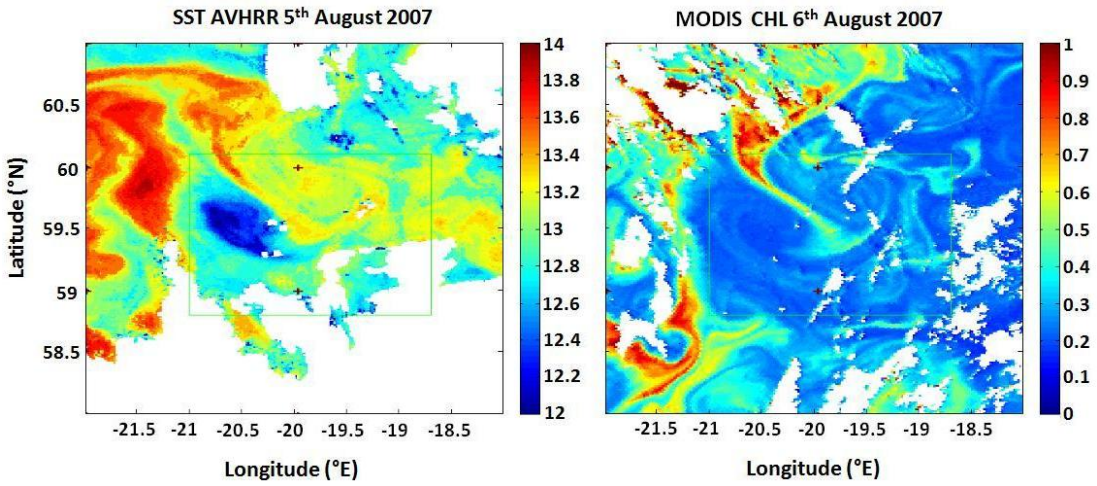

Figure 5.6. (a) Sea Surface Temperature satellite image (Advanced Very High Resolution Radiometer, AVHRR, NOAA Satellite and Information service) and (b) chlorophyll-*a* satellite image (MODIS Ocean Color, NASA); at the beginning of the second survey.

The higher pH values observed in the north of the study area (Figure 5.3e) were associated with the cyclonic eddy and the central jet positions, whereas the lower pH values observed were associated with the anti-cyclonic eddy (Figure 5.5). The SST satellite image from the beginning of the second survey showed higher temperature in the cyclonic eddy area (Figure 5.6), whereas a colder patch was observed at the anti-cyclonic eddy location, which was also observed in the SST measurements from the TSG system (Figure 5.3a). The difference in chlorophyll-*a* concentrations between the two eddies was less pronounced than differences in temperature and pH

(Figure 5.3f and 5.6b). Nevertheless, higher chlorophyll-*a* concentration was observed within the central jet and in the north of the survey area, associated with the cyclonic eddy position.

Cast	***Position relative to the eddies***	***Cast***	***Position relative to the eddies***
16204	associated with core of C	16247	central jet
16209	associated with core of AC, boundary of central jet	16260	near periphery of AC
16212	far periphery of C	16262	near periphery of C
16222	background	16274	associated with core of AC
16226	background	16280	far periphery of AC
16231	associated with core of AC	16285	associated with core of C
16235	near periphery of AC	16286	associated with core of AC

Table 5.1. List of the CTD casts and their positions related to the location of the two eddies: cyclonic (C) and anti-cyclonic (AC) (R. Pidcock, *pers. comm.*).

5.4.4. Differences between the two eddies

The positions of the stations sampled in the region of the eddy structures are provided in Table 5.1. The CTD profiles sampled at different times during the cruise showed clear differences in temperature, nitrate, DIC and chl-*a* concentrations within the two eddy cores (Figure 5.7). Surface water temperatures were higher within the cyclonic eddy (casts 16204, 16247, 16262 and 16285) and the temperature difference between the two eddy cores was approximately 0.5 °C (Figure 5.7a). Nitrate and DIC concentrations showed similar trends, with overall higher concentrations within the anti-cyclonic eddy (casts 16231, 16274 and 16286) than in the cyclonic eddy (Figure 5.7b and 5.7c). The difference in surface concentrations was up to 3 µmol l^{-1} for nitrate and up to 20 µmol kg^{-1} for DIC. Enhanced biological activity (higher chlorophyll-*a* concentrations) was observed between the start and the end of the cruise within both eddies, with highest chl-*a* concentrations in the cyclonic eddy (Figure 5.7d). The chlorophyll-*a* concentration within the cyclonic eddy was 0.23 µg l^{-1} at the start of the cruise (cast 16204), and had increased to 0.88 µg l^{-1} at the end of

the cruise (cast 16285). The chlorophyll-*a* concentration within the anti-cyclonic eddy was 0.13 µg l^{-1} at the start of the cruise (cast 16231), and had increased to 0.59 µg l^{-1} at the end of the cruise (cast 16286) (Figure 5.7d).

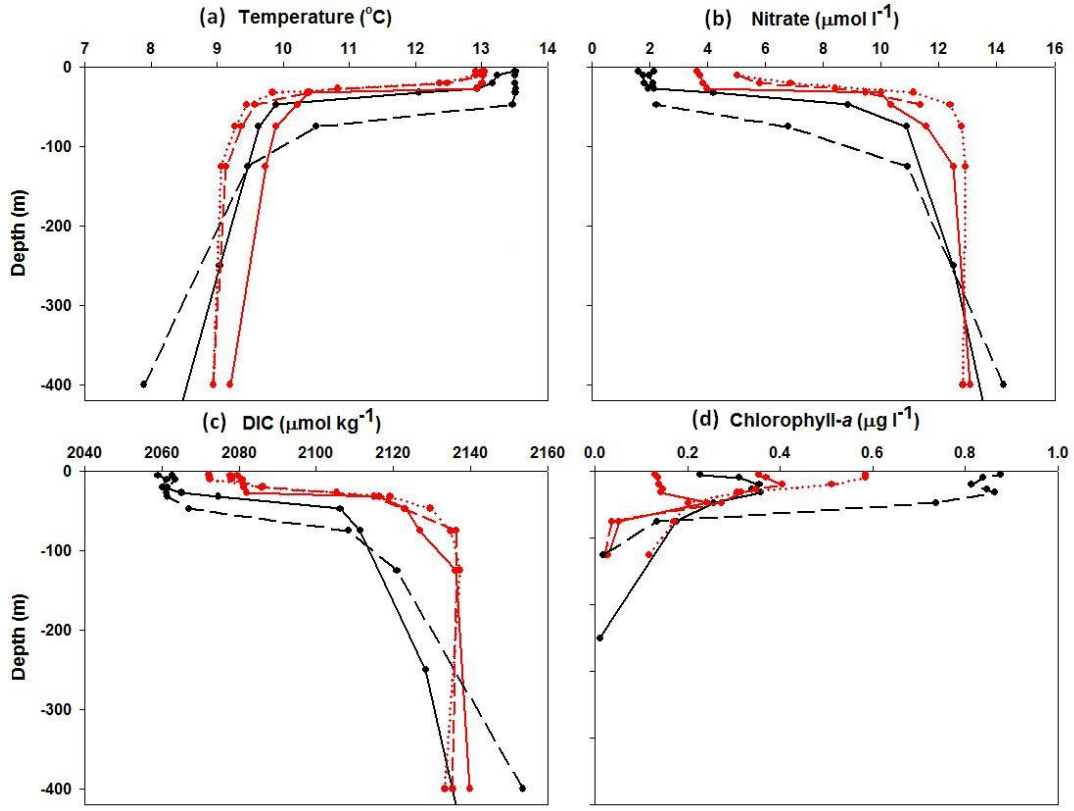

Figure 5.7. Depth profiles of (a) temperature (°C), (b) nitrate concentrations (µmol l^{-1}), (c) DIC concentrations (µmol kg^{-1}), and (d) chlorophyll-*a* concentrations (µg l^{-1}) for the casts sampled within the cyclonic eddy core: casts 16204 (black line) and 16285 (dashed black line); and within the anti-cyclonic eddy core: casts 16231 (red line), 16274 (dashed red line) and 16286 (dotted red line).

The observed differences between the two eddies could be due to different stages of development of the two eddies, in which case the local upwelling associated with the cyclonic and the anti-cyclonic eddy would have occurred over different timescales. This could explain the chlorophyll-*a* increase and the lower nitrate and DIC concentrations within the cyclonic eddy, and higher nitrate and DIC concentrations within the anti-cyclonic eddy associated with lower chlorophyll-*a* concentrations.

These results agree with previous observations of changes in the carbonate chemistry associated with a cyclonic eddy activity reported for the North Pacific sub-tropical

gyre (Chen et al. 2008). Enhanced DIC concentrations of approximately 30 µmol kg^{-1} on average were observed within the eddy core compared to the background concentration outside the eddy. Furthermore, higher chlorophyll-*a* concentration was observed in the eddy core. The differences in DIC and nitrate concentrations observed in this study between the anti-cyclonic eddy and the background region (not affected by the presence of the eddy; Table 5.1) ranged between 10 and 20 µmol kg^{-1} and between 1 and 3 µmol l^{-1}, for DIC and nitrate respectively, hence similar to the differences in concentration between the anti-cyclonic and the cyclonic eddy (Figure 5.8).

However, previous observations of CO_2 transport within a single eddy in the North Atlantic Ocean (Chipman et al. 1993) have shown eddy diffusive transport of CO_2 into the mixed layer to be negligible compared with the effect of other processes such as air-sea CO_2 gas exchange and biological CO_2 utilization/respiration.

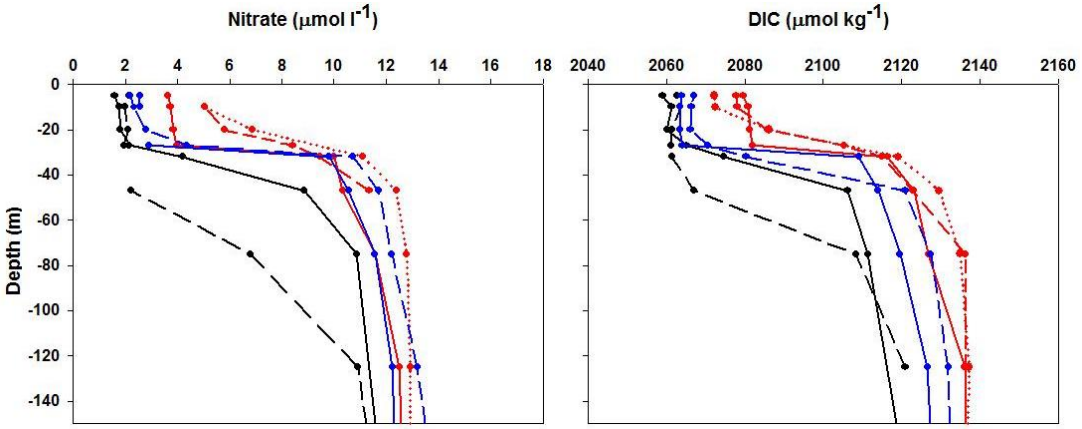

Figure 5.8. Profile distributions of nitrate concentrations (left) and DIC concentrations (right) for the casts sampled within the cyclonic eddy core: casts 16204 (black line) and 16285 (dashed black line); the anti-cyclonic eddy core: casts 16231 (red line), 16274 (dashed red line) and 16286 (dotted red line); and outside the eddy dipole (background): casts 16222 (blue line) and 16226 (dashed blue line).

Finally, the increase in chlorophyll-*a* concentration observed towards the end of the cruise in both eddies seemed to be reflected in the pH distribution, showing higher values in the whole survey area towards the end of the cruise compared to earlier on the cruise (Figure 5.9).

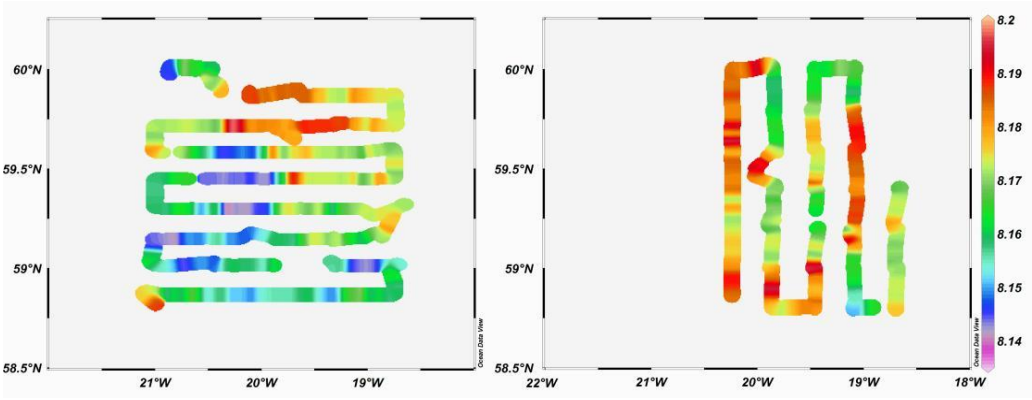

Figure 5.9. Surface pH distributions at the beginning (second survey, August 5-10th) and at the end (third survey, August 11-15th) of the cruise.

5.5. Conclusions

High spatial resolution pH measurements were obtained on cruise D321, and a detailed observation of the variability of the carbonate system was possible. The mesoscale activity observed in the Iceland Basin was shown to affect the spatial and temporal distribution of the carbonate system and was associated with the presence and development of an eddy dipole. Clear differences were observed within the eddy dipole, composed of a cyclonic eddy and an anti-cyclonic mode water eddy. The surface characteristics within the cyclonic eddy showed higher SST, lower nitrate and DIC concentrations, higher pH and higher chlorophyll-*a* concentration. The anti-cyclonic eddy was characterized by lower SST, higher surface nitrate and DIC concentrations, lower surface pH and lower chlorophyll-*a* concentration; suggesting more recent upwelling within the anti-cyclonic eddy core compared to the cyclonic eddy. The increase in primary productivity throughout the cruise was reflected in an overall increase in surface water pH values, showing a more uniform distribution later in the cruise as opposed to the beginning of the cruise when lower pH values were observed in the anti-cyclonic eddy. The importance of mesoscale eddies in local air-sea CO_2 flux is often subject to debate due to the two opposite processes affecting the surface DIC concentration. While no observation of air-sea CO_2 flux was possible (due to a problem with the measurement of the CO_2 standards), this study showed however the complexity of the carbonate system distribution associated with mesoscale activity.

Chapter 6

Summary and perspectives

6.1. Introduction

The work presented in this thesis aimed to determine and quantify the different processes that affect the carbonate system in the North Atlantic Ocean. The results obtained for various regions of the North Atlantic Ocean showed important spatial, seasonal and inter-annual variability. More precisely, this study has shown that the carbonate system was strongly affected by natural processes such as winter mixing, upwelling, remineralization, mesoscale eddies, and air and sea temperature.

As a result of anticipated future anthropogenic CO_2 emissions and climate change, the physical and biological forcings on the carbonate system will change, leading to large uncertainties in the magnitude and direction of the climate-ocean feedbacks. The results presented in this study hence confirm the need of a better understanding of the physical and biological processes controlling the carbonate system. In addition, this study highlights the importance of continuous ocean monitoring (such as time-series programs), especially in regions which will be most strongly affected by future changes such as high latitude and upwelling regions.

6.2. Summary

In order to compare the carbonate system distribution in the three North Atlantic regions studied in this thesis, the three datasets have been combined in order to look at the geographical differences (Figure 6.1). A strong spatial variability of DIC was associated with the SST distribution (Figure 6.1b and 6.1a), while SSS and TA showed similar distributions (Figure 6.1c and 6.1d). Overall, the distributions of SST and DIC were strongly correlated ($r = -0.803$; $n = 340$; $p < 0.0001$; Appendix 7) in the three study regions (Table 6.1); showing a decrease in DIC and an increase in SST with decreasing latitude (Figure 6.1). As expected, the SSS and TA distributions were also strongly correlated ($r = 0.899$; $n = 308$; $p < 0.0001$; Appendix 8) for the whole dataset.

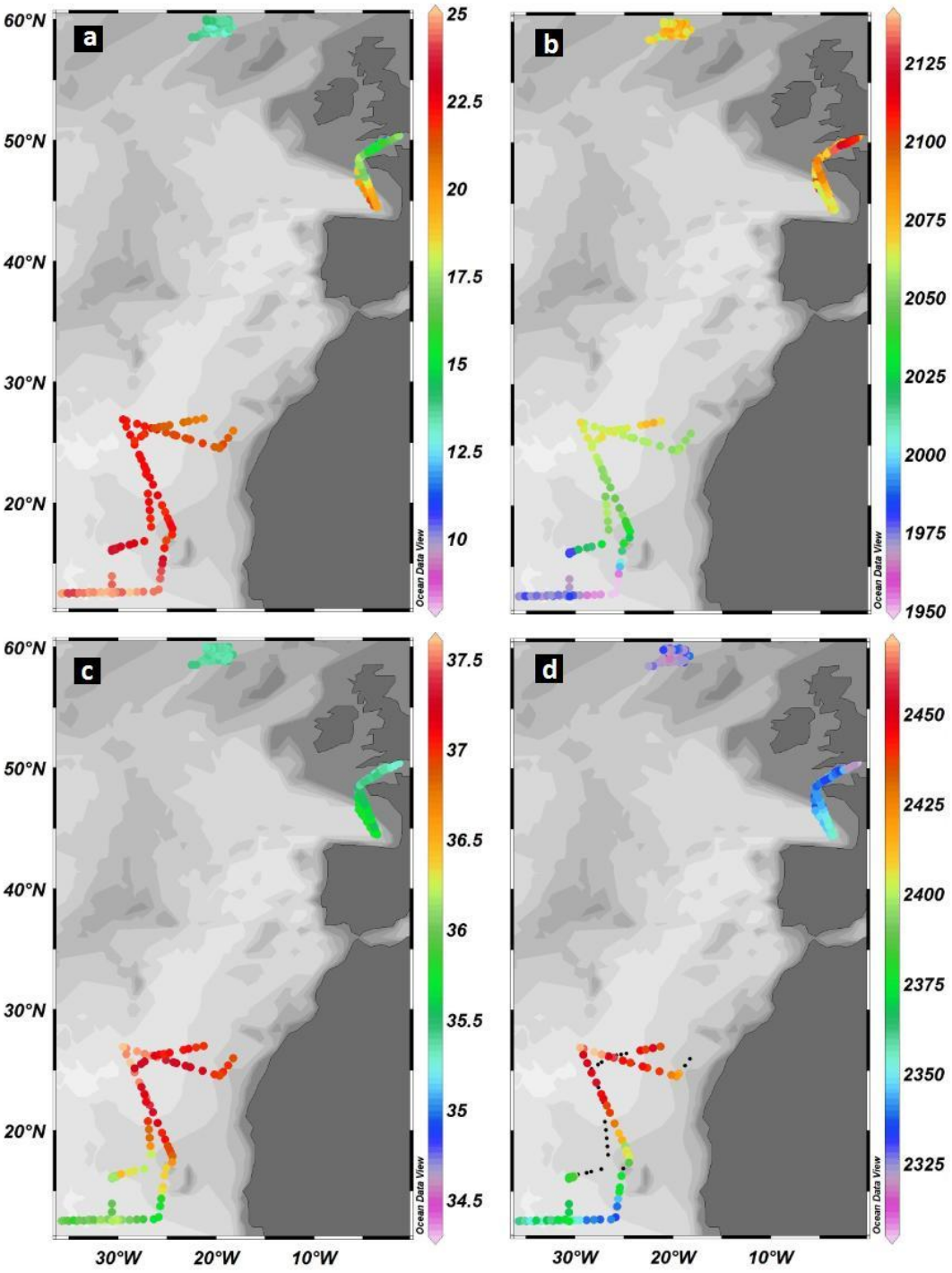

Figure 6.1. Surface water distributions of (a) Temperature (°C); (b) DIC (µmol kg^{-1}); (c) Salinity; and (d) TA (µmol kg^{-1}).

	DIC	*TA*	*Temperature*	*Salinity*
Latitude	0.663 n = 340	-0.641 n = 308	-0.836 n = 356	-0.733 n = 356
Longitude	0.756 n = 340	-0.425 n = 308	-0.624 n = 356	-0.615 n = 356
DIC		-0.249 n = 292	-0.803 n = 340	-0.381 n = 340
TA			0.573 n = 308	0.899 n = 308
Temperature				0.679 n = 356

Table 6.1. Pearson product-moment correlation coefficient (r) observed between DIC, TA, SST, SSS, Latitude and Longitude (n represents the number of samples; $p < 0.0001$).

The carbonate system was therefore strongly influenced by the hydrographic properties (temperature and salinity). The seasonal variability of the carbonate system in the Northeast Atlantic Ocean was controlled by both physics (winter mixing) and biological activity (spring/summer drawdown), and showed an increase in DIC in autumn/winter due to winter mixing, and a decrease in DIC during periods of high biological activity (chapter 3). This was also observed in the high latitude North Atlantic where the physics appeared to control the biological response associated with the presence of mesoscale eddies, and therefore the DIC and pH distributions (chapter 5). However, no significant relationship was observed between the chlorophyll *a*-fluorescence data and the DIC and TA distributions in the high latitude North Atlantic, which can be attributed to poor spatial resolution in the sampling. In the oligotrophic region of the sub-tropical Northeast Atlantic, no significant relationship was observed between the chlorophyll *a*-fluorescence data and the DIC and TA distributions (chapter 4) which is most likely due to the oligotrophic nature of this region.

Although the physics appeared to be the main forcing on the carbonate system in this study (through the influence of events such as coastal upwelling, mesoscale eddies, wind speed, and differences in winter mixing and temperature); the role of biological activity in the seasonality of the carbonate system is highly important. However,

physical forcings tend to set the level for biological drawdown and therefore highly contribute to the variability of the carbonate system and CO_2 fluxes.

6.3. Recommendations and perspectives

6.3.1. Quality controlled carbonate system databases

A range of projects generate large datasets of quality controlled surface ocean CO_2 measurements for the world's oceans. The Carbon Dioxide Information Analysis Center (CDIAC) is responsible of grouping the data and information of programs such as the GLobal Ocean Data Analysis Project (GLODAP), which represents a high quality dataset as part of the Joint Global Ocean Flux Study (JGOFS), the World Ocean Circulation Experiment (WOCE) and Ocean Atmosphere Carbon Exchange Study (OACES) projects (Key et al. 2004); the International Ocean Carbon Coordination Project (IOCCP); the Surface Ocean CO_2 Atlas (SOCAT) project; the CARbon IN the Atlantic Ocean (CARINA) data synthesis project; and the Volunteer Observing Ship (VOS) programs. This approach is important in order to compare past and future measurements and to study the impact of climate change and anthropogenic CO_2 on the oceanic carbon cycle.

6.3.2. Importance of climate models

While direct measurements are crucial, it is also important to predict the changes in the carbonate system and marine ecosystem that may occur with future climate change and anthropogenic CO_2 emissions. In order to determine the positive and negative feedbacks of climate change on the ocean carbon cycle and carbon sequestration, climate-ocean coupled models are required (Bopp et al. 2005 and 2001; Schmittner 2005; Schneider et al. 2008). Although there are still large uncertainties on the model results (Schmittner et al. 2005; Watson 2008), the use of such coupled climate-ocean models is important, along with continuous observations, to obtain alternative solutions and to reduce the impacts of climate change. Furthermore, it is important to note that some of the model predictions made over the last decade are currently being observed in the oceans.

6.3.2.1. Ocean circulation

Several climate-ocean models have predicted a decrease in ocean circulation associated with future climate change (Bopp et al. 2005 and 2001; Schmittner et al. 2005). More particularly, Schmittner et al. (2005) predicted a possible weakening of the North Atlantic thermohaline circulation of up to 25% by the end of the century. It is therefore important to improve our understanding of ocean circulation as it determines surface nutrients supply and consequently primary productivity (Najjar et al. 2007). Schneider et al. (2008) concluded that the changes in ocean circulation and nutrient cycling as a result of climate change will impact primary production and export production, and thus requires a better understanding of the controlling mechanisms.

A strong relationship has been observed between marine productivity and climate variability such as changes in upper-ocean temperature and stratification, in both models and satellite ocean-color observations (Schneider et al. 2008; Behrenfeld et al. 2006). More precisely, changes in temperature and ocean stratification seem to have decreased net primary production over the past decade (Behrenfeld et al. 2006). However, productivity and export processes are still poorly understood and are therefore difficult to include in models (Schneider et al. 2008).

Future warming of the ocean surface could be responsible for a decrease in oceanic carbon uptake due to a decreased solubility of CO_2 with increasing temperature, and the weakening of ocean circulation which will also reduce the penetration of anthropogenic carbon (Bopp et al. 2005; Sarmiento et al. 1998). Bopp et al. (2005) reported a possible decrease in carbon export by up to 25% when future CO_2 atmospheric concentrations will reach four times the CO_2 pre-industrial conditions (set at approximately 286 ppm), and a decrease in primary productivity of 15%. Major phytoplankton groups such as diatoms, key players in the biological carbon pump, would be affected by the reduction in nutrient inputs associated with future climate change and would be replaced by smaller phytoplankton groups (Bopp et al. 2005). This will hence have a strong feedback on the global carbon cycle by reducing the efficiency of the biological carbon pump (Bopp et al. 2005).

6.3.2.2. High latitudes

The increase in sea surface and air temperature due to anthropogenic greenhouse gas emissions is responsible for the decrease in sea-ice and the melting of glaciers (Levitus et al. 2000 and 2001; Barnett et al. 2005). Some areas of the world's oceans are thought to be more affected in a high CO_2 world, such as the high latitude regions where enhanced ocean acidification and undersaturation of calcium carbonate is expected due to water freshening (sea ice melting) and increased carbon uptake (Steinacher et al. 2009; Orr et al. 2005).

Model estimates of ocean acidification in the Arctic Ocean suggest that undersaturation with respect of aragonite could be observed in the surface waters as early as 2016 (atmospheric CO_2 concentration of 409 ppm); and for the whole water column by the end of the century (atmospheric CO_2 concentration of 765 ppm), with a decrease in pH of up to 0.45 (Steinacher et al. 2009). These model estimates based on direct observations (Jutterström and Anderson 2005) agree with recent studies showing seasonal surface aragonite undersaturation influenced by sea ice melting (Bates et al. 2009). Similar predictions have been made for the Southern Ocean where undersaturation with respect to aragonite could also be observed for the entire Southern Ocean's surface by 2100 (Orr et al. 2005). This is expected to have severe impacts on marine ecosystems in these high latitude regions (Royal Society 2005).

6.3.3. Carbon sequestration and geo-engineering

A mechanistic and quantitative understanding of biogeochemical cycles is required to predict future changes in our oceans. Ocean acidification is an important consequence of rising atmospheric CO_2 concentrations due to the penetration of anthropogenic CO_2 into the ocean which alters the carbonate chemistry. However, other severe changes as a result of increasing greenhouse gas emissions are expected, including global warming, sea-ice and glacier melting, bleaching of coral reefs, undersaturation of calcium carbonate, and weakening of the oceanic CO_2 uptake. The increase in the efficiency of the biological pump is one of the major challenges that geo-engineering policies are trying to achieve in order to improve carbon export efficiency in the future. The reduction of greenhouse gases emissions is however the

most important first step in the process of reducing atmospheric CO_2 concentrations, but radical actions will most likely be needed (Royal Society 2009). Due to the uncertainty of the economic and ecologic impacts of the geo-engineering scenarios, no program can commence until we have seriously determined the risks of such actions.

Among the scenarios investigated in order to reduce atmospheric CO_2 concentrations (Royal Society 2009), the stimulation of carbon sequestration by ocean iron fertilization has received much attention (Lampitt et al. 2008). While natural iron fertilization in the Southern Ocean have been shown to enhance short-term carbon export (Pollard et al. 2009; Blain et al. 2007), the efficiency of artificial iron fertilization to enhance carbon export is still uncertain (Boyd et al. 2007). However, some possible side-effects are expected such as enhanced ocean acidification and undersaturation of calcium carbonate in the deeper layers, or coastal eutrophication (Royal Society 2009; Lampitt et al. 2008). It is hence still unsure whether this option is globally significant regarding its efficacy compare to the risks and side effects predicted and therefore still demand further investigation (Lampitt et al. 2008).

6.3.4. Atlantic Ocean vs. Pacific Ocean

Finally, while this thesis has been focused on the North Atlantic Ocean, it is interesting to compare this ocean basin with the rest of the Atlantic Ocean as well as with the Pacific Ocean in terms of carbon sequestration. As explained earlier, the North Atlantic Ocean is characterized by the formation of the North Atlantic Deep Waters which make this ocean basin the biggest sink of anthropogenic CO_2. In fact, the North Atlantic carbon storage was estimated to approximately 23% of the global oceanic anthropogenic CO_2, while it covers only 15% of the global ocean area (Sabine et al. 2004). While a large difference in anthropogenic CO_2 content is observed between the North Atlantic and the North Pacific, the Southern hemisphere shows similar distributions in both basins and stores approximately 60% of the total oceanic anthropogenic CO_2 (Sabine et al. 2004).

Appendices

Appendix 1:

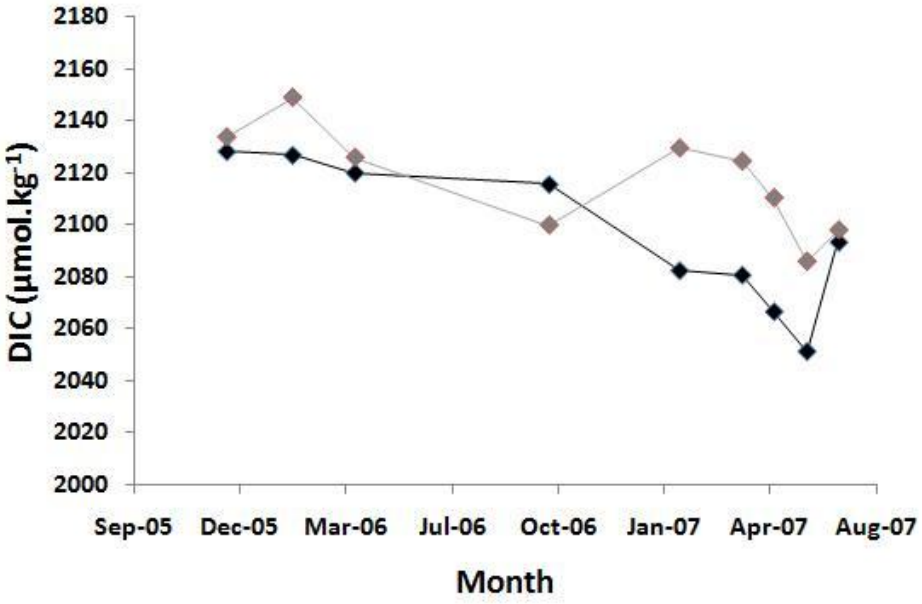

Figure A.3. Comparison of the DIC data (µmol kg^{-1}) measured from the *Pride of Bilbao* (black line) and the DIC calculated from the *Santa Maria f*CO_2 data (grey line; chapter 3).

Appendix 2:

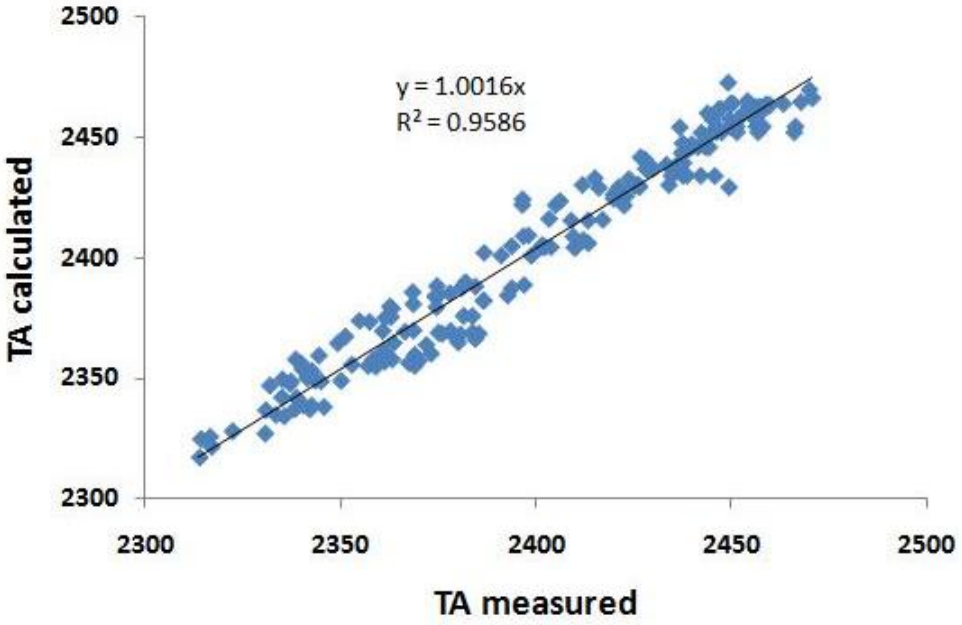

Figure A.4. Comparison of TA measured and TA (µmol kg^{-1}) calculated from temperature and salinity data (Lee et al. 2006) in the Sub-Tropical North Atlantic Ocean (chapter 4).

Appendix 3:

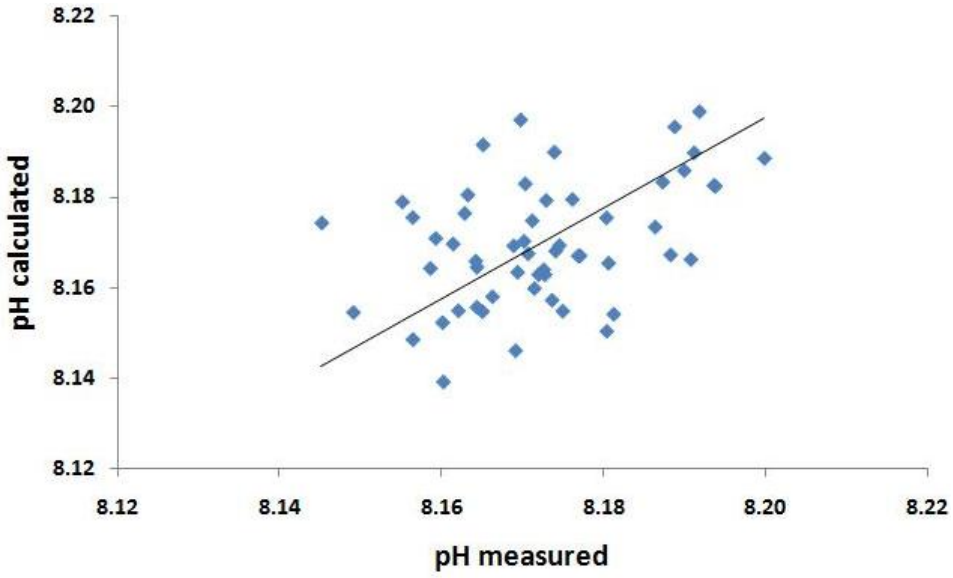

Figure A.5. Comparison of pH measured and pH calculated from DIC and TA measurements for the sub-tropical Northeast Atlantic Ocean (chapter 4).

Appendix 4:

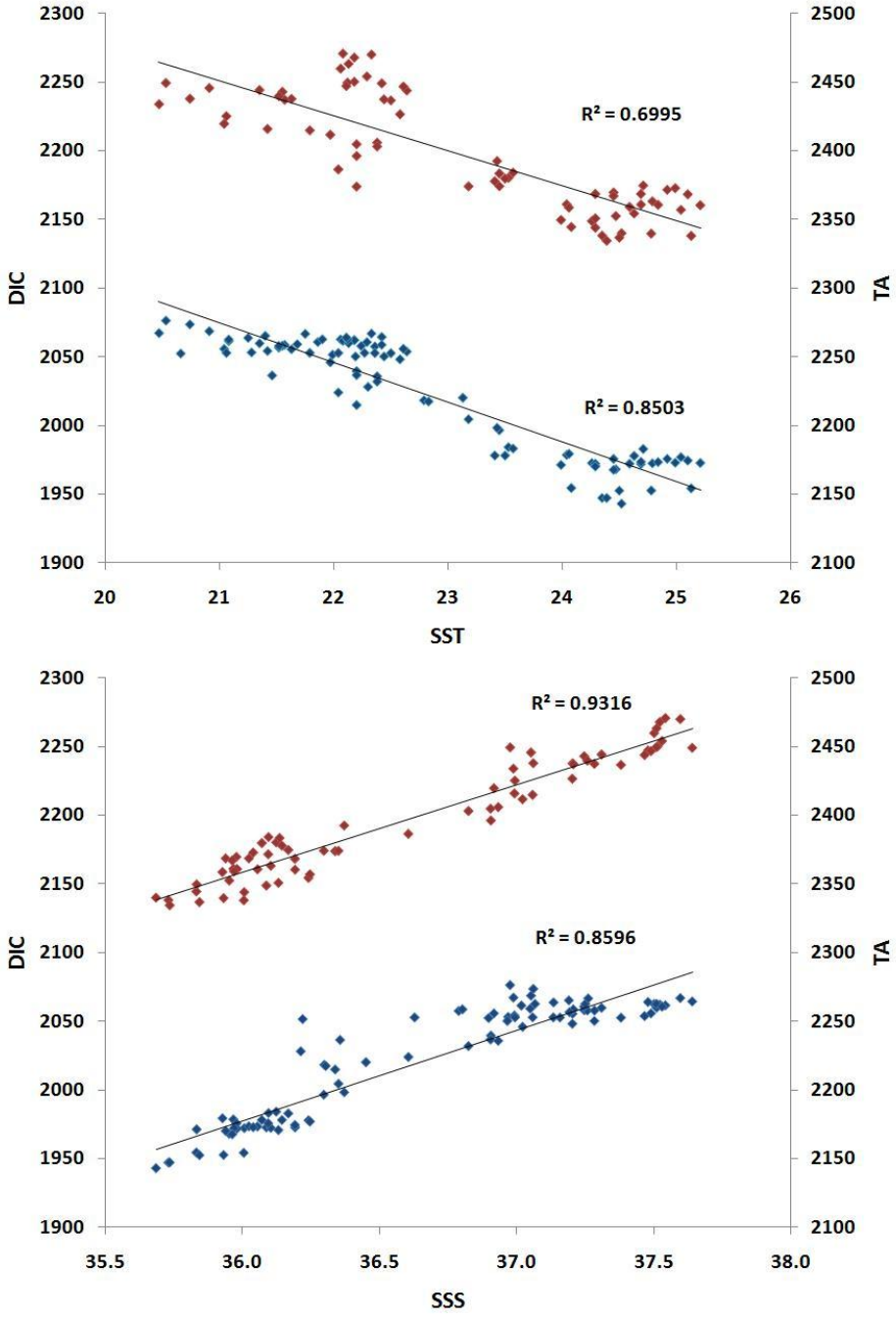

Figure A.6. Correlation observed between the underway DIC (µmol kg^{-1}; blue dots), underway TA (µmol kg^{-1}; red dots), and the SST data (°C; top panel); and between the underway DIC (µmol kg^{-1}; blue dots), underway TA (µmol kg^{-1}; red dots) and the SSS data (bottom panel) for the sub-tropical Northeast Atlantic Ocean (chapter 4).

Appendix 5:

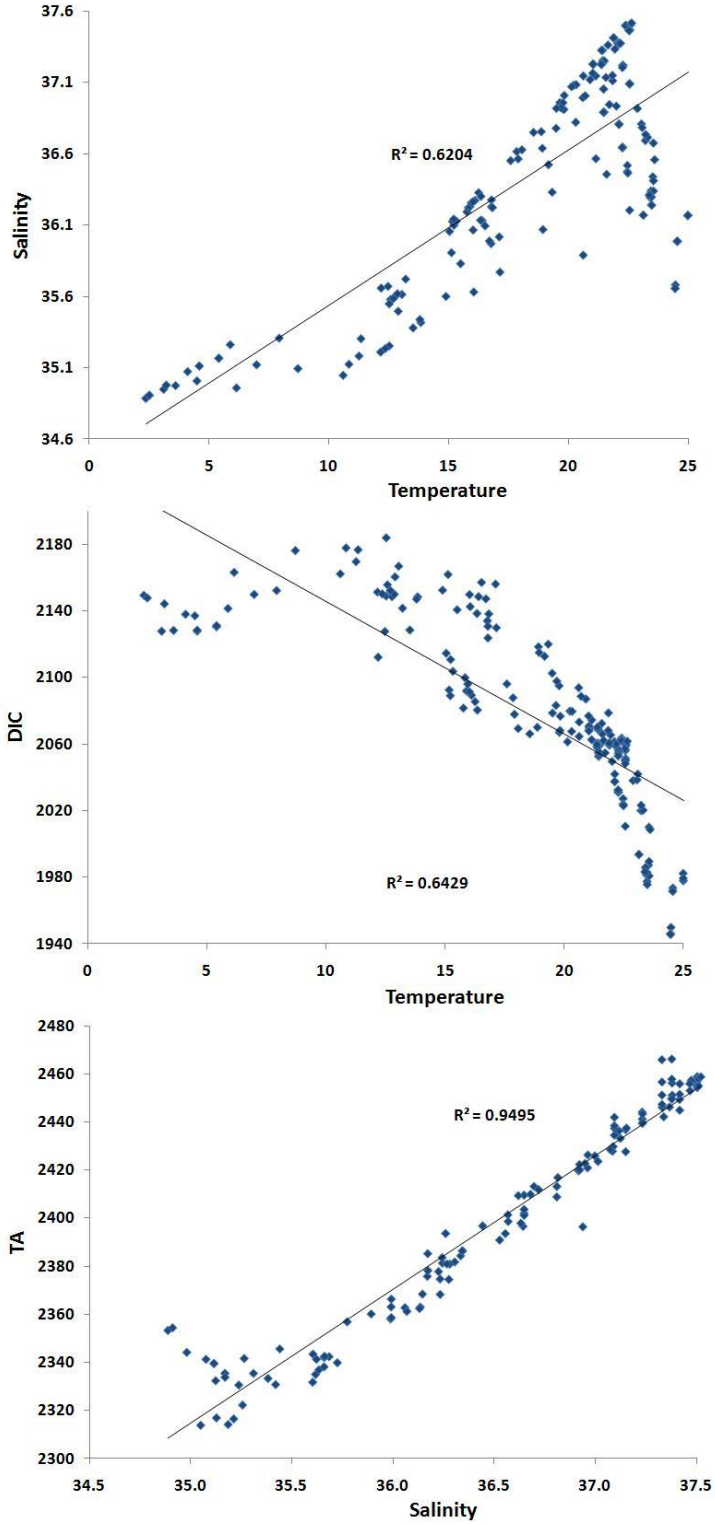

Figure A.7. Correlation observed between the salinity and temperature depth distributions; the DIC (µmol kg^{-1}) and temperature (°C) depth distribution; and the TA (µmol kg^{-1}) and salinity depth distribution for the sub-tropical Northeast Atlantic Ocean (chapter 4).

Appendix 6:

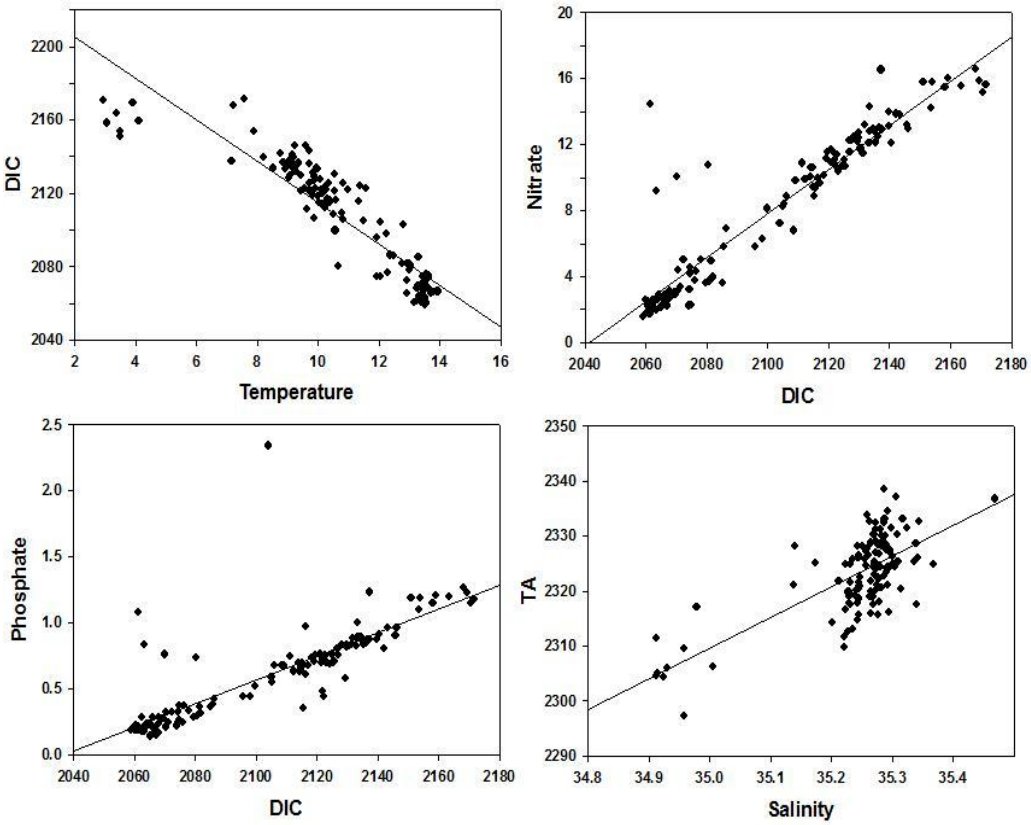

Figure A.8. Correlation observed between the depth distributions of DIC and Temperature (top left); Nitrate and DIC (top right); Phosphate and DIC (bottom left); and TA and Salinity (bottom right) in the Iceland Basin (chapter 5).

Appendix 7:

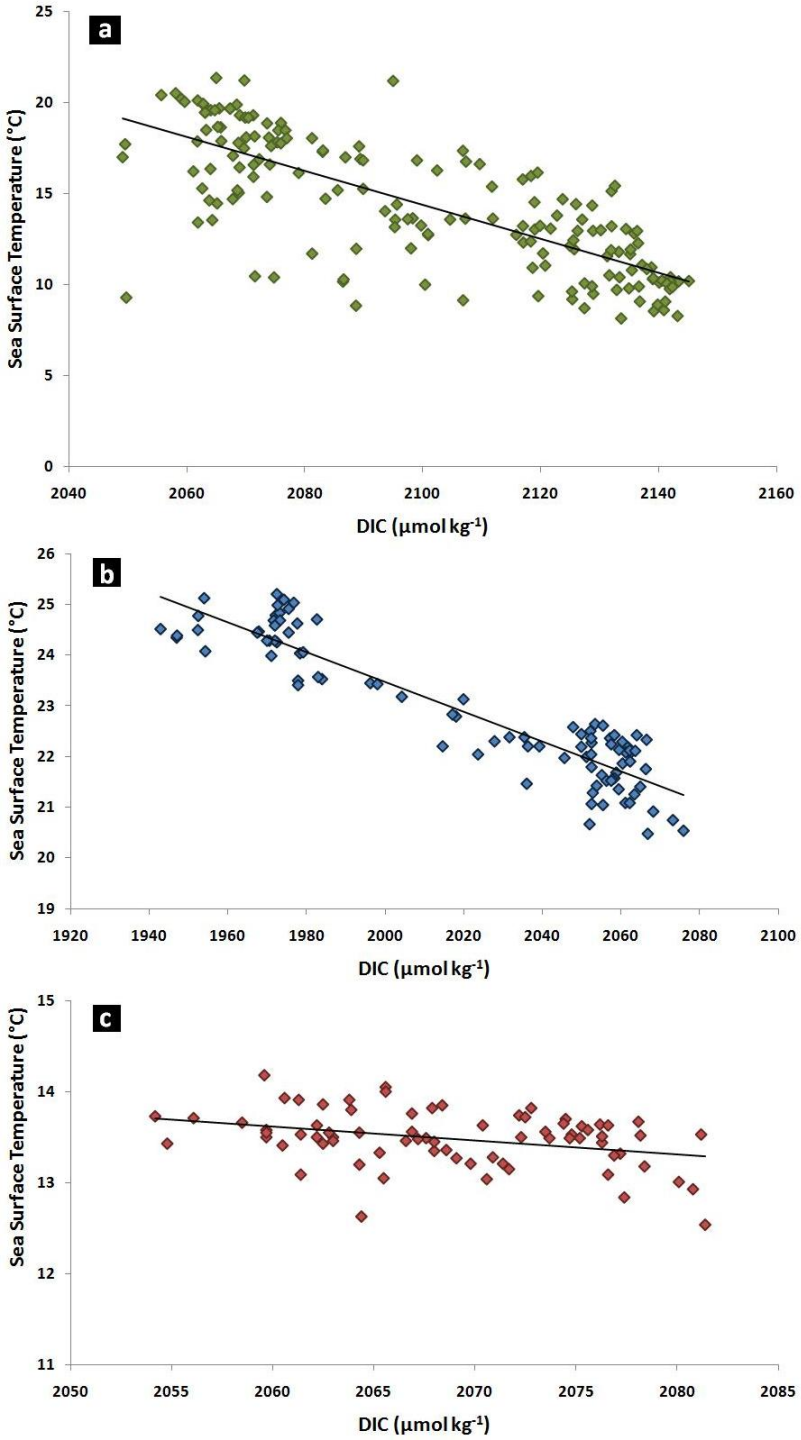

Figure A.9. Correlation observed between sea surface DIC (µmol kg^{-1}) and temperature (°C) data for (a) the Northeast Atlantic Ocean (chapter 3); (b) the sub-tropical Northeast Atlantic Ocean (chapter 4); and (c) the Iceland Basin (chapter 5).

Appendix 8:

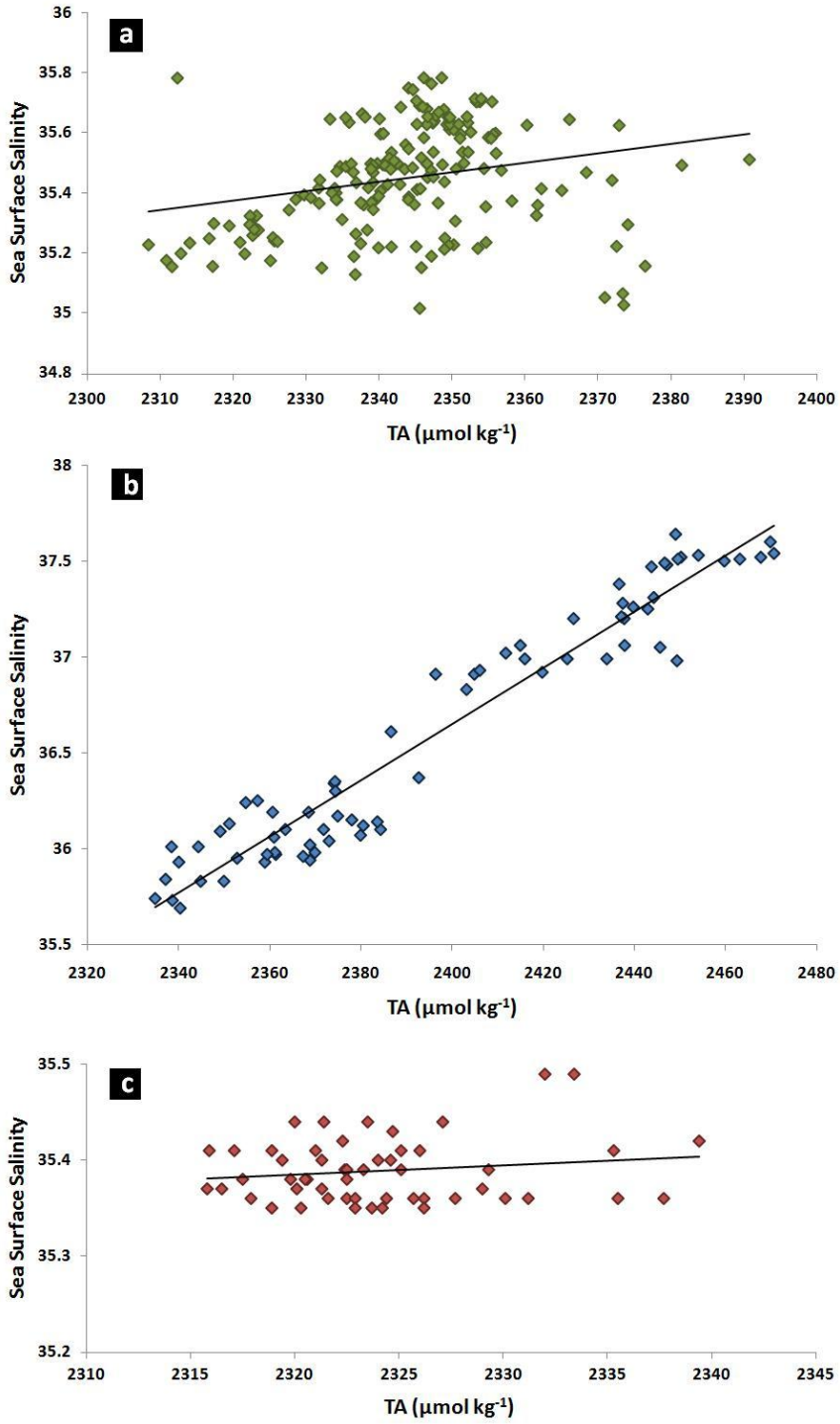

Figure A.10. Correlation observed between sea surface TA (µmol kg^{-1}) and salinity data for (a) the Northeast Atlantic Ocean (chapter 3); (b) the sub-tropical Northeast Atlantic Ocean (chapter 4); and (c) the Iceland Basin (chapter 5).

References

Álvarez, M., Fernández, E., Pérez, F.F., 1999. Air-sea CO_2 fluxes in a coastal embayment affected by upwelling: physical versus biological control. *Oceanol. Acta* **22,** 499-515.

Anderson, L.A., Sarmiento, J.L., 1994. Redfield ratios of remineralization determined by nutrient data analysis. *Global Biogeochem. Cycles* **8,** 65-80.

Anderson, T.R., Totterdell, L.J., 2004. Modelling the response of the biological pump to climate change. In: Follows, M. and Oguz, T. (Eds.). The Ocean Carbon Cycle and Climate, *NATO Science Series IV* **40**, Kluwer, 65-96.

Allen, J.T., Brown, L., Sanders, R., Moore, C.M., Mustard, A., Fielding, S., Lucas, M., Rixen, M., Savidge, G., Henson, S., Mayor, D., 2005. Diatom carbon export enhanced by silicate upwelling in the northeast Atlantic. *Nature* **437,** 728-732.

Bange, H.W., Naqvi, S.W.A., Codispoti, L.A., 2005. The nitrogen cycle in the Arabian Sea. *Progr. Oceanogr.* **65,** 145-158.

Bargeron, C.P., Hydes, D.J., Woolf, D.K., Kelly-Gerreyn, B.A., Qurban, M.A., 2006. A regional analysis of new production on the northwest European shelf using oxygen fluxes and a ship-of-opportunity. *Estuarine, Coastal and Shelf Science* **69**, 478-490.

Barnett, T.P., Pierce, D.W., AchutaRao, K.M., Glecker, P.J., Santer, B.D., Gregory, J.M., Washington, W.M., 2005. Penetration of human-induced warming into the World's Oceans. *Science* **309,** 284-287.

Bates, N.R., Michaels, A.F., Knap, A.H., 1996a. Seasonal and interannual variability of oceanic carbon dioxide species at the US JGOFS Bermuda Atlantic time-series study (BATS) site. *Deep-Sea Res. II* **43**, 347-383.

Bates, N.R., Michaels, A.F., Knap, A.H., 1996b. Alkalinity changes in the Sargasso Sea: geochemical evidence of calcification? *Mar. Chem.* **51,** 347-358.

Bates, N.R., 2001. Interannual variability of oceanic CO_2 and biogeochemical properties in the Western North Atlantic subtropical gyre. *Deep-Sea Res. II* **48**, 1507-1528.

Bates, N.R., 2007. Interannual variability of the oceanic CO_2 sink in the subtropical gyre of the North Atlantic Ocean over the last 2 decades. *J. Geophys. Res.* **112,** C09013, doi:10.1029/2006JC003759.

Bates, N.R., Mathis, J.T., Cooper, L.W., 2009. Ocean acidification and biologically induced seasonality of carbonate saturation states in the western Arctic Ocean. *J. Geophys. Res.* **114,** C11007, doi:10.1029/2008JC004862.

Bates, R.G., Bower, V.E., 1954. Standard potential of the silver-silver-chloride electrode from 0° to 95 °C and the thermodynamic properties of dilute hydrochloric acid solutions. *Journal of Research of the National Bureau of Standards* **53,** 283-290.

Bates, R.G., 1964. Determination of pH, Theory and Practice. John Wiley & Sons, Inc, Second edition, New York, 435pp.

Behrenfeld, M.J., O'Malley, R.T., Siegel, D.A., McClain, C.R., Sarmiento, J.L., Feldman, G.C., Milligan, A.J., Falkowski, P.G., Letelier, R.M., Boss, E.S., 2006. Climate-driven trends in contemporary ocean productivity. *Nature* **444,** 752-755.

Bellerby, R.G.J., Turner, D.R., Millward, G.E., Worsfold, P.J., 1995. Shipboard flow injection determination of sea water pH with spectrophotometric detection. *Analytica Chimica Acta* **309,** 259-270.

Bellerby, R.G.J., Olsen, A., Johannessen, T., Croot, P., 2002. A high precision spectrophotometric method for on-line shipboard seawater pH measurements: the automated marine pH sensor (AMpS). *Talanta* **56,** 61-69.

Benson, B.B., Krause, D., 1984. The concentration and isotopic fractionation of oxygen dissolved in freshwater and seawater in equilibrium with the atmosphere. *Limnol. Oceanogr.* **29,** 620-632.

Bibby, T.S., Gorbunov, M.Y., Wyman, K.W., Falkowski, P.G., 2008. Photosynthetic community responses to upwelling in mesoscale eddies in the subtropical North Atlantic and Pacific Oceans. *Deep-Sea Res. II* **55,** 1310-1320.

Blain, S., Quéguiner, B., Armand, L., Belviso, S., Bombled, B., Bopp, L., Bowie, A., Brunet, C., Brussaard, C., Carlotti, F., Christaki, U., Corbière, A., Durand, I., Ebersbach, F., Fuda, J.-L., Garcia, N., Gerringa, L., Griffiths, B., Guigue, C., Guillerm, C., Jacquet, S., Jeandel, C., Laan, P., Lefèvre, D., Lo Monaco, C., Malits, A., Mosseri, J., Obernosterer, I., Park, Y.-H., Picheral, M., Pondaven, P., Remenyi, T., Sandroni, V., Sarthou, G., Savoye, N., Scouarnec, L., Souhaut, M., Thuiller, D., Timmermans, K., Trull, T., Uitz, J., van Beek, P., Veldhuis, M., Vincent, D., Viollier, E., Vong, L., Wagener, T., 2007. Effect of natural iron fertilization on carbon sequestration in the Southern Ocean. *Nature* **446,** 1070-1075.

Bopp, L., Monfray, P., Aumont, O., Dufresne, J.-L., Le Treut, H., Madec, G., Terray, L., Orr, J.C., 2001. Potential impact of climate change on marine export production. *Global Biogeochem. Cycles* **15**, 81-99.

Bopp, L., Aumont, O., Cadule, P., Alvain, S., Gehlen, M., 2005. Response of diatoms distribution to global warming and potential implications: a global model study. *Geophys. Res. Lett.* **32,** L19606, doi:10.1029/2005GL023653.

Borges, A.V., Frankignoulle, M., 2003. Distribution of surface carbon dioxide and air-sea exchange in the English Channel and adjacent areas. *J. Geophys. Res.* **108,** C53140, doi:10.1029/2000JC000571.

Borges, A.V., Schiettecatte, L.-S., Abril, G., Delille, B., Gazeau, F., 2006. Carbon dioxide in European coastal waters. *Estuarine, Coastal and Shelf Science* **70,** 375-387.

Boyd, P.W., Jickells, T., Law, C.S., Blain, S., Boyle, E.A., Buesseler, K.O., Coale, K.H., Cullen, J.J., de Baar, H.J.W., Follows, M., Harvey, M., Lancelot, C., Levasseur, M., Owens, N.P.J., Pollard, R., Rivkin, R.B., Sarmiento, J., Schoemann, V., Smetacek, V., Takeda, S., Tsuda, A., Turner, S., Watson, A.J., 2007. Mesoscale Iron enrichment experiments 1993-2005: synthesis and future directions. *Science* **315,** 612-617.

Brewer, P.G., Goldman, J.C., 1976. Alkalinity changes generated by phytoplankton growth. *Limnol. Oceanogr.* **21,** 108-117.

Broerse, A.T.C., Ziveri, P., van Hinte, J.E., Honjo, S., 2000. Coccolithophore export production, species composition, and coccolith-$CaCO_3$ fluxes in the NE Atlantic (34ºN 21ºW and 48ºN 21ºW). *Deep-Sea Res. II* **47,** 1877-1905.

Byrne, R.H., 1987. Standardization of standard buffers by visible spectrometry. *Analytical Chemistry* **59,** 1479-1481.

Caldeira, K., Wickett, M. E., 2003. Anthropogenic carbon and ocean pH. *Nature* **425**, 365.

Campbell, D.M., Millero, F.J., Roy, R., Roy, L., Lawson, M., Vogel, K.M., Porter-Moore, C.P., 1993. The standard potential for the hydrogen-silver, silver chloride cell in synthetic seawater. *Mar. Chem.* **44,** 221-233.

Carr, M.-E., 2002. Estimation of potential productivity in Eastern Boundary Currents using remote sensing. *Deep-Sea Res. II* **49,** 59-80.

Chen, F., Cai, W.-J., Wang, Y., Rii, Y.M., Bidigare, R.R., Benitez-Nelson, C.R., 2008. The carbon dioxide system and net community production within a cyclonic eddy in the lee of Hawaii. *Deep-Sea Res. II* **55,** 1412-1425.

Chipman, D.W., Marra, J., Takahashi, T., 1993. Primary production at 47°N and 20°W in the North Atlantic Ocean: a comparison between the ^{14}C incubation method and the mixed layer carbon budget. *Deep-Sea Res. II* **40,** 151-169.

Clayton, T.D., Byrne, R.H., 1993. Spectrophotometric sea water pH measurements: total hydrogen ion concentration scale calibration of *m*-cresol purple and at-sea results. *Deep-Sea Res. I* **40,** 2115-2129.

Copin-Montégut, G., Avril, B., 1993. Vertical distribution and temporal variation of dissolved organic carbon in the North-Western Mediterranean Sea. *Deep-Sea Res.* **40,** 1963-1972.

Copin-Montégut, C., Avril, B., 1995. Continuous pCO_2 measurements in surface water of the Northeastern tropical Atlantic. *Tellus B* **47,** 86-92.

Corbière, A., Metzl, N., Reverdin, G., Brunet, C., Takahashi, T., 2007. Interannual and decadal variability of the oceanic carbon sink in the North Atlantic subpolar gyre. *Tellus B* **59**, 168-178.

Covington, A.K., Whitfield, M., 1988. Recommendations for the determination of pH in seawater and estuarine waters. *Pure and Applied Chemistry* **60,** 865-870.

Culberson, C.H., 1981. Direct potentiometry. In: Whitfield, M. and Jagner, D. (Eds.). *Marine Electrochemistry,* Wiley, New York, 187-261.

Cullen, J.J., 1991. Hypotheses to explain high-nutrient conditions in the open sea. *Limnol. Oceanogr.* **36,** 1578-1599.

de Baar, H.J.W., Boyd, P.W., Coale, K.H., Landry, M.R., Tsuda, A., Assmy, P., Bakker, D.C.E., Bozec, Y., Barber, R.T., Brzezinski, M.A., Buesseler, K.O., Boyé, M., Croot, P.L., Gervais, F., Gorbunov, M.Y., Harrison, P.J., Hiscock, W.T., Laan, P., Lancelot, C., Law, C.S., Levasseur, M., Marchetti, A., Millero, F.J., Nishioka, J., Nojiri, Y., van Oijen, T., Riebesell, U., Rijkenberg, M.J.A., Saito, H., Takeda, S., Timmermans, K.R., Veldhuis, M.J.W., Waite, A.M., Wong, C.-S., 2005. Synthesis of iron fertilization experiments: from the Iron Age in the Age of Enlightenment. *J. Geophys. Res.* **110,** C09S16, doi:10.1029/2004JC002601.

De La Rocha, C.L., Passow, U., 2007. Factors influencing the sinking of POC and the efficiency of the biological carbon pump. *Deep-Sea Res. II* **54,** 639-658.

DelValls, T.A., Dickson, A.G., 1998. The pH of buffers based on 2-amino-2-hydroxymethyl-1,3-propanediol ('TRIS') in synthetic sea water. *Deep-Sea Res. I* **45,** 1541-1554.

Dickson, A.G., Riley, J.P., 1979. The estimation of acid dissociation constants in seawater from potentiometric titrations with strong base: I. The ion product of water-K_w. *Mar. Chem.* **7,** 89-99.

Dickson, A.G., 1981. An exact definition of total alkalinity and a procedure for the estimation of alkalinity and total inorganic carbon from titration data. *Deep-Sea Res.* **28,** 609-623.

Dickson, A.G., 1987. Standardization of the (AgCl + H_2 = Ag + HCl) cell from 273.15 to 318.15 K. *Journal of Chemical Thermodynamics* **19,** 993-1000.

Dickson, A.G., Millero, F.J., 1987. A comparison of the equilibrium constants for the dissociation of carbonic acid in seawater media. *Deep-Sea Res.* **34**, 1733-1743.

Dickson, A.G., 1990. Standard potential of the reaction: $AgCl_{(s)} + H_{2(g)} = Ag_{(s)} + HCl_{(aq)}$, and the standard acidity constant of the ion HSO_4^- in synthetic sea water from 273.15 to 318.15 K. *Journal of Chemical Thermodynamics* **22,** 113-127.

Dickson, A.G., 1993. The measurement of sea water pH. *Mar. Chem.* **44,** 131-142.

Dickson, A.G., Goyet, C., (Eds.) 1994. Handbook of methods for the analysis of the various parameters of the carbon dioxide system in sea water. DOE (U.S. Department of Energy), ORNL/CDIAC. Carbon Dioxide Information Analysis Center, Oak Ridge National Laboratory, Oak Ridge, Tenn., U.S.A.

Dickson, A.G., Sabine, C.L., Christian, J.R. (Eds.) 2007. Guide to best practices for ocean CO_2 measurements. PICES Special Publication 3, IOCCP report No. 8, 191 pp.

Dickson, A.G., 2010. The carbon dioxide system in sea water: equilibrium chemistry and measurements. In: Riebesell, U., Fabry, V.J., Hansson, L., Gattuso, J.-P. (Eds.). Guide to best practices in ocean acidification research and data reporting.

Dickson, R., Lazier, J., Meincke, J., Rhines, P., Swift, J., 1996. Long-term coordinated changes in the convective activity of the North Atlantic. *Prog. Oceanog.* **38**, 241-295.

Doney, S.C., Fabry, V.J., Feely, R.A., Kleypas, J.A., 2009a. Ocean acidification: the other CO_2 problem. *Annual Review of Marine Science* **1,** 169-192.

Doney, S.C., Tilbrook, B., Roy, S., Metzl, N., Le Quéré, C., Hood, M., Feely, R.A., Bakker, D., 2009b. Surface-ocean CO_2 variability and vulnerability. *Deep-Sea Res. II* **56,** 504-511.

Doney, S.C., Lima, I., Feely, R.A., Glover, D.M., Lindsay, K., Mahowald, N., Moore, J.K., Wanninkhof, R., 2009c. Mechanisms governing interannual variability in upper-ocean inorganic carbon system and air-sea CO_2 fluxes: physical climate and atmospheric dust. *Deep-Sea Res. II* **56,** 640-655.

Dore, J.E., Karl, D.M., 1996. Nitrification in the euphotic zone as a source for nitrite, nitrate, and nitrous oxide at station ALOHA. *Limnol. Oceanogr.* **41,** 1619-1628.

Dore, J.E., Lukas, R., Sadler, D.W., Church, M.J., Karl, D.M., 2009. Physical and biogeochemical modulation of ocean acidification in the central North Pacific. *Proc. Natl Acad. Sci.* **106,** 12235-12240.

Dugdale, R.C., Goering, J.J., 1967. Uptake of new and regenerated forms of nitrogen in primary productivity. *Limnol. Oceanogr.* **12,** 196-206.

Dumousseaud, C., Achterberg, E.P., Tyrrell, T., Charalampopoulou, A., Schuster, U., Hartman, M., Hydes, D.J., 2010. Contrasting effects of temperature and winter mixing on the seasonal and inter-annual variability of the carbonate system in the Northeast Atlantic Ocean. *Biogeosciences* **7,** 1481-1492.

Eppley, R.W., Peterson, B.J., 1979. Particulate organic matter flux and planktonic new production in the deep ocean. *Nature* **282,** 677-680.

Fabry, V.J., 2008. Marine calcifiers in a high-CO_2 ocean. *Science* **320**, 1020-1022.

Falkowski, P.G., Ziemann, D., Kolber, Z., Bienfang, P.K., 1991. Role of eddy pumping in enhancing primary production in the ocean. *Nature* **352,** 55-58.

Falkowski, P., Scholes, R.J., Boyle, E., Canadell, J., Canfield, D., Elser, J., Gruber, N., Hibbard, K., Hogberg, P., Linder, S., Mackenzie, F.T., Moore III, B., Pedersen, T., Rosenthal, Y., Seitzinger, S., Smetacek, V., Steffen, W., 2000. The

Global Carbon Cycle: a test of our knowledge of Earth as a system. *Science* **290,** 291-296.

Feely, R.A., Sabine, C.L., Lee, K., Berelson, W., Kleypas, J., Fabry, V.J., Millero, F.J., 2004. Impact of anthropogenic CO_2 on the $CaCO_3$ system in the oceans. *Science* **305**, 362-366.

Feely, R.A., Sabine, C.L., Hernandez-Ayon, J.M., Ianson, D., Hales, B., 2008. Evidence for upwelling of corrosive "acidified" water onto the continental shelf. *Science* **320,** 1490-1492.

Findlay, H.S., Tyrrell, T., Bellerby, R.G.J., Merico, A., Skjelvan, I., 2008. Carbon and nutrient mixed layer dynamics in the Norwegian Sea. *Biogeosciences* **5**, 1395-1410.

Fischer, G., Karakas, G., Blaas, M., Ratmeyer, V., Nowald, N., Schlitzer, R., Helmke, P., Davenport, R., Donner, B., Neuer, S., Wefer, G., 2007. Mineral ballast and particle settling rates in the coastal upwelling system off NW Africa and the South Atlantic. *Int. J. Earth Sci.* **98,** 281-298.

Frankignoulle, M., Canon, C., Gattuso, J.-P., 1994. Marine calcification as a source of carbon dioxide: positive feedback of increased atmospheric CO_2. *Limnol. Oceanogr*. **39,** 458-462.

Frankignoulle, M., Bourge, I., Canon, C., Dauby, P., 1996a. Distribution of surface seawater partial CO_2 pressure in the English Channel and in the Southern Bight of the North Sea. *Cont. Shelf Res.* **16**, 381-395.

Frankignoulle, M., Elskens, M., Biondo, R., Bourge, I., Canon, Ch., Desgain, S., Dauby, P., 1996b. Distribution of inorganic carbon and related parameters in surface seawater of the English Channel during spring 1994. *Journal of Marine Systems* **7**, 427-434.

Frankignoulle, M., Borges, A.V., 2001. European continental shelf as a significant sink for atmospheric carbon dioxide. *Global Biogeochem. Cycles* **15,** 569-576.

Friis, K., Kortzinger, A., Wallace, D.W.R., 2003. The salinity normalization of marine inorganic carbon chemistry data. *Geophys. Res. Lett.* **31,** 1085, doi:10.1029/2002GL015898.

Garcia, H.E., Gordon, L.I., 1992. Oxygen solubility in seawater: better fitting equations. *Limnol. Oceanogr.* **37,** 1307-1312.

González-Dávila, M., Santana-Casiano, J.M., 2003a. Seasonal and interannual variability of sea-surface carbon dioxide species at the European Station for Time Series in the Ocean at the Canary Islands (ESTOC) between 1996 and 2000. *Global Biogeochem. Cycles* **17,** 1076, doi:10.1029/2002GB001993.

González-Dávila, M., Santana-Casiano, J.M., Dafner, E.V., 2003b. Winter mesoscale variations of carbonate system parameters and estimates of CO_2 fluxes in the Gulf of Cadiz, northeast Atlantic Ocean (February 1998). *J. Geophys. Res.* **108,** doi:10.1029/2001JC001243.

González-Dávila, M., Santana-Casiano, J.M., de Armas, D., Escánez, J., Suarez-Tangil, M., 2006. The influence of island generated eddies on the carbon dioxide system, south of the Canary Islands. *Mar. Chem.* **99,** 177-190.

Goyet, C., Poisson, A., 1989. New determination of carbonic acid dissociation constants in seawater as a function of temperature and salinity. *Deep-Sea Res.* **36,** 1635-1654.

Goyet, C., Adams, R., Eischeid, G., 1998. Observations of the CO_2 system properties in the tropical Atlantic Ocean. *Mar. Chem.* **60,** 49-61.

Goyet, C., Gonçalves, R.I., Touratier, F., 2009. Anthropogenic carbon distribution in the eastern South Pacific Ocean. *Biogeosciences* **6,** 149-156.

Grasshoff, K., 1983. Determination of nutrients. In: Grasshoff, K., Ehrhardt, M., Kremling, K. (Eds.). Methods of Seawater Analysis, second edition. Verlag Chemie GmbH, Basel, 125-188.

Gruber, N., Sarmiento, J.L., Stocker, T.F., 1996. An improved method for detecting anthropogenic CO_2 in the oceans. *Global Biogeochem. Cycles* **10,** 809-837.

Gruber, N., Keeling, C.D., Bates, N.R., 2002. Interannual variability in the North Atlantic Ocean carbon sink. *Science* **298**, 2374-2378.

Gruber, N., Gloor, M., Mikaloff Fletcher, S.E., Doney, S.C., Dutkiewicz, S., Follows, M.J., Gerber, M., Jacobson, A.R., Joos, F., Lindsay, K., Menemenlis, D., Mouchet, A., Müller, S.A., Sarmiento, J.L., Takahashi, T., 2009. Oceanic sources, sinks, and transport of atmospheric CO_2. *Global Biogeochem. Cycles* **23,** GB1005, doi:10.1029/2008GB003349.

Hansson, I., 1973. A new set of pH scales and standard buffers for sea water. *Deep-Sea Res.* **20,** 479-491.

Hardman-Mountford, N.J., Moore, G., Bakker, D.C.E., Watson, A.J., Schuster, U., Barciela, R., Hines, A., Moncoiffé, G., Brown, J., Dye, S., Blackford, J., Somerfield, P.J., Holt, J., Hydes, D.J., Aiken, J., 2008. An operational monitoring system to provide indicators of CO_2-related variables in the ocean. *ICES Journal of Marine Science* **65,** 1498-1503.

Hofmann, D.J., Butler, J.H., Tans, P.P., 2009. A new look at atmospheric carbon dioxide. *Atmospheric Environment* **43,** 2084-2086.

Holley, S.E., Hydes, D.J., 1995. Procedures for the determination of dissolved oxygen in seawater. *James Rennell Centre for Ocean Circulation*, 33 pp.

Holligan, P.M., Fernández, E., Aiken, J., Balch, W.M., Boyd, P., Burkill, P.H., Finch, M., Groom, S.B., Malin, G., Muller, K., Purdie, D.A., Robinson, C., Trees, C.C., Turner, S.M., van der Wal, P., 1993. A biogeochemical study of the coccolithophore, *Emiliana huxleyi*, in the North Atlantic. *Global Biogeochem. Cycles* **7,** 879-900.

Hunter, K.A., 1998. The temperature dependence of pH in surface seawater. *Deep-Sea Res. I* **45,** 1919-1930.

Hydes, D.J., Yool, A., Campbell, J.M., Crisp, N.A., Dodgson, J., Dupee, B., Edwards, M., Hartman, S.E., Kelly-Gerreyn, B.A., Lavin, A.M., González-Pola, C.M., Miller, P., 2003. Use of a Ferry-Box system to look at shelf sea and ocean margin processes. In: Dahlin, H., Flemming, N.C., Nittis, K., Petersson, S.E. (Eds.).

Building of the European Capacity in Operational Oceanography. *Elsevier Oceanography Series* **69,** 297-303.

Hydes, D.J., Hartman, M.C., Bargeron, C.P., Campbell, J.M., Curé, M.S., Woolf, D.K., 2008. A study of gas exchange during the transition from deep winter mixing to spring bloom in the Bay of Biscay measured by continuous observation from a ship of opportunity. *Journal of Operational Oceanography* **1(2)**, 41-50.

Hydes, D.J., Hartman, M.C., Kaiser, J., Campbell, J.M., 2009. Measurement of dissolved oxygen using optodes in a FerryBox system. *Estuarine, Coastal and Shelf Science* **83,** 485-490, doi:10.1016/j.ecss.2009.04.014.

Iglesias-Rodriguez, D., Halloran, P.R., Rickaby, R.E.M., Hall, I.R., Colmenero-Hidalgo, E., Gittins, J.R., Green, D.R.H., Tyrrell, T., Gibbs, S.J., von Dassow, P., Rehm, E., Armbrust, E.V., Boessenkool, K.P., 2008. Phytoplankton calcification in a High-CO_2 world. *Science* **320,** 336-340.

IPCC, 2001. Climate Change 2001: The Scientific Basis. Contribution of Working Group I to the Third Assessment Report of the Intergovernmental Panel on Climate Change. Houghton, J.T., Ding, Y., Griggs, D.J., Noguer, M., van der Linden, P.J., Dai, X., Maskell, K., Johnson, C.A. (Eds.). Cambridge University Press, Cambridge, United Kingdom and New York, NY, USA, 881 pp.

IPCC, 2007. Climate Change 2007: Synthesis Report. Contribution of Working Groups I, II and III to the Fourth Assessment Report of the Intergovernmental Panel on Climate Change. IPCC, Geneva, Switzerland, 104pp.

Johnson, K.M., Wills, K.D., Butler, D.B., Johnson, W.K., Wong, C.S., 1993. Coulometric total carbon dioxide analysis for marine studies: maximizing the performance of an automated gas extraction system and coulometric detector. *Mar. Chem.* **44,** 167-187.

Jutterström, S., Anderson, L.G., 2005. The saturation of calcite and aragonite in the Arctic Ocean. *Mar. Chem.* **94,** 101-110.

Karl, D.M., Bates, N.R., Emerson, S., Harrison, P.J., Jeandel, C., Llinás, O., Liu, K.-K., Marty, J.-C., Michaels, A.F., Miquel, J.C., Neuer, S., Nojiri, Y., Wong, C.S.,

2003. Temporal studies of biogeochemical processes determined from ocean time-series observations during the JGOFS era. In: Fasham, M.J.R. (Ed.). Ocean Biogeochemistry: The Role of the Ocean Carbon Cycle in Global Change, Springer, 239-265.

Karstensen, J., Stramma, L., Visbeck, M., 2008. Oxygen minimum zones in the eastern tropical Atlantic and Pacific oceans. *Prog. Oceanogr.* **77,** 331-350.

Keeling, C.D., 1960. The concentration and isotopic abundances of carbon dioxide in the atmosphere. *Tellus* **12,** 200-203.

Kelly-Gerreyn, B.A., Hydes, D.J., Jégou, A.M., Lazure, P., Fernand, L.J., Puillat, I., Garcia-Soto, C., 2006. Low salinity intrusions in the western English Channel. *Cont. Shelf Res.* **26**, 1241-1257.

Key, R.M., Kozyr, A., Sabine, C.L., Lee, K., Wanninkhof, R., Bullister, J.L., Feely, R.A., Millero, F.J., Mordy, C., Peng, T.-H., 2004. A global ocean carbon climatology: results from Global Data Analysis Project (GLODAP). *Global Biogeochem. Cycles* **18,** GB4031, doi:10.1029/2004GB002247.

Kirkwood, D., 1996. Nutrients: practical notes on their determination in seawater. *ICES Techniques in marine environmental sciences* **25**. Copenhagen, International Council for the Exploration of the Sea.

Körtzinger, A., Koeve, W., Kähler, P., Mintrop, L., 2001. C:N ratios in the mixed layer during the productive season in the northeast Atlantic Ocean. *Deep-Sea Res. I* **48**, 661-688.

Lamb, M.F., Sabine, C.L., Feely, R.A., Wanninkhof, R., Key, R.M., Johnson, G.C., Millero, F.J., Lee, K., Peng, T.-H., Kozyr, A., Bullister, J.L., Greeley, D., Byrne, R.H., Chipman, D.W., Dickson, A.G., Goyet, C., Guenther, P.R., Ishii, M., Johnson, K.M., Keeling, C.D., Ono, T., Shitashima, K., Tilbrook, B., Takahashi, T., Wallace, D.W.R., Watanabe, Y.W., Winn, C., Wong, C.S., 2002. Consistency and synthesis of Pacific Ocean CO_2 survey data. *Deep-Sea Res. II* **49,** 21-58.

Lampitt, R.S., Achterberg, E.P., Anderson, T.R., Hughes, J.A., Iglesias-Rodriguez, M.D., Kelly-Gerreyn, B.A., Lucas, M., Popova, E.E., Sanders, R.,

Shepherd, J.G., Smythe-Wright, D., Yool, A., 2008. Ocean fertilization: a potential means of geoengineering? *Phil. Trans. R. Soc. A* **366,** 3919-3945.

Landry, M.R., Barber, R.T., Bidigare, R.R., Chai, F., Coale, K.H., Dam, H.G., Lewis, M.R., Lindley, S.T., McCarthy, J.J., Roman, M.R., Stoecker, D.K., Verity, P.G., White, J.R., 1997. Iron and grazing constraints on primary production in the central equatorial Pacific: an EqPac synthesis. *Limnol. Oceanogr.* **42,** 405-418.

Lee, K., Millero, F.J., Byrne, R.H., Feely, R.A., Wanninkhof, R., 2000. The recommended dissociation constants for carbonic acid in seawater. *Geophys. Res. Lett.* **27,** 229-232.

Lee, K., Tong, L.T., Millero, F.J., Sabine, C.L., Dickson, A.G., Goyet, C., Park, G.-H., Wanninkhof, R., Feely, R.A., Key, R.M., 2006. Global relationships of total alkalinity with salinity and temperature in surface waters of the world's oceans. *Geophys. Res. Lett.* **33**, L19605, doi:10.1029/2006GL027207.

Le Quéré, C., Rödenbeck, C., Buitenhuis, E.T., Conway, T.J., Langelfelds, R., Gomez, A., Labuschagne, C., Ramonet, M., Nakazawa, T., Metzl, N., Gillett, N., Heimann, M., 2007. Saturation of the Southern Ocean CO_2 sink due to recent climate change. *Science* **316**, 1735-1738.

Levitus, S., Antonov, J.I., Boyer, T.P., Stephens, C., 2000. Warming of the World Ocean. *Science* **287,** 2225-2229.

Levitus, S., Antonov, J.I., Wang, J., Delworth, T.L., Dixon, K.W., Broccoli, A.J., 2001. Anthropogenic warming of Earth's climate system. *Science* **292,** 267-270.

Lewis, E., Wallace, D.W.R., 1998. Program Developed for CO2 System Calculations. ORNL/CDIAC-105. Carbon Dioxide Information Analysis Center, Oak Ridge National Laboratory, U.S. Department of Energy, Oak Ridge, Tennessee.

Lovenduski, N.S., Gruber, N., Doney, S.C., 2008. Toward a mechanistic understanding of the decadal trends in the Southern Ocean carbon sink. *Global Biogeochem. Cycles* **22,** GB3016, doi:10.1029/2007GB003139.

Lueker, T.J., Dickson, A.G., Keeling, C.D., 2000. Ocean pCO_2 calculated from dissolved inorganic carbon, alkalinity, and equations for K_1 and K_2: validation based on laboratory measurements of CO_2 in gas and seawater at equilibrium. *Mar. Chem.* **70,** 105-119.

Luterbacher, J., Liniger, M.A., Menzel A., Estrella, N., Della-Marta, P.M., Pfister, C., Rutishauser T., Xoplaki, E., 2007. Exceptional European warmth of autumn 2006 and winter 2007: historical context, the underlying dynamics, and its phonological impacts. *Geophys. Res. Lett.* **34,** L12704, doi:10.1029/2007GL029951.

Martin, A.P., Wade, I.P., Richards, K.J., Heywood, K.J., 1998. The PRIME eddy. *J. Mar. Res.* **56,** 439-462.

Martin, A.P., Richards, K.J., 2001. Mechanisms for vertical nutrient transport within a North Atlantic mesoscale eddy. *Deep-Sea Res. II* **48,** 757-773.

Martin, J.H., Fitzwater, S.E., 1988. Iron deficiency limits phytoplankton growth in the north-east Pacific subarctic. *Nature* **331,** 341-343.

Martin, J.H., Gordon, R.M., Fitzwater, S.E., 1991. The case for iron. *Limnol. Oceanogr.* **36,** 1793-1802.

Matear, R.J., Hirst, A.C., 2003. Long-term changes in dissolved oxygen concentrations in the ocean caused by protracted global warming. *Global Biogeochem. Cycles* **17,** doi:10.1029/2002GB001997.

McElligott, S., Byrne, R.H., Lee, K., Wanninkhof, R., Millero, F.J., Feely, R.A., 1998. Discrete water column measurements of CO_2 fugacity and pH_T in seawater: A comparison of direct measurements and thermodynamic calculations. *Mar. Chem.* **60,** 63-73.

McGillicuddy Jr., D.J., Robinson, A.R., Siegel, D.A., Jannasch, H.W., Johnson, R., Dickey, T.D., McNeil, J., Michaels, A.F., Knap, A.H., 1998. Influence of mesoscale eddies on new production in the Sargasso Sea. *Nature* **394,** 263-266.

McGillicuddy Jr., D.J., Anderson, L.A., Bates, N.R., Bibby, T., Buesseler, K.O., Carlson, C.A., Davis, C.S., Ewart, C., Falkowski, P.G., Goldthwait, S.A., Hansell,

D.A., Jenkins, W.J., Johnson, R., Kosnyrev, V.K., Ledwell, J.R., Li, Q.P., Siegel, D.A., Steinberg, D.K., 2007. Eddy/wind interactions stimulate extraordinary mid-ocean plankton blooms. *Scien*ce **316,** 1021-1026.

Mehrbach, C., Culberson, C.H., Hawley, J.H., Pytkowicz, R.M., 1973. Measurement of the apparent dissociation constants of carbonic acid in seawater at atmospheric pressure. *Limnol. Oceanogr.* **18**, 897-907.

Mellon, M.G., Morris, V.N., 1925. Standardizing acids and bases with Borax. *Industrial and Engineering Chemistry* **17,** 145-146.

Millero, F.J., Lee, K., Roche, M., 1998a. Distribution of Alkalinity in the Surface Waters of the Major Oceans. *Mar. Chem.* **60**, 111-130.

Millero, F.J., Dickson, A.G., Eischeid, G., Goyet, C., Guenther, P., Johnson, K.M., Key, R.M., Lee, K., Purkenson, D., Sabine, C.L., Schottle, R.G., Wallace, D.W.R., Lewis, E., Winn, C.D., 1998b. Assessment of the quality of the shipboard measurements of total alkalinity on the WOCE Hydrographic Program Indian Ocean CO2 survey cruises 1994-1996. *Mar. Chem.* **63**, 9-20.

Mittelstaedt, E., 1983. The upwelling area off Northwest Africa – A description of phenomena related to coastal upwelling. *Prog. Oceanog.* **12,** 307-331.

Mojica Prieto, F.J., Millero, F.J., 2002. The values of pK_1 + pK_2 for the dissociation of carbonic acid in seawater. *Geochimica et Cosmochimica Acta*, **66,** 2529-2540.

Monterey, G., Levitus, S., 1997. Seasonal variability of mixed layer depth for the world ocean. NOAA Atlas, NESDIS 14, Washington D.C., 96 pp.

Morel, A., Prieur, L., 1977. Analysis of variations in ocean color. *Limnol. Oceanogr.* **22(4),** 709-722.

Najjar, R.G., Jin, X., Louanchi, F., Aumont, O., Caldeira, K., Doney, S.C., Dutay, J.-C., Follows, M., Gruber, N., Joos, F., Lindsay, K., Maier-Reimer, E., Matear, R.J., Matsumoto, K., Monfray, P., Mouchet, A., Orr, J.C., Plattner, G.-K., Sarmiento, J.L., Schlitzer, R., Slater, R.D., Weirig, M.-F., Yamanaka, Y., Yool, A., 2007. Impact of

circulation on export production, dissolved organic matter, and dissolved oxygen in the ocean: results from Phase II of the Ocean Carbon-cycle Model Intercomparison Project (OCMIP-2). *Global Biogeochem. Cycles* **21,** GB3007, doi:10.1029/2006GB002857.

Nemzer, B.V., Dickson, A.G., 2005. The stability and reproducibility of TRIS buffers in synthetic seawater. *Mar. Chem.* **96,** 237-242.

Nightingale, P.D., Malin, G., Law, C.S., Watson, A.J., Liss, P.S., Liddicoat, M.I., Boutin, J., Upstill-Goddard, R.C., 2000. In situ evaluation of air-sea gas exchange parameterizations using novel conservative and volatile tracers. *Global Biogeochem. Cycles* **14,** 373-387.

Ohline, S.M., Reid, M.R., Husheer, S.L.G., Currie, K.I., Hunter, K., 2007. Spectrophotometric determination of pH in seawater off Taiaroa Head, Otago, New Zealand: Full-spectrum modeling and prediction of pCO_2 levels. *Mar. Chem.* **107,** 143-155.

Orr, J.C., Fabry, V.J., Aumont, O., Bopp, L., Doney, S.C., Feely, R.A., Gnanadesikan, A., Gruber, N., Ishida, A., Joos, F., Key, R.M., Lindsay, K., Maier-Reimer, E., Matear, R., Monfray, P., Mouchet, A., Najjar, R.G., Plattner, G-K., Rodgers, K.B., Sabine, C.L., Sarmiento, J.L., 2005. Anthropogenic ocean acidification over the twenty-first century and its impact on calcifying organisms. *Nature* **437**, 681-686.

Oschlies, A., Schulz, K.G., Riebesell, U., Schmittner, A., 2008. Simulated 21st century's increase in oceanic suboxia by CO_2-enhanced biotic carbon export. *Global Biogeochem. Cycles* **22,** doi:10.1029/2007GB003147.

Padin, X.A., Vázquez-Rodríquez, M., Ríos, A.F., Pérez, F.F., 2007. Surface CO_2 measurements in the English Channel and Southern Bight of North Sea using voluntary observing ships. *Journal of Marine Systems* **66,** 297-308.

Padin, X.A., Castro, C.G., Ríos, A.F., Pérez, F.F., 2008. fCO_2^{SW} variability in the Bay of Biscay during ECO cruises. *Cont. Shelf Res.* **28,** 904-914.

Padin, X.A., Navarro, G., Gilcoto, M., Rios, A.F., Pérez, F.F., 2009. Estimation of air-sea CO_2 fluxes in the Bay of Biscay based on empirical relationships and remotely sensed observations. *Journal of Marine Systems* **75**, 280-289.

Patey, M.D, Rijkenberg, M.J.A., Statham, P.J., Stinchcombe, M.C., Achterberg, E.P., Mowlem, M., 2008. Determination of nitrate and phosphate in seawater at nanomolar concentrations. *Trac-Trends in Analytical Chemistry* **27(2),** 169-182.

Pearson, K., 1901. On lines and planes of closest fit to systems of points in space. *Philosophical Magazine* **2(6),** 559-572.

Peng, T.-H., Wanninkhof, R., Feely, R.A., 2003. Increase of anthropogenic CO_2 in the Pacific Ocean over the last two decades. *Deep-Sea Res. II* **50,** 3065-3082.

Pérez, F.F., Mintrop, L., Llinás, O., Glez-Dávila, M., Castro, C.G., Alvarez, M., Körtzinger, A., Santana-Casiano, M., Rueda, M.J., Ríos, A.F., 2001. Mixing analysis of nutrients, oxygen and inorganic carbon in the Canary Islands region. *Journal of Marine Systems* **28,** 183-201.

Pidcock, R.E.M., Allen, J.T., Painter, S.C., Martin, A.P., Martin, P., Srokosz, M., Popova, E.K., Lucas, M., 2007. Real-time assessment of a developing eddy dipole in the Iceland Basin. Poster presented at the NATO Undersea Research Centre's Rapid Environmental Assessment (REA) Conference, Villa Marigola, Lerichi, Italy, September 25^{th} -27^{th}.

Pierre, C., Vangriesheim, A., Laube-Lenfant, E., 1994. Variability of water masses and of organic production-regeneration systems as related to eutrophic, mesotrophic and oligotrophic conditions in the northeast Atlantic Ocean. *Journal of Marine Systems* **5,** 159-170.

Pierrot, D., Lewis, E., Wallace, D.W.R., 2006. *MS Excel Program Developed for CO_2 System Calculations.* ORNL/CDIAC-105. Carbon Dioxide Information Analysis Center, Oak Ridge National Laboratory, U.S. Department of Energy, Oak Ridge, Tennessee.

Pollard, R.T., Read, J.F., Holliday, N.P., 2004. Water masses and circulation pathways through the Iceland Basin during Vivaldi 1996. *J. Geophys. Res.* **109,** C04004, doi:10.1029/2003JC002067.

Pollard, R.T., Salter, I., Sanders, R.J., Lucas, M.I., Moore, C.M., Mills, R.A., Statham, P.J., Allen, J.T., Baker, A.R., Bakker, D.C.E., Charette, M.A., Fielding, S., Fones, G.R., French, M., Hickman, A.E., Holland, R.J., Hughes, J.A., Jickells, T.D., Lampitt, R.S., Morris, P.J., Nédélec, F.H., Nielsdóttir, M., Planquette, H., Popova, E.E., Poulton, A.J., Read, J.F., Seeyave, S., Smith, T., Stinchcombe, M., Taylor, S., Thomalla, S., Venables, H.J., Williamson, R., Zubkov, M.V., 2009. Southern Ocean deep-water carbon export enhanced by natural iron fertilization. *Nature* **457,** 577-581.

Prowe, A.E.F., Thomas, H., Pätsch, J., Kühn, W., Bozec, Y., Schiettecatte, L., Borges, A.V., de Baar, H.J.W., 2009. Mechanisms controlling the air–sea CO_2 flux in the North Sea. *Cont. Shelf Res.* **29**, 1801-1808.

Read, J.F., Pollard, R.T., 2001. A long-lived eddy in the Iceland Basin 1998. *J. Geophys. Res.* **106,** 11411-11421.

Revelle, R., Suess, H.E., 1957. Carbon dioxide exchange between atmosphere and ocean and the question of an increase of atmospheric CO_2 during the past decades. *Tellus* **9,** 18-27.

Ridgwell, A., Zeebe, R.E., 2005. The role of the global carbonate cycle in the regulation and evolution of the Earth system. *Earth and Planetary Science Letters* **234,** 299-315.

Riebesell, U., Zondervan, I., Rost, B., Tortell, P.D., Zeebe, R.E., Morel, F.M.M., 2000. Reduced calcification of marine plankton in response to increased atmospheric CO_2. *Nature* **407,** 364-367.

Robertson, J.E., Robinson, C., Turner, D.R., Holligan, P., Watson, A.J., Boyd, P., Fernandez, E., Finch, M., 1994. The impact of a coccolithophore bloom on oceanic carbon uptake in the northeast Atlantic during summer 1991. *Deep-Sea Res. I* **41**, 297-314.

Roy, R.N., Roy, L.N., Vogel, K.M., Porter-Moore, C., Pearson T., Good, C.E., Millero, F.J., Campbell, D.M., 1993. The dissociation constants of carbonic acid in seawater at salinities 5 to 45 and temperatures 0 to 45ºC. *Mar. Chem.* **44,** 249-267.

Royal Society, 2005. Ocean Acidification due to increasing atmospheric carbon dioxide. Policy document 12/05. ISBN 0-85403-617-2.

Royal Society, 2009. Geoengineering the climate: science, governance and uncertainty. Policy document 10/09. ISBN 0-85403-773-5.

Sabine C.L., Feely, R.A., Gruber, N., Key, R.M., Lee, K., Bullister, J.L., Wanninkhof, R., Wong, C.S., Wallace, D.W.R., Tilbrook, B., Millero, F.J., Peng, T-H. Kozyr, A., Ono, T., Rios, A.F., 2004. The oceanic sink for anthropogenic CO_2. *Science* **305**, 367-371.

Sambrotto, R.N., Savidge, G., Robinson, C., Boyd, P., Takahashi, T., Karl, D.M., Langdon, C., Chipman, D., Marra, J., Codispoti, L., 1993. Elevated consumption of carbon relative to nitrogen in the surface ocean. *Nature* **363,** 248-250.

Santana-Casiano, J.M., González-Dávila, M., Rueda, M.-J., Llinás, O., González-Dávila, E.-F., 2007. The interannual variability of oceanic CO_2 parameters in the northeast Atlantic subtropical gyre at the ESTOC site. *Global Biogeochem. Cycles* **21,** doi:10.1029/2006GB002788.

Santana-Casiano, J.M., González-Davila, M., Ucha, I.R., 2009. Carbon dioxide fluxes in the Benguela upwelling system during winter and spring: a comparison between 2005 and 2006. *Deep-Sea Res. II* **56,** 533-541.

Sarmiento, J.L., Hughes, T.M.C., Stouffer, R.J., Manabe, S., 1998. Simulated response of the ocean carbon cycle to anthropogenic climate warming. *Nature* 393, 245-249.

Sarmiento, J.L., Gruber, N., 2002. Sinks for anthropogenic carbon. *Physics Today* **55,** 30-36.

Sarmiento, J.L., Gruber, N., 2006. Ocean Biogeochemical Dynamics. Princeton University Press, 503 pp.

Schneider, B., Bopp, L., Gehlen, M., Segschneider, J., Frolicher, T.L., Cadule, P., Friedlingstein, P., Doney, S.C., Behrenfield, M.J., Joos, F., 2008. Climate-induced interannual variability of marine primary and export production in three global coupled climate carbon cycle models. *Biogeosciences* **5,** 597-614.

Schmitter, A, Latif, M., Schneider, B., 2005. Model projections of the North Atlantic thermohaline circulation for the 21st century assessed by observations. *Geophys. Res. Lett.* **32,** L23710, doi:10.1029/2005GL024368.

Schuster, U., Watson, A.J., 2007. A variable and decreasing sink for atmospheric CO_2 in the North Atlantic. *J. Geophys. Res.* **112**, C11006, doi:10.1029/2006JC003941.

Schuster, U., Watson, A.J., Bates, N.R., Corbière, A., Gonzalez-Davila, M., Metzl, N., Pierrot, D., Santana-Casiano, M., 2009. Trends in North Atlantic sea-surface fCO_2 from 1990 to 2006. *Deep-Sea Res. II* **56**, 620-629.

Seidel, M.P., DeGrandpre, M.D., Dickson, A.G., 2008. A sensor for in situ indicator-based measurements of seawater pH. *Mar. Chem.* **109,** 18-28.

Smith, W.H., Hood, D.W., 1964. pH measurements in the ocean; a sea water secondary buffer system. In: Miyake, Y. and Koyama, T. (Eds.). *Recent researches in the fields of hydrosphere, atmosphere and nuclear geochemistry*, Maruzen Co., Tokyo, 185-202.

Soetaert, K., Hofmann, A.F., Middelburg, J.J., Meysman, F.J.R., Greenwood, J., 2007. The effect of biogeochemical processes on pH. *Mar. Chem.* **105,** 30-51.

Somavilla, R., González-Pola, C., Rodriguez, C., Josey, S.A., Sánchez, R.F., 2009. Large changes in the hydrographic structure of the Bay of Biscay after the extreme mixing of winter 2005. *J. Geophys. Res.* **114**, C01001, doi:10.1029/2008JC004974.

Sørensen, S.P.L., 1909. Enzymstudien II: Mitteilung. Über die Messung und die Bedeutung der Wasserstoffionenkonzentration bei enzymatischen Prozessen. *Biochemische Zeitschrift* **21,** 131-200.

Steinacher, M., Joos, F., Frölicher, T.L., Plattner, G.-K., Doney, S.C., 2009. Imminent ocean acidification in the Arctic projected with the NCAP global coupled carbon cycle-climate model. *Biogeosciences* **6,** 515-533.

Steinberg, D.K., Carlson, C.A., Bates, N.R., Goldthwait, S.A., Madin, L.P., Michaels, A.F., 2000. Zooplankton vertical migration and the active transport of dissolved organic and inorganic carbon in the Sargasso Sea. *Deep-Sea Res.* **47,** 137-158.

Stramma, L., Müller, T.J., 1989. Some observations of the Azores Current and the North Equatorial Current. *J. Geophys. Res.* **94,** 3181-3186

Stramma, L., Huttl, S., Schafstall, J., 2005. Water masses and currents in the upper tropical northeast Atlantic off northwest Africa. *J. Geophys. Res.* **110,** C12006, doi:10.1029/2005JC002939.

Stramma, L., Brandt, P., Schafstall, J., Schott, F., Fischer, J., Körtzinger, A., 2008a. Oxygen minimum zone in the North Atlantic south and east of the Cape Verde Islands. *J. Geophys. Res.* **113,** C04014, doi:10.1029/2007JC004369.

Stramma, L., Johnson, G.C., Sprintall, J., Mohrholz, V., 2008b. Expanding Oxygen-Minimum Zones in the Tropical Oceans. *Science* **320,** 655-658.

Stramma, L., Visbeck, M., Brandt, P., Tanhua, T., Wallace, D., 2009. Deoxygenation in the oxygen minimum zone of the Eastern tropical North Atlantic. *Geophysical Research Letters* **36,** L20607, doi:10.1029/2009GL039593.

Sweeney, C., Gloor, E., Jacobson, A.R., Key, R.M., McKinley, G., Sarmiento, J.L., Wanninkhof, R., 2007. Constraining global air-sea gas exchange for CO_2 with recent bomb CO_2 measurements. *Global Biogeochem. Cycles* **21,** GB2015, doi:10.1029/2006GB002784.

Sweeney, E.N., McGillicuddy Jr., D.J., Buesseler, K.O., 2003. Biogeochemical impacts due to mesoscale eddy activity in the Sargasso Sea as measured at the Bermuda Atlantic Time-Series Study (BATS). *Deep-Sea Res. II* **50,** 3017-3039.

Takahashi, T., Sutherland, S.C., Sweeney, C., Poisson, A., Metzl, N., Tilbrook, B., Bates, N., Wanninkhof, R., Feely, R.A., Sabine, C., Olafsson, J., Nojiri, Y., 2002. Global sea-air CO_2 flux based on climatological surface ocean pCO_2 and seasonal biological and temperature effects. *Deep-Sea Res. II* **49**, 1601-1622.

Takahashi, T., Sutherland, S.C., Wanninkhof, R., Sweeney, C., Feely, R.A., Chipman, D.W., Hales, B., Friederich, G., Chavez, F., Sabine, C., Watson, A., Bakker, D.C.E., Schuster, U., Metzl, N., Yoshikawa-Inoue, H., Ishii, M., Midorikawa, T., Nojiri, Y., Körtzinger, A., Steinhoff, T., Hoppema, M., Olafsson, J., Arnarson, T.S., Tilbrook, B., Johannessen, T., Olsen, A., Bellerby, R., Wong, C.S., Delille, B., Bates, N.R., de Baar, H.J.W., 2009. Climatological mean and decadal change in surface ocean pCO_2, and net sea-air CO_2 flux over the global oceans. *Deep-Sea Res. II* **56**, 554-577.

Thomas, H., Prowe, A.E.F., Lima, I.D., Doney, S.C., Wanninkhof, R., Greatbatch, R.J., Schuster, U., Corbière, A., 2008. Changes in the North Atlantic Oscillation influence CO_2 uptake in the North Atlantic over the past 2 decades. *Global Biogeochem. Cycles* **22,** GB4027, doi:10.1020/2007GB003167.

Tomczak, M., Godfrey, J.S., 2003. Regional Oceanography: An Introduction (second ed.). Daya Publishing House, Delhi, 390p.

Torres, R., Turner, D.R., Silva, N., Rutllant, J., 1999. High short-term variability of CO_2 fluxes during an upwelling event off the Chilean coast at 30ºS. *Deep-Sea Res. I* **46,** 1161-1179.

Touratier, F., Goyet, C., 2004a. Definition, properties, and Atlantic Ocean distribution of the new tracer TrOCA. *Journal of Marine Systems* **46,** 169-179.

Touratier, F., Goyet, C., 2004b. Applying the new TrOCA approach to assess the distribution of anthropogenic CO_2 in the Atlantic Ocean. *Journal of Marine Systems* **46,** 181-197.

Touratier, F., Azouti, L., Goyet, C., 2007. CFC-11, $\Delta^{14}C$ and ^{3}H tracers as a means to assess anthropogenic CO_2 concentrations in the ocean. *Tellus B* **59,** 318-325.

Tseng, C.-M., Wong, G.T.F., Chou, W.-C., Lee, B.-S., Sheu, D.-D., Liu, K.-K., 2007. Temporal variations in the carbonate system in the upper layer at the SEATS station. *Deep-Sea Res. II* **54**, 1448-1468.

Tyrrell, T., Schneider, B., Charalampopoulou, A., Riebesell, U., 2008. Coccolithophores and calcite saturation state in the Baltic and Black Seas. *Biogeosciences* **5**, 485-494.

Urrère, M.A., Knauer, G.A., 1981. Zooplankton fecal pellet fluxes and vertical transport of particulate organic material in the pelagic environment. *Journal of Plankton Research* **3,** 369-387.

Vantrepotte, V., Brunet, C., Mériaux, X., Lécuyer, E., Velluci, V., Santer, R., 2007. Bio-optical properties of coastal waters in the Eastern English Channel. *Estuarine, Coastal and Shelf Science* **72,** 201-212.

Vogel, A., 1978. A textbook of quantitative inorganic analysis. Longman Inc, Fourth edition, New York, 925 pp.

Wanninkhof, R., 1992. Relationship between wind speed and gas exchange over the ocean. *J. Geophys. Res.* **97,** 7373-7382.

Wanninkhof, R., Lewis, E., Feely, R.A., Millero, F.J., 1999. The optimal carbonate dissociation constants for determining surface water *p*CO2 from alkalinity and total inorganic carbon. *Mar. Chem.* **65**, 291-301.

Watson, A.J., 2008. Certainty and uncertainty in climate change predictions: what use are climate models? *Environ. Resource Econ.* **39,** 37-44.

Wedborg, M., Turner, D.R., Anderson, L.G., Dyrssen, D., 1999. Determination of pH. In: Grasshoff, K., Kremling, K., Ehrhardt, M. (Eds.). *Methods of seawater analysis*, Wiley-VCH, third edition, Weinheim, 109-125.

Weiss, R.F., 1974. Carbon dioxide in water and seawater: the solubility of a non-ideal gas. *Mar. Chem.* **2,** 203-215.

Welschmeyer, N.A., 1994. Fluorometric analysis of chlorophyll *a* in the presence of chlorophyll *b* and pheopigments. *Limnol. Oceanogr.* **39,** 1985-1992.

Whitfield, M., Butler, R.A., Covington, A.K., 1985. The determination of pH in estuarine waters I: Definition of pH scales and the selection of buffers. *Oceanologica Acta* **8,** 423-432.

Williams, R.G., Follows, M.J., 1998. Eddies make ocean deserts bloom. *Nature* **394,** 228-229.

Wolf-Gladrow, D.A., Riebesell, U., Burkhardt, S., Bijma, J., 1999. Direct effects of CO_2 concentration on growth and isotopic composition of marine plankton. *Tellus B* **51,** 461-476.

Wolf-Gladrow, D.A., Zeebe, R.E., Klaas, C., Körtzinger, A., Dickson, A.G., 2007. Total Alkalinity: the explicit conservative expression and its application to biogeochemical processes. *Mar. Chem.* **106,** 287-300.

Wollast, R., Chou, L., 2001. The carbon cycle at the ocean margin in the northern Gulf of Biscay. *Deep-Sea Res. II* **48**, 3265-3293.

Yool, A., Martin, A.P., Fernandez, C., Clark, D.R., 2007. The significance of nitrification for oceanic new production. *Nature* **447,** 999-1002.

Zeebe, R.E., Wolf-Gladrow, D.A., 2001. CO_2 in seawater: equilibrium, kinetics, isotopes. Elsevier Oceanography Series 65, 346 pp.

Zhang, H., Byrne, R.H., 1996. Spectrophotometric pH measurements of surface seawater at in-situ conditions: absorbance and protonation behaviour of thymol blue. *Mar. Chem.* **52,** 17-25.

Zondervan, I., Zeebe, R.E., Rost, B., Riebesell, U., 2001. Decreasing marine biogenic calcification: a negative feedback on rising atmospheric pCO_2. *Global Biogeochem. Cycles* **15,** 507-516.